96-0002042

Department of Energy
Washington, DC 20585

RECEIVED
1996 MAY 14 PM 2:32
DNF SAFETY BOARD

MAY 07 1996

The Honorable John T. Conway
Chairman
Defense Nuclear Facilities Safety Board
625 Indiana Avenue, N.W.
Suite 700
Washington, D.C. 20004

Dear Mr. Conway:

The Implementation Plan for Defense Nuclear Facilities Safety Board Recommendation 93-2 requires a quarterly status report. Enclosed is the Department of Energy's quarterly status report for the second quarter of Fiscal Year 1996.

Sincerely,

Victor Stello, Jr.
Principal Deputy Assistant Secretary
for Safety and Quality
Defense Programs

Enclosure

cc:
Mark Whitaker, S-3.1, w/encl.

RECEIVED
1996 MAY 14 PM 2:32
DNF SAFETY BOARD

96/2042

QUARTERLY STATUS OF THE IMPLEMENTATION PLAN FOR DEFENSE NUCLEAR FACILITIES SAFETY BOARD RECOMMENDATION 93-2 SECOND QUARTER FISCAL YEAR 1996

The Nuclear Criticality Experiments Steering Committee (NCESC), as delineated in the Implementation Plan for the Defense Nuclear Facilities Safety Board (DNFSB) Recommendation 93-2, met twice during the second quarter of Fiscal Year 1996. An updated roster of NCESC and Subcommittee membership is attached to this report. Accomplishments and key issues discussed by the NCESC during this period of time are as follows:

- The NCESC completed an extensive review of the full program requirements for maintaining the Department's nuclear criticality predictive capability. The results of this review were documented in a report entitled, "The Department of Energy Nuclear Criticality Predictability Program," dated January 17, 1996. Along with presenting programmatic requirements, the NCESC report recommends a course of action for the institutionalization of this program. The Assistant Secretary for Defense Programs concurred with the NCESC's recommended course of action, and on February 13, 1996, sent a memorandum to the affected Program Secretarial Officers (PSOs) requesting their support. As of March 31, 1996, negotiations with cognizant PSOs on the funding of this activity are continuing.

- The NCESC conducted its annual program review at the Los Alamos Critical Experiments Facility (LACEF) in March 1996. This review highlighted accomplishments and issues requiring resolution in each of the five major program element areas. A copy of the agenda from the program review is attached. Also attached is a copy of the most recent LACEF Semi-Annual Progress Report which describes in technical detail the nuclear criticality experimental activities being conducted at the LACEF. One noteworthy accomplishment announced at the review was that the LACEF had recently won the Don Summers/Los Alamos National Laboratory Quality Excellence Award. Candidates for this award are evaluated through a rigorous process similar to that used for evaluating applicants for the prestigious Malcolm Baldridge quality award for business excellence. This is truly a momentous accomplishment by the LACEF and its staff.

The NCESC has continued to make significant progress in addressing the key issues surrounding the maintenance of the Department's nuclear criticality predictive capability. The focus of the Committee in the next quarter will be to resolve the short-term funding situation with assistance from Departmental management and begin work on laying the foundation for long-term resolution of the funding situation with a view towards institutionalization of the nuclear criticality predictability program. In addition, the NCESC will use the technical subcommittees, with additional expertise as required, to continue assessing and prioritizing needs from the nuclear criticality predictability community.

Attachments

COMMITTEE MEMBERSHIP

NUCLEAR CRITICALITY EXPERIMENTS STEERING COMMITTEE (ALL DOE FEDS)

	PHONE NO.	FAX NO.	ORGAN.
Paul Vogel (Co-Chairman)	301-903-4312	6624	DP-16
Roger Dintaman (Co-Chairman)	301-903-3642	6628	DP-13
Matt Hutmaker	301-903-3921	3419	NE-40
Dennis Cabrilla	301-903-7468	1959	EM-4
Al Evans	301-903-4896	9513	ER-13
Ivon Fergus	301-903-6364	4672	EH-22
George Kachadorian	202-426-1320	1480	HR-21
Burton Rothleder	301-903-3726	1182	EH-31
Bob Walston (nonvoting)	505-845-5694	6431	DOE/AL

METHODOLOGY AND EXPERIMENTS SUBCOMMITTEE (FEDS AND CONTRACTORS)

	PHONE NO.	FAX NO.	ORGAN.
Ivon Fergus (Chairman)	301-903-6364	4672	EH-22
Dennis Cabrilla	301-903-7468	1959	EM-4
Dennis Galvin	301-903-2972	8754	DP-45
Burton Rothleder	301-903-3726	1182	EH-31
Rick Anderson	505-667-4839	5-3657	LANL
J. Blair Briggs	208-526-7628	0528	INEL
Ed Fujita	708-252-4866	4500	ANL
R. Michael Westfall	615-574-5267	3527	ORNL

TRAINING SUBCOMMITTEE (FEDS AND CONTRACTORS)

	PHONE NO.	FAX NO.	ORGAN.
George Kachadorian	202-426-1320	1480	HR-21
Nick Delaplane	202-586-9403	7734	EM-121
Dick Trevillian	301-903-3074	4672	EH-11
Henry Harper	208-533-7775	7623	ANL
Tom Mclaughlin	505-667-7628	5-4970	LANL

Attachment 2

DOE/LACEF PROGRAM REVIEW
MARCH 12-13, 1996
LOS ALAMOS NATIONAL LABORATORY
TA-18, BUILDING 30 CONFERENCE ROOM

MARCH 12, 1996

8:00	R. Anderson	Welcome, Introduction of Participants
8:10	R. Dintaman/P.Vogel	DOE/NCESC Overview
8:20	R. Walston	DOE/AL Overview
8:30	R. Anderson	NIS-6 Overview
8:40	R. Scarlett	NN-20 R&D Program
8:50	E.M. Hanson	NMSM Program Overview
9:00	D. Cobb	Non-Proliferation Program Overview
9:10	J. Pratt	NEST Program Overview
9:20	D. Rutherford	International/Domestic Safeguards Program
9:30	BREAK	
10:00	B. Partain	Facility Status, Compliance Efforts
10:30	R. Paternoster	LACEF Program Overview & Status
10:50	K. Butterfield	LACEF Support of NEST & TA-55
11:10	R. Sanchez/ P. Jaegers	Variable Spectrum Experiments for Untested Matrix Materials
11:40	C. Cappiello	APT and LWR Target Experiments
12:00	WORKING LUNCH	

DOE/LACEF PROGRAM REVIEW
MARCH 12-13, 1996
LOS ALAMOS NATIONAL LABORATORY
TA-18, BUILDING 30 CONFERENCE ROOM

12:20 W. Casson	Dosimetry Measurements
12:40 C. Cappiello	Status of Acquisition of New Materials
1:00 R. Kimpland	Excursion Kinetics in Solution and Metal Systems
1:20 W. Myers	Excursions in Underground Repositories
1:50 C. Goulding	Sub-Critical Measurements
2:10 BREAK	
2:30 R. Paternoster	Russian Critical Experiment Activities
2:50 K. Coop	Sub-critical Measurements for Waste Assay
3:10 D. Loaiza/ R. Sanchez	Delayed Neutron Parameters
3:30 D. Glenn	Molybdenum-99 Production Experiments
4:00 R. Sanchez	Actinide Critical Masses
4:10 R. Paternoster	New Initiatives
4:30 OPEN DISCUSSION	

MARCH 13, 1996

8:00 M. Westfall	Analytical Codes
8:30 C. Parks	Nuclear Data
9:00 B. Briggs	Benchmarking
9:30 N. Pruvost	Critical Experiments Archiving

DOE/LACEF PROGRAM REVIEW
MARCH 12-13, 1996
LOS ALAMOS NATIONAL LABORATORY
TA-18, BUILDING 30 CONFERENCE ROOM

9:40 S. Vessard	Criticality Safety Training
9:50 T. McLaughlin	Criticality Safety Classes
10:10 BREAK	
10:30 Budget Discussions	
11:50 WORKING LUNCH	
12:30 NCESC MEETING	
2:30 MES MEETING	

LA-UR-95-4336

Los Alamos Critical Experiments Facility Semi-Annual Progress Report

April 1, 1995 — September 30, 1995

Compiled by
R. Paternoster

With Contributions by:
R. Anderson, D. Barton, J. Bounds, G. Brunson, K. Butterfield, C. Cappiello, W. Casson, A. Criscuolo, R. Damjanovich, D. Glenn, C. Goulding, P. Jaegers, R. Kimpland, D. Loaiza, W. Myers, D. Rutherford, R. Sanchez, and W. Stratton

Photograph: by Chris J. Lindberg

LA-UR-95-4336

Los Alamos Critical Experiments Facility
Semi-Annual Progress Report

April 1, 1995 — September 30, 1995

Compiled by
R. Paternoster

With Contributions by:
R. Anderson, D. Barton, J. Bounds, G. Brunson, K. Butterfield,
C. Cappiello, W. Casson, A. Criscuolo, R. Damjanovich, D. Glenn,
C. Goulding, P. Jaegers, R. Kimpland, D. Loaiza, W. Myers, D. Rutherford,
R. Sanchez, and W. Stratton

TABLE OF CONTENTS

Tables

Figures

PREFACE

This Progress Report is a compilation of the unclassified research activities of the Los Alamos Critical Experiments Facility (LACEF), a part of the Los Alamos National Laboratory, from the period Apr. 1 through September 30, 1995. The previous progress report documenting research from Oct. 1 through Mar. 30, 1995 was LA-UR-95-2151. These reports are issued to document the results of critical experiments and nuclear criticality safety research at LACEF. They are issued as a timely compilation of research results, and not meant to be construed as a publication-ready manuscript.

1.0 PROGRAM HIGHLIGHTS

R. Paternoster and R. Anderson

The Los Alamos Critical Experiments Facility (LACEF) is the last of a number of US facilities once operated for benchmark critical experiments, research reactor development, and criticality safety-related experimentation. Recent studies by the USDOE and the DNFSB analyzing the changing DOE mission show the overwhelming need for a critical experiments facility. The mission of LACEF is evolving to support a broader class of experiments, while becoming increasingly focused to provide high-resolution benchmark data in a cost-effective manner. Other programs using the LACEF and LACEF personnel fulfilled national security needs involving Category 1 configurations of fissile materials. Currently no other U.S. national laboratory facility could complete this diverse set of programs with Category 1 nuclear materials.

Implementation of the Defense Nuclear Facilities Safety Board (DNFSB) Recommendation 93-2 (criticality experiment capability) includes expanding and updating the current nuclear criticality database. To that end, the Nuclear Criticality Experiments Steering Committee (NCESC) has compiled and prioritized a list of experiments [1,2] solicited from the criticality community. The current LACEF program emphasizes the high priority experiments from this list. (Table 1.1)

Table 1.1. Experiments from NCESC List with number and status.

	Experiment Focus	Experiment No. [1]	Status
1)	Low-power solution-fueled benchmark experiments based on the SHEBA assembly	206, 207	In Progress
2)	Development of sub-critical reactivity measurements	505	In Progress
3)	Array experiment incorporating intermediate energy configurations applicable to waste matrices	102, 502a	Planning
4)	Critical mass measurements for actinides	601	In Progress
5)	Applications of prompt-burst metal assemblies to dosimetry and accident analysis	503, 504	In Progress

SHEBA (Solution High-Energy Burst Assembly) is a solution fueled reactor which uses 5% enriched UO_2F_2 (uranyl fluoride) solution for fuel. The SHEBA machine is the only operating solution critical assembly in the U.S. An important effect in solution reactors is the formation and the reactivity effect of the voids caused by radiolytic gas production. During the second half of FY95 SHEBA completed research on solution excursions (Section 4). In addition, SHEBA performed static irradiations of uranyl nitrate solutions (U(93)NH) to examine the validity of production of the medical isotope Mo-99 in a solution fueled reactor. In FY96 the present SHEBA fuel will be replaced with a 20% enriched uranyl nitrate (U(20)NH) fuel in an effort to demonstrate high-efficiency, Mo-99 continuous production and extraction technology.

Precise replacement measurements to determine the critical mass of $^{237}Np_{93}$ were performed by replacing small samples of neptunium, uranium, or empty aluminum cans in the center of the FLATTOP assembly (Section 2). The neptunium sample is clad with nickel. The FLATTOP critical assembly is operated above delayed-critical by inserting the control rods all the way in. The worth of each sample is then estimated through the measured asymptotic reactor period and the Inhour

equation. These measurements were repeated tens of times to obtain better statistics and reduce the error of the measurements. Once the cross section data for $^{237}Np_{93}$ was benchmarked, we were able to use TWODANT to estimate the critical mass for a bare neptunium sphere. The calculation yielded a mass of 56 ± 2 kg at a density of 20.45 g/cc. Knowing precisely the critical mass of these elements not only will validate storage mass limits reported in the standard ANSI/ANS-8.15-1981, "Nuclear Criticality Control of Special Actinide Elements," but will optimize the geometry needed for safe disposition of these materials.

Among the experiments planned are measurements of the critical masses of Np-237, Am-241, and other actinide isotopes which now exist in the DOE complex, but have no direct measurements of critical mass. Some of these isotopes, Np-237 for instance, are threshold fissioners. If a fast critical experiment is constructed from a threshold fissioner, the "dollar" value of delayed neutrons may be very small or zero, due to the threshold character of the fission cross section and the soft spectrum of delayed neutrons. LACEF in conjunction with a University of New Mexico graduate student are measuring the delayed neutron fraction on Np-237.

LACEF is designing two critical experiment to incorporate elements of several high-priority NCESC experiments [1,2]. Specifically, elements of the following are being designed into the assembly.

1. Experiment 102 - Large Array of Small Units,
2. Experiment 501 - Assessment Program for Materials Used to Transport and Store Discrete Items and Weapons Components,
3. Experiment 502a - Absorption Properties of Waste Matrices, and
4. Experiment 609 - Validation of Calculational Methodology in the Intermediate Energy Range

The specifications and intial design concepts are presented.

Understanding the dynamic behavior of metal and solution assemblies is a central theme of LACEF research. Recent unpublished studies at Los Alamos have suggested the possivility of autocatalytic excursions in geologic storage arrays containing vitrified plutonium. Two studies have been completed at LACEF to examine such possibilities. The first examines criticality in Pu/SiO_2 and $Pu/SiO_2/H_2O$ mixtures. A copy of this paper is included in Appendix 1 of this progress report. The second paper examines the dynamic behavior of these systems (Section 4.0).

Acceptance testing of the new Godiva transport system and automated vault door was completed on March 30, 1995 and Godiva-IV nuclear operations resumed in early April. Godiva IV and SHEBA were used for irradiations to simulate metal and solution accidents in the 23rd Nuclear Accident Dosimetry (NAD) intercomparison workshop held from June 12-16, 1995. This first NAD workshop to be held since 1987 was sponsored by the DOE Office of Worker Safety and Hazards Management. Prior to the workshop a characterization of the Godiva IV in the free-field configuration and with the HPRR shields (Concrete, Steel, and Lucite) was completed.

Safety training activities (Section 7) were completed during the second half of FY95. The NCSC classes include three "hands-on" lab exercises involving construction of multiplying assemblies and operation of a critical assembly. Five Nuclear Criticality Safety Classes were completed during the second half of FY95 and a total of nine classes in FY95.

Documentation, compliance, and personnel training activities continued during this period. In accordance with DOE Order 5480.22, the new TSRs (Technical Safety Requirements) were revised, reviewed, approved within the Laboratory, and submitted for approval to the DOE on September 24 (Section 10).

References

1. D. Rutherford, "Forecast of Criticality Experiments and Experimental Programs Needed to Support Nuclear Operations in the United States of America: 1994-199," Los Alamos National Laboratory Report LA-12683, July 1994.

2. US Department of Energy Annual Report for the Defense Nuclear Facilities Safety Board Recommendation 93-2. Submitted to the DNFSB July 26, 1994.

2.0 CRITICAL EXPERIMENTS CORE CAPABILITY

2.1. Critical Mass of $^{237}Np_{93}$

R. Sanchez, J. Bounds, P. Jaegers

Neptunium-237 is produced primarily by successive neutron capture events in U-235 or through the (n,2n) reaction in U-238. These nuclear reactions (see Eq. 1) lead to the production of U-237, which decays by beta emission into Np-237.

$$U_{92}^{235}(n, \gamma)U_{92}^{236};\ U_{92}^{236}(n, \gamma)U_{92}^{237} \rightarrow \beta \rightarrow Np_{93}^{237} \quad (1)$$

$$U_{92}^{238}(n, 2n)U_{92}^{237} \rightarrow \beta \rightarrow Np_{93}^{237} \quad (1)$$

It is estimated that a typical 1000 MW (electric) light water reactor (LWR) operating at a load factor of 80% produces on the order of 13 kg of Np-237 per year [1]. Some of this neptunium has been separated from irradiated fuel elements and at the present is being stored in a liquid form. This is adequate from the point of view of criticality safety because the fission cross section for Np-237 at thermal energies is quite low and any moderation of the neutron population would tend to increase its critical mass to infinity. However, for long-term storage, the neptunium liquid solutions would be converted into oxide and metal forms because these forms are less movable and less likely to leak out of containers. At the present, there is a great uncertainty about the critical mass of Np-237 in oxide and metal forms as seen in the standard ANSI/ANS-8.15-1981 "Nuclear Criticality Control of Special Actinide Elements" [2]. Knowing precisely the critical mass of this element not only will validate the storage mass limits reported in the standard but will also optimize the geometry needed for safe disposition of these materials.

The criticality of Np-237 is governed by several factors. For instance, it is well known that nuclides with an even number of neutrons, such as Np-237, exhibit a sharp threshold in their fission cross section. For Np-237, the threshold occurs at approximately 500 keV. Above this neutron energy, the fission cross section is comparable to that of U-235. On the other hand, below this threshold, the fission cross section is quite low. Thus, Np-237 can only become critical in a fast neutron spectrum. Another factor that affects the critical mass of this element is the inelastic scattering cross section of Np-237. A low inelastic scattering cross section in a fast spectrum will enhance criticality because fewer neutrons will scatter below the fission threshold where they will be unable to cause fissions.

2.1.1 Experiment

The experiment consists of replacing small samples of neptunium, 93.2% U-235 (Oy), or empty aluminum cans in the center of a fast critical reflected assembly, known as Flattop. This critical assembly is operated above delayed-critical by inserting the three control rods to their full-in position. The worth of each sample is estimated through the measured asymptotic reactor period and the Inhour equation. These measurements are repeated tens of times to obtain better statistics and reduce the error of the measurements.

Table 2.1 shows the dimensions, weights, and isotopic composition of the samples used for these experiments. Note that the neptunium sample is clad with nickel, but the uranium sample is bare.

Table 2.1. Properties of the replacement samples

	Uranium Sample	Np-237 sample	Empty Al can
Weight of metal	29.909 g	28.393 g	——
Weight of can	——	0.773 g	0.476 g
Dimensions			
Length (in.)	0.5015	0.4890	0.4975
Outside Diameter (in)	0.4990	0.4865	0.4865
Thickness		Nickel clad	Al wall thickness
Ends (in.)	——	0.0035	0.010
Sides (in.)	——	0.0057	0.010
Isotopic composition, wt%			
Uranium		**Neptunium**	
U-234	1.1	Np-237	99.87
U-235	93.2	Other elements	0.13
U-236	0.2		
U-238	5.5		

Figure 2.1 shows the Flattop critical assembly used for this experiment. This machine consists of a driver core of fissile material that sits in the center of a natural uranium reflector 48 cm (19 in.) in diameter .

Two driver cores are available for the Flattop assembly. The Oy core has a mass of approximately 16.22 kg and has a 1.27-cm (0.5-in.)diameter glory hole where mass adjustment buttons and the Np-237, Oy, or the empty aluminum can samples can be placed. For this core, the maximum excess reactivity available when the Oy sample is in the center of the glory hole is approximately 49 ¢ above delayed-critical.

The other available core is made of delta-phase plutonium (95% Pu-239, 5% Pu-240) and has a mass of approximately 5.9 kg. It also has a 1.27-cm (0.5 in) diameter where mass adjustment buttons and the various samples can be placed. The maximum excess reactivity when the Oy sample is loaded in the center of the glory hole is approximately 44 ¢ above delayed-critical.

The natural uranium reflector consists of two movable quarter spheres mounted on keyed tracks and the stationary hemisphere which contains the control rod voids. Three natural uranium control rods are inserted from the bottom into the stationary natural uranium hemisphere. Two of them are approximately 17.8 cm (7 in) long and 1.27 cm (0.5 in.) in diameter and worth 26 ¢ when the Oy is present and 40 ¢ when the plutonium core is in the Flattop assembly. The third control rod is 10.2 cm (4 in.) long and 2.54 cm (1 in.) in diameter. It is worth $1.10 when the Oy core is present and $1.60 when the plutonium core is in the Flattop assembly. For more details about the description of Flattop, see reference [3].

2.1.2 Computer Models

Two computer models were developed with the help of TWODANT [4] and MCNP [5] to simulate the Flattop assembly and the samples that were placed in the center of this assembly. Figure 2.1 shows these models.

The TWODANT code used the sixteen group Hansen-Roach neutron cross section library [6] and the thirty group MENDF5 library. For the MCNP model, the MCNP code was operated in the *k*-code (eigenvalue) mode using continuous-energy cross sections based on the Evaluated Nuclear Data File, ENDF/B-V and ENDF/B-VI, and on evaluations from the Nuclear Theory and Applications group at Los Alamos [5].

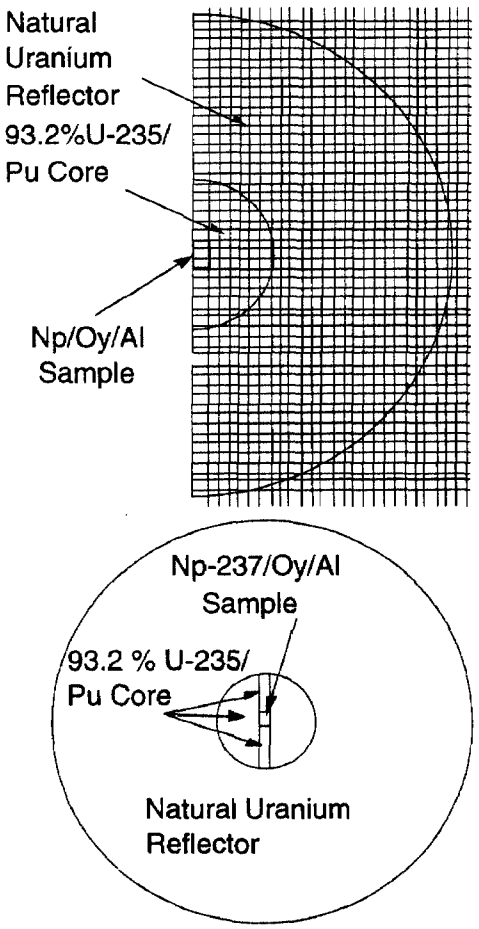

Figure 2 1. TWODANT and MCNP computer models.

Both codes calculate the multiplication factor, k_{eff}, of the system when the different samples are placed in the center of the assembly. These results will be compared with those obtained in the experiments.

2.1.3 Results

Table 2.2 lists the experimental and computational results. As seen in this table, the experiments show that when the 93.2% U-235 (Oy) is present, the Oy sample is worth 3.41 ± 0.4 ¢ more than the neptunium sample. The TWODANT calculation shows that the Oy sample is worth 2.16 ¢ more than the neptunium sample when Hansen-Roach cross sections are used and 2.19 ¢ more when the MENDF5 cross section library is used.

Table 2.2. Experimental and computational results.

Experimental Results

Oy Core	**Pu Core**
$\Delta\rho$ (Oy-Np) = 3.41 $\pm$ 0.39 ¢	
$\Delta\rho$ (Oy-Al) = 22.44 $\pm$ 0.22 ¢	$\Delta\rho$ (Oy-Np) = 6.41 $\pm$ 0.40 ¢
$\Delta\rho$ (Np-Al) = 18.95 $\pm$ 0.32 ¢	

Computational Results

TWODANT (Oy Core)	**TWODANT (Pu Core)**
Hansen-Roach Cross Sections	**Hansen-Roach Cross Sections**
$\Delta\rho$ (Oy-Np) = 2.16 ¢	
$\Delta\rho$ (Oy-Al) = 23.95 ¢	$\Delta\rho$ (Oy-Np) = 5.31 ¢
$\Delta\rho$ (Np-Al) = 21.78 ¢	
MENDF5	**MENDF5**
$\Delta\rho$ (Oy-Np) = 2.19 ¢	
$\Delta\rho$ (Oy-Al) = 22.66 ¢	$\Delta\rho$ (Oy-Np) = 7.85 ¢
$\Delta\rho$ (Np-Al) = 20.48 ¢	
MCNP (Oy Core)	**MCNP (Pu Core)**
ENDF/B-V	**ENDF/B-V**
k_{eff}(Np) = 1.00081 $\pm$ 0.0004	k_{eff}(Np) = 1.0115 $\pm$ 0.0004
k_{eff}(Oy) = 1.00035 $\pm$ 0.0004	k_{eff}(Oy) = 1.0133 $\pm$ 0.0004
k_{eff}(Al) = 1.00029 $\pm$ 0.0004	
ENDF/B-VI	**ENDF/B-VI**
k_{eff}(Np) = 0.9991 $\pm$ 0.0004	k_{eff}(Np) = 1.0128 $\pm$ 0.0004
k_{eff}(Oy) = 0.99898 $\pm$ 0.0004	k_{eff}(Oy) = 1.0136 $\pm$ 0.0004
k_{eff}(Al) = 0.99771 $\pm$ 0.0004	

When the plutonium core is present, the experiment shows that the Oy sample is worth 6.41 $\pm$ 0.4 ¢ more than the neptunium sample. The results obtained from TWODANT are 5.31 ¢ when using Hansen-Roach and 7.85 ¢ when using MENDF5 cross section libraries.

These comparisons agree well considering that in the TWODANT model, the driver fissile material core and the natural uranium reflector were approximated with a step function and are not perfect spheres. Other measurements included the worth of the Oy and neptunium samples with respect to a void, which was represented by an empty aluminum can. These experimental results also agree well with the results obtained from TWODANT.

Finally, the MCNP code was used to calculate the k_{eff} for the different configurations. After one-thousand cycles, the central reactivity contributions from the three different samples in the Oy core showed no difference (the k_{eff} values were within one standard deviation of each other) when using ENDF/B-V. On the other hand, when using ENDF/B-VI, the MCNP calculations showed that the Oy and neptunium samples were more reactive than the aluminum empty can, but there was no

difference between the Oy and neptunium samples. Similar MCNP kcode calculations were performed, this time assuming a plutonium core. The MCNP computational results showed that the neptunium sample was worth less than the Oy sample when using the ENDF/B-V cross section library, which agrees with the experiment. However, when we used the ENDF/B-VI cross section library, the central reactivity contributions from the neptunium and Oy samples showed no difference after 1000 cycles. As expected, the MCNP results, for the most part, were not able to account for the small reactivity contributions of the different samples.

The uncertainty in the critical mass of Np-237 depends on the mass of the sample used for the experiment. It is obvious that the larger the neptunium mass used, the greater the reduction in the uncertainty of the critical mass. The variance as a function of the mass availability of Np-237 has been calculated by Hansen [7]. According to this reference, when using a 30-g sample, the uncertainty is between 18 and 20% of the estimated Np-237 critical mass.

Because the experimental and TWODANT results were in good agreement, a simpler version of the TWODANT code was used to estimate the critical mass of Np-237. The ONEDANT [8] code yielded a critical mass of 56 kg. The uncertainty of this measurement, based on a 30-g sample, was ± 10 kg.

References

1. Seifritz, W. and Wydler, P., "Criticality of Neptunium-237 and Its Possible Utilization in Nuclear Reactors," *Nuclear Science and Engineering* **72**, 273 (1979).
2. Nuclear Criticality Control of Special Actinide Elements, ANSI/ANS-8.15-1981.
3. Paternoster, R., et al., Safety Analysis Report for the Los Alamos Critical Experiments Facility (LACEF) and the Hillside Vault (PL-26), Los Alamos National Laboratory Controlled Publication LA-CP-92-235 (1994).
4. Alcouffe, R., et al., "User's Guide for TWODANT: A Code Package for Two-Dimensional, Diffusion-Accelerated, Neutral-Particle Transport," LA-10049-M (1992).
5. Briesmeister, J., "MCNP-A General Monte Carlo N-Particle Transport Code," Los Alamos National Laboratory report LA-12625 (1993).
6. Hansen, G. and Roach, W., "Six and Sixteen Group Cross Sections for Fast and Intermediate Critical Assemblies," Los Alamos Scientific Laboratory report LA-2543-MS (1961).
7. Hansen, G., et al., "Uncertainty in the Np-237 Critical Mass," Memorandum T-2-M-1388, May 27, 1983.
8. O'Dell R., et al., "User's Manual for ONEDANT: A Code Package for One-Dimensional, Diffusion-Accelerated, Neutral-Particle Transport," Los Alamos National Laboratory report LA-9184-M (1982).

2.2. Specifications for New Experiments

R. Anderson and R. Paternoster

The following two sections contain more detailed specifications for two benchmark critical experiments. These experiments were originally included in the NCESC (Nuclear Criticality Experiments Steering Committee) list of prioritized list of experiments. These improved

specifications are being used to design the experiments. The preliminary concepts represent the current state of design.

Experiment Program 609: Validation of Calculational Methodology in the Intermediate Energy Range

DOE Contractor Who Needs Experimental Data
All DOE Reactor and Non-Reactor Nuclear Facilities

Experimental Category
Highly Enriched Uranium, Low-Enriched Uranium, Plutonium

Application
Process Operations and Materials Disposition
Waste Handling and Storage
Transportation
Ill-Defined Safety Margin
Enhancement of Criticality Safety Knowledge Base

Status
Planning Stage

Priority
MES-High

Description of Operation and Experimental Data Needed

Department of Energy fissile materials handling operations in the past have emphasized metal and metal-compound systems and solutions systems. Thus, critical experiments activities have concentrated in making measurements appropriate to these interests. These critical experiments resulted in systems in which the fissions took place primarily at high energies (above neutron energies of about 100 keV) or at near thermal energies (below neutron energies of about 1 eV). Little or no information is available for systems in which the fissions take place primarily between neutron energies of 1 eV and 100 keV. Most importantly, the fission cross sections for 239-Pu and 235-U, the fissile materials of most interest to the DOE complex, are not validated by critical experiment.

Today, and in the future, the DOE is undertaking new types of operations, including decontamination and decommissioning and materials disposition. In D&D operations and materials disposition operations systems are expected in which the fissions take place primarily in the range between 1 eV and 100 keV. These types of systems are produced when the fissile material is contained in a matrix of heavy material, such as SiO_2, aluminum, steel, etc. For example, these situations are expected when in the various fissile materials vitrification schemes, and in the disposal of contaminated building debris.

When the heavy non-fissile materials are present in large amounts, that is, when the non-fissile/fissile ratio is high, the fission causing spectra are intermediate in character. While the cross sections for the heavy non-fissile materials may need to be tested in their own rights (see Experiment Programs 102 and 502, for example), the lack of testing for the fissile materials fission cross sections in the intermediate energy range also requires experimental testing. This experiment also has the interesting possibility that the experiment could demonstrate configurations in which the uranium critical mass is actually less than the corresponding plutonium critical mass.

Experiments which produce the tests for intermediate range fission cross sections may be constructed by interleaving thin (up to several millimeters thick) fuel plates or rods with comparable and slightly thicker plates or rods of the non-fissile materials. This experiment is done most easily using plates which are divided into two sections and assembled using a horizontal or vertical assembly device (see Fig. 2.2). The thickness of the plates of non-fissile materials in this array-type experiment are adjusted to moderate the neutron spectrum to the desired energy range. Sensitive adjustments in this experiment are possible because the absorption and moderation produced per interaction by the heavy non-fissile materials is typically small compared to hydrogen.

The experiment priorities remain to be set. However, we expect to begin experiments with the following fissile materials: high-enriched uranium, plutonium, and low-enriched uranium.

This experiment plan also encompasses the objectives of Experiment 502i.

These experiments further two objectives set forth in DNFSB Recommendation 93-2:

The prediction of the critical state of a system by methods that use theory must be benchmarked against good and well characterized critical experiments, and

Experiments should be targeted at the major sources of discrepancy between theory and experiments

Matrix Intermediate-energy X-section Experiment
(NCESC Expt. 609, 502i)
Preliminary Concept

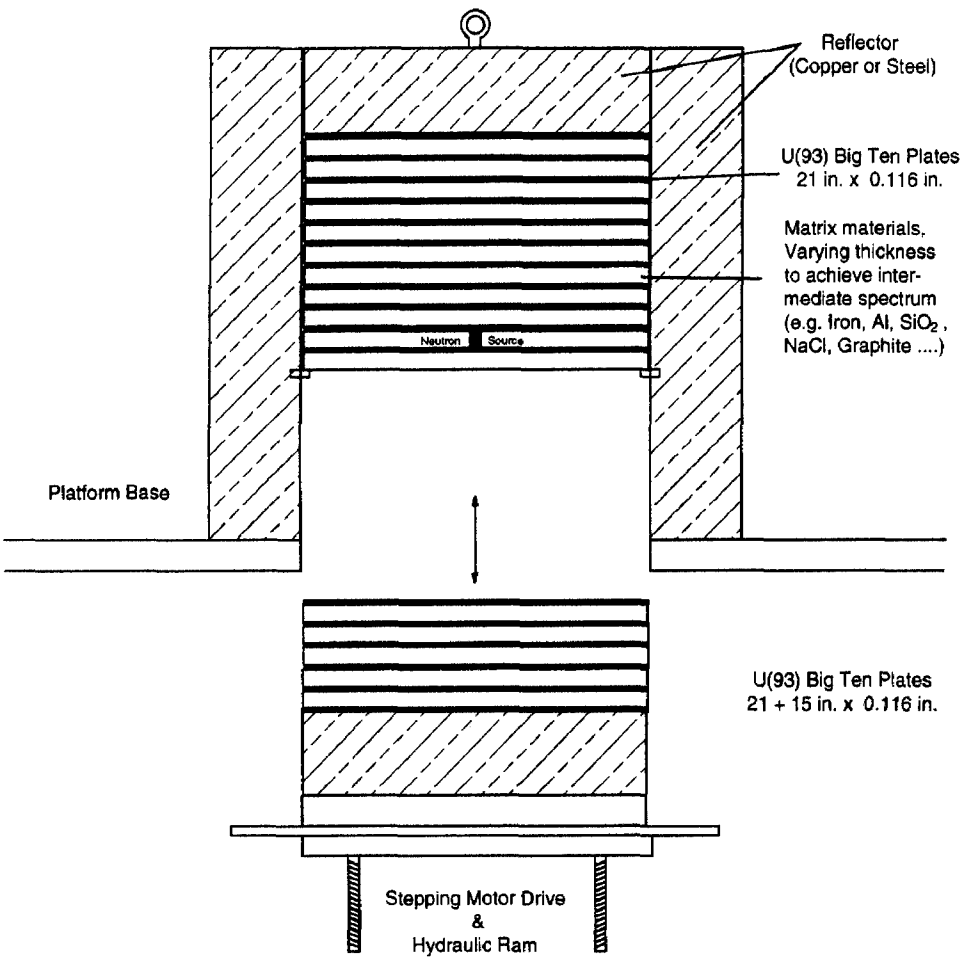

Figure 2.2. Preliminary design concept of intermediate energy spectrum experiment.

Experiment Program 102: Large Array of Small Units

DOE Contractor Who Needs Experimental Data
All DOE Non-Reactor Nuclear Facilities

Experimental Category
Highly Enriched Uranium, Low-Enriched Uranium, Plutonium

Application
Process and Storage Operations
Waste Handling and Storage
Transportation

Ill-Defined Safety Margin
Enhancement of Criticality Safety Knowledge Base

Status
Planning Stage

Priority
MES-High

Description of Operation and Experimental Data Needed

Available experimental data for highly enriched uranium (and plutonium) have properties which differ from those encountered in actual storage arrays because of differences in the couplings which exist between the various fissile units in the array. This is of importance because the experimental data, which is used to test the calculational methodology (principally the Monte Carlo codes), represents an incomplete test of the cross section features which are present in actual storage and process situations. This concern applies to both uranium and plutonium, both of which, in the future, will likely require storage and process operations which are of a different character than the storage and process conditions encountered thus far in the DOE complex.

As a result, an experiment should be performed which addresses issues related to calculations of the type described above. The principal goals of this experiment are to show that the calculational methodologies treat correctly the neutron coupling between units and the impacts of important nonfissile materials.

This is best done by measuring critical configurations under conditions where the neutron coupling between fissile units is varied to the maximum extent possible and where the impacts of the nonfissile materials are maximized, while at the same time the experimental uncertainties due to other features of the experiment are minimized. This will be accomplished by:

(1) varying the size, shape, number, position, and composition of the fissile units. Initial experiments will concentrate on fissile units which are sealed containers of highly enriched or low-enriched uranium solution. The composition of the fissile units may be varied by using highly enriched uranium or plutonium metal. Other fuel compositions, such as sealed containers of plutonium solution or low-enriched uranium solution, may also be added.

(2) varying the inter-unit coupling by performing both bare and reflected experiments which utilize various interstitial absorber/moderator and reflector materials. The interstitial absorber/moderator and reflector materials will be selected on the basis of the need for experimental tests of the cross sections for these material types and on the potential for these materials to modify the inter-unit coupling to the maximum extent possible. Essentially, this means changing the inter-unit neutron spectrum. Some materials whose properties will be evaluated are SiO_2, PVC and fluorinated PVC, materials loaded with strong absorbers such as gadolinium or boron, Al_2O_3, CaCl, cellulose, celotex, concrete, depleted uranium, expanded borated polyfoam, Fe_2O_3, firedike, foamglas, kerosene, lead, plexiglass, polyethylene, TBP, etc.

Experiments are expected to utilize a horizontal split table as a platform for the assembly (see Fig. 2.3). Some fissile units and associated interstitial moderator/absorber or reflector material would be placed on each side of the horizontal split table. The experiment would be performed by closing the table and determining the critical separation for the table components. Accompanying

calculations will demonstrate the abilities of the various calculational methodologies to properly describe actual situations. In addition, this experiment is expected to address questions concerning one of the outstanding critical experiment anomalies, a series of critical measurements using collections of slabs and cylindrical containers of high-enriched uranyl nitrate solution. The results of these measurements have consistently disagreed non-conservatively with the results of calculations.

These experiments further two objectives set forth in DNFSB Recommendation 93-2:

The prediction of the critical state of a system by methods that use theory must be benchmarked against good and well characterized critical experiments, and

Experiments should be targeted at the major sources of discrepancy between theory and experiments

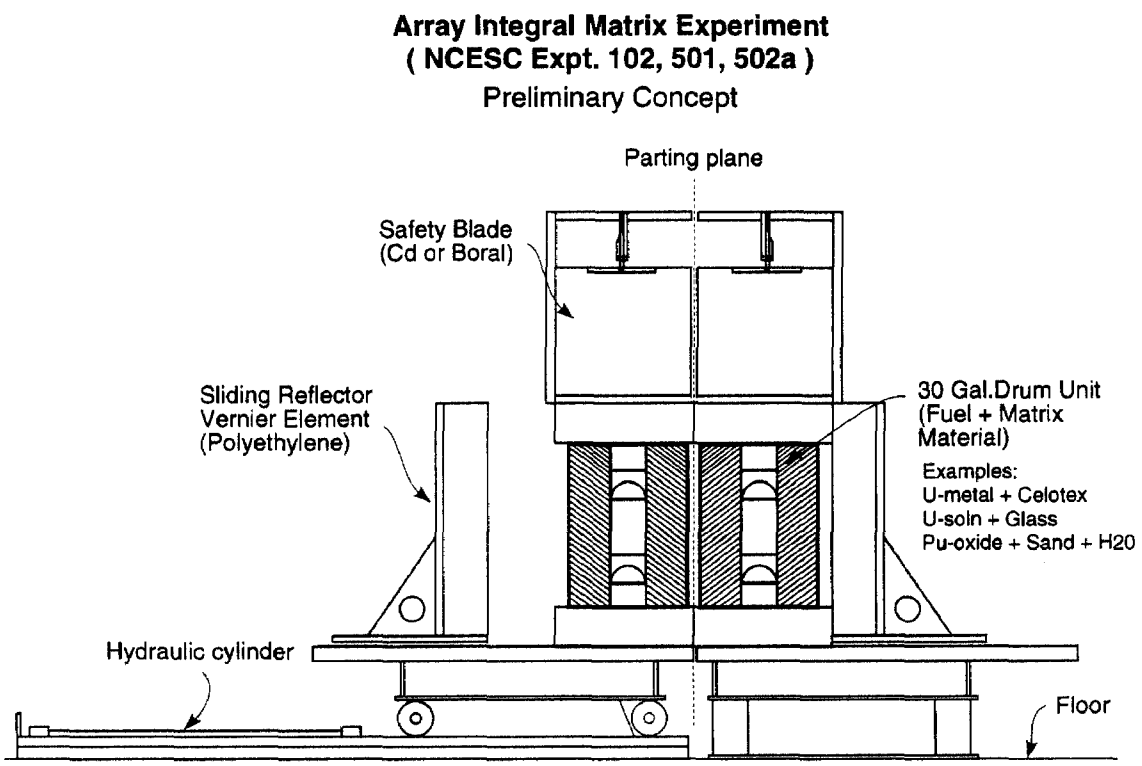

Figure 2.3. Preliminary design concept for Array Integral Matrix Experiment.

2.3. Compilation of Recent Big Ten Measurements.

J. Bounds, P. Jaegers, D. Barton, and D. Rutherford

Big Ten is one of the benchmark critical assemblies at LACEF. It is a right circular cylinder 33 in. in diameter and 38 in. in length, composed of 10 metric tons of uranium with an average core enrichment of 10%. Big Ten has been the focus of a recent detailed model calculation. To support the model, the experimental values of total excess reactivity and delayed-critical control rod positions have been compiled for the present configuration and are presented below.

Figure 2.4 shows the distribution of measurements of total excess reactivity in Big Ten over the last 3 1/2 years. These measurements were made under normal operating conditions and typically at the beginning of an operation to verify that the assembly was behaving normally. The measurements were performed by a variety of operators. The resulting distribution of measurements is nearly a normal bell shape. However, examination of the time evolution of the reactivity, Fig. 2.5, shows a distinct annual dip in total excess reactivity in June. June is the month in which the kiva receives the most direct sunlight and so is the warmest of the year. Only a few of these measurements also recorded the temperature, as it is required only for high-power operations, but a thermocouple has since been installed to gather data from normal operations.

Effects of temperature are also evident in the control rod positions required for steady-state operation (see Fig. 2.6). As with the reactivity measurements, the data spans 3 1/2 years and was obtained by several operators. Most are routine determinations of critical position when starting up for the day and lack the precision possible with the assembly. Note that except for two sets of data, the operators clearly tend to favor either one rod out or both rods at nearly the same position when making this measurement. The two series of measurements, at 19°C and 24°C, were made after this data was first compiled in April, as an intentional effort to map out the DC curve of control rod positions at different temperatures.

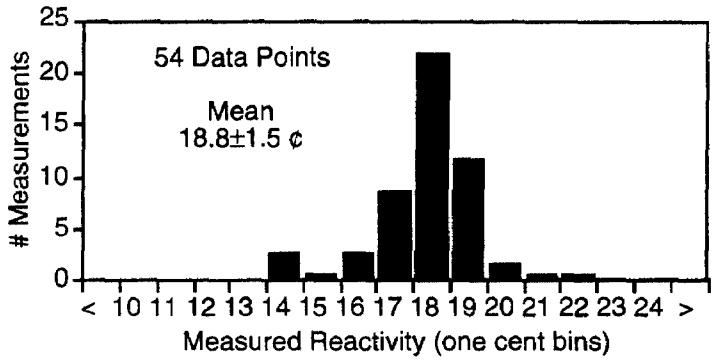

Figure 2.4. Distribution of measured excess reactivity for Big Ten with all rods in.

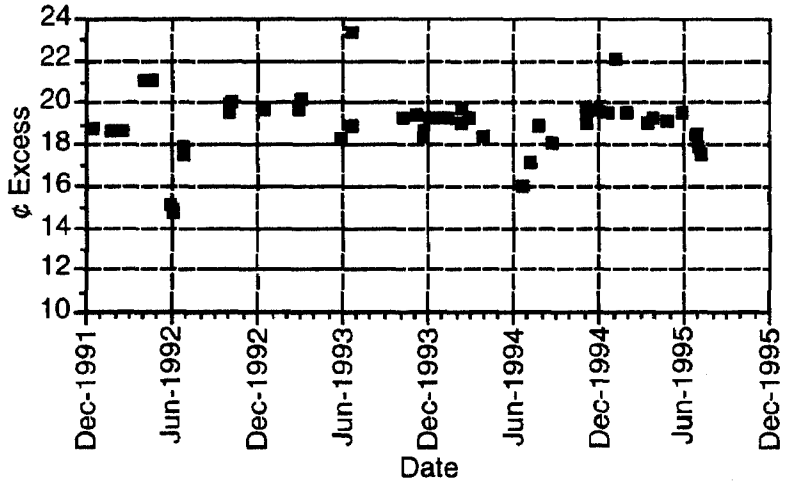

Figure 2.5. Measurements of total excess reactivity in Big Ten. Note annual dips in June.

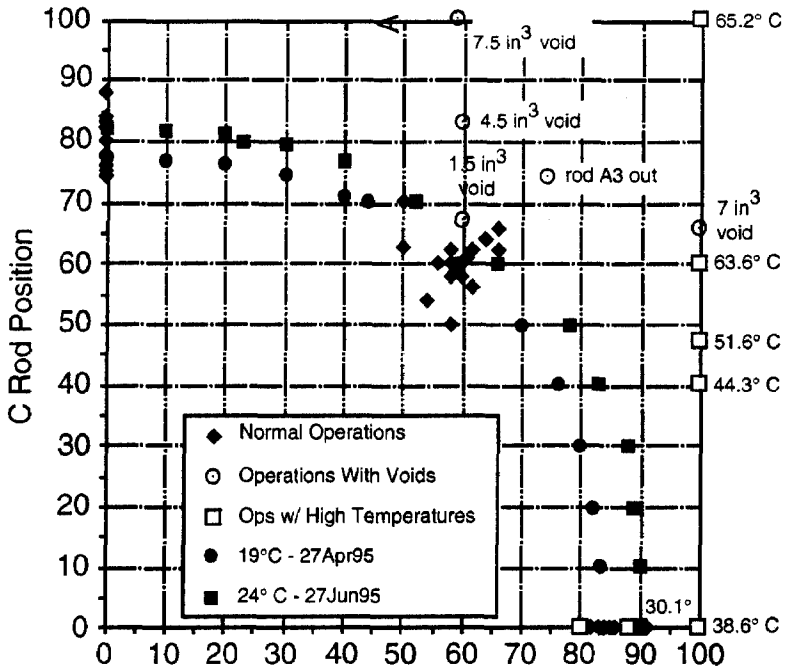

Figure 2.6. Control rod positions for DC operation of Big Ten.

Of the control rod measurements, 83 were in normal operations in Big Ten's present configuration, five were from operations with voids, and eight were from operations at higher than normal temperatures. The variations of control rod positions under normal conditions appear to be ±5% for either rod.

2.4. Fission Chamber Progress.
J. Bounds, P. Jaegers, D. Barton, and D. Rutherford

The collection of fission chamber data on Big Ten and Flattop was completed in this period, but the data has not been fully analyzed. The fission chambers are small proportional counters, which have microgram quantities of fissionable material on the inner walls of their tubes. With three or four isotope tubes in a single detector, the neutron flux of a given critical assembly can be measured simultaneously. An assembly with a relatively faster neutron spectrum will fission relatively more U-238, for example.

Figure 2.7 shows the data from Flattop, Big Ten, and a short data set from room-return neutrons as the detector sat outside of Big Ten. The two assembly data sets have very nearly the same number of counts in U-235 but differ in the other isotopes, because Flattop is a faster-spectrum machine than Big Ten. The room return clearly favors the thermal fissioning isotopes U-235 and Pu-239.

Interest has been expressed for using the fission chambers in SHEBA and Skua, as well as making new fission chambers for other experiments.

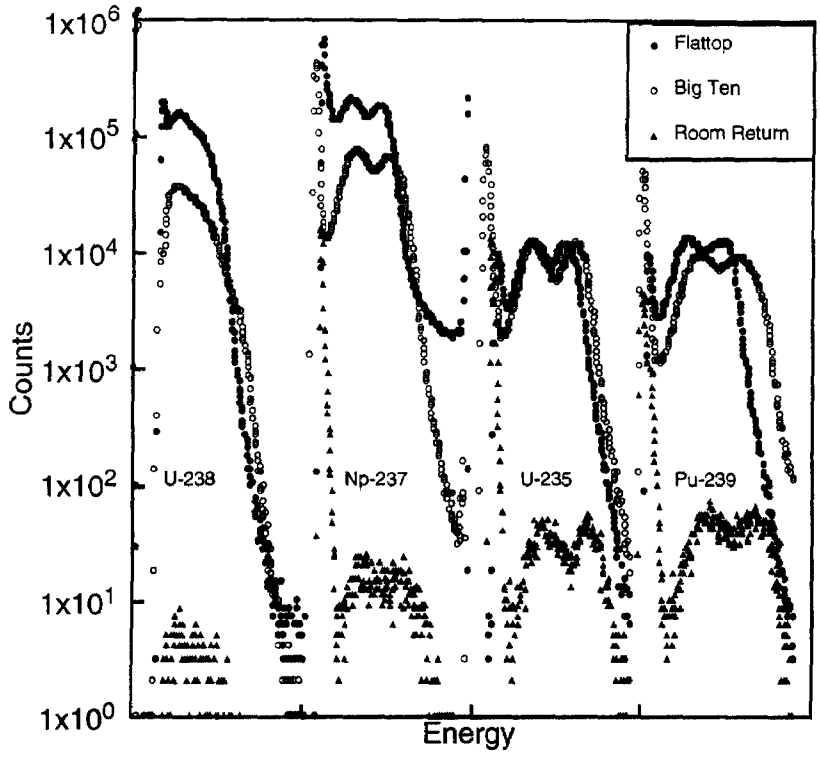

Figure 2.7. Fission chamber data. The four chambers are multiplexed into one spectrum for each machine.

2.5. Measurements of Delayed Neutron Parameters for ^{235}U and ^{237}Np

D. Loaiza, R. Sanchez, and G. Brunson

2.5.1. Introduction

The purpose of this experiment is to measure the delayed neutron period, yield, and the delayed neutron fraction for the six groups of delayed neutrons from ^{235}U and ^{237}Np. In addition, this experiment will support the objectives set forth by Defense Nuclear Facility Safety Board (DNFSB) Recommendation 93-2.

There is still a great interest in detailed delayed neutron phenomena to help understand the role of delayed neutrons in the fission process, especially for actinides. To study the delayed neutron phenomena, a well-suited source is required; the bare ^{235}U metal assembly "Godiva IV" at LACEF provides the source of neutrons. Godiva IV will provide shots of about 10^{16} total fissions for the "infinite" and "instantaneous" irradiation needed to accentuate the shorter and longer periods of delayed neutrons.

2.5.2. Experimental Set Up

A preliminary sketch for the general experiment is shown in Fig. 2.8. The Godiva IV assembly, the sample transfer system, and the detection system will be located in Kiva 3. The transfer system is being built by the design team. The transfer system needs to transport a small sample of ^{235}U and ^{237}Np from the point of irradiation to the counting room in less than 200 ms, and stop at the same position after each shot. The detection system used for the experiment will be a well counter.

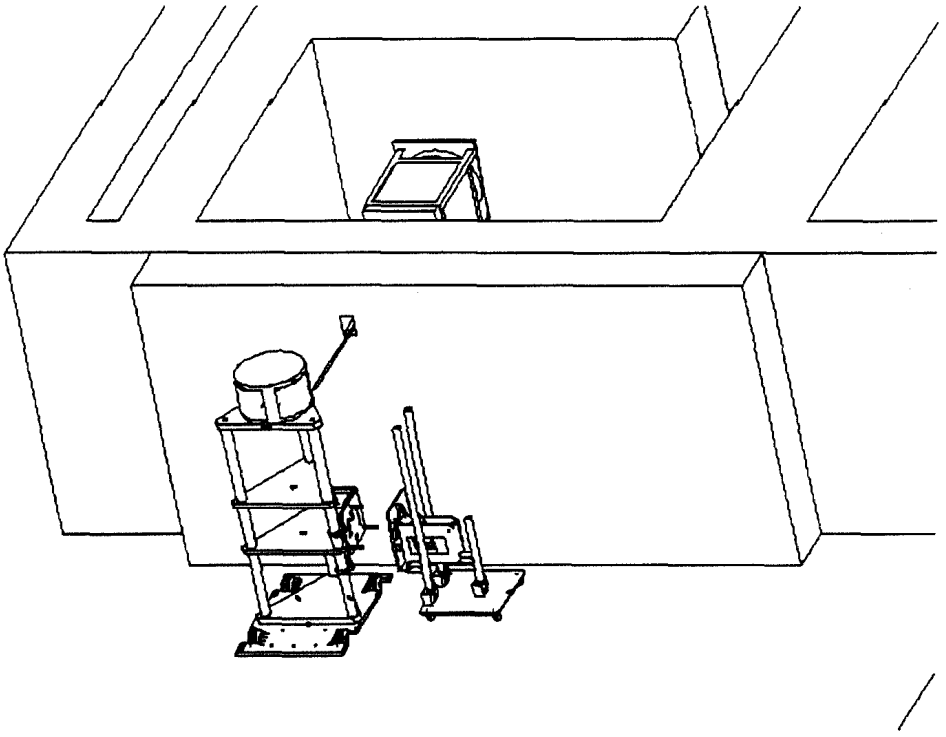

Figure 2.8. Schematic view of the ^{237}Np delayed neutron experimental set up.

2.5.3. Neutron Detection System

The neutron detection system consists of 20 He-3 tubes embedded in a cylindrical configuration inside the polyethylene. The entire arrangement of the well counter is shown in Fig. 2.9. This device is 58 cm by 59 cm by 72 cm high. The counter has a central cavity 17.78 cm in diameter and has an active depth of 40 cm. The counter is surrounded by 10 cm of polyethylene lined with a 1.5-mm-thick sheet of cadmium. The layer of cadmium is intended to absorb background thermal neutrons that are created outside the cavity.

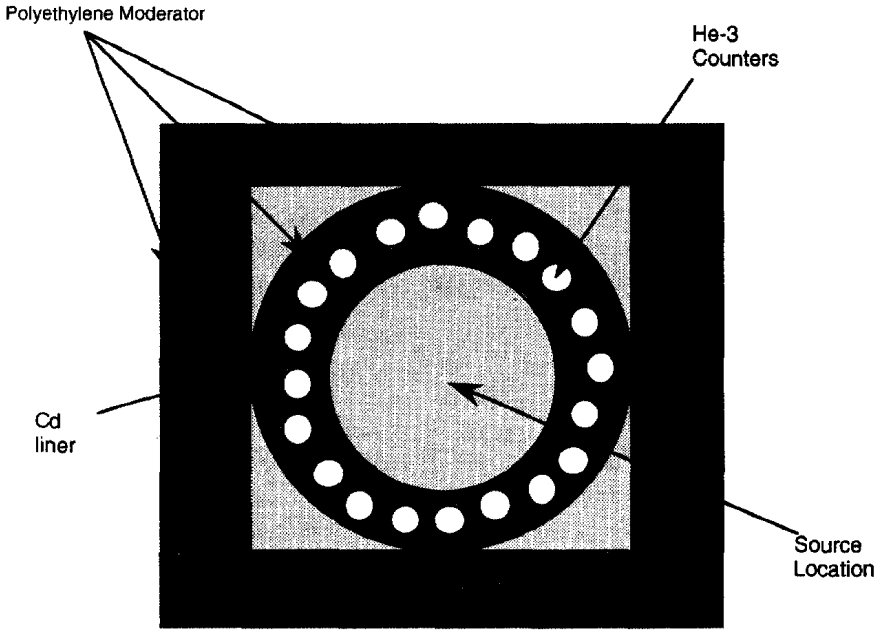

Figure 2.9. Cross sectional view of the well counter.

2.5.4. Calibration of the Well Counter

An Am/Li calibrated neutron source was used to determine the detector efficiency. The absolute neutron emission rate of this source was determined relative to a standard source in a graphite pile to an accuracy of 3 to 6%; the relative emission rate of the source was known to an accuracy of approximately 4%. The reported source strength was 1.75×10^3 neutrons per second. This Am/Li source was selected because its neutron energy spectrum is very similar to that of delayed neutrons. The absolute efficiency calculated for the well counter was 29.04% ± 0.062.

2.5.5. The High-Voltage Plateau

The well counter is used to study the phenomena of counting neutrons. Changes in the counting rate should be caused by changes in the neutron population and not by changes in the environment such as atmospheric pressure, temperature, humidity, or voltage. For the experiment at hand, all these factors can be neglected except voltage changes. It is highly desirable to have a detection system for which a change in the counting rate is negligible, when the HV changes for a reason beyond our control. Figure 2.10 shows the HV plateau curve obtained while varying the HV from 1100 V to 1600 V. From this figure, the high operating voltage for the well counter was determined to be 1350 V.

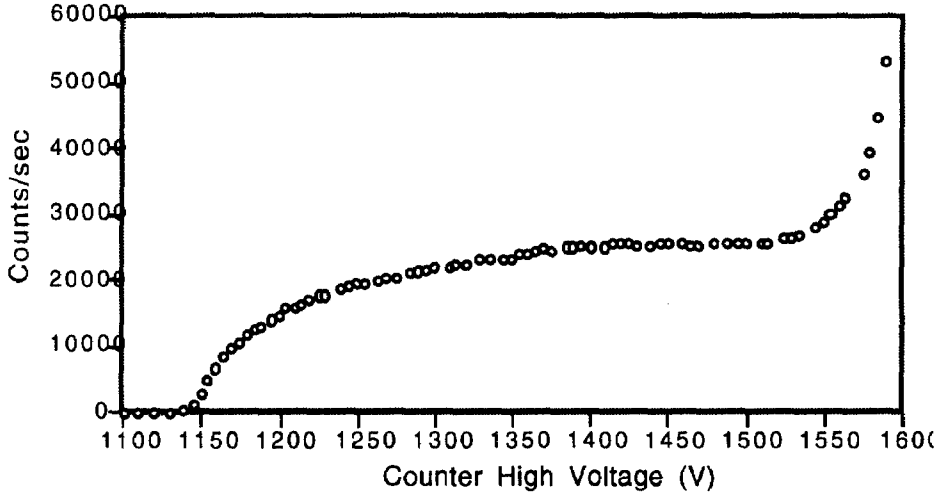

Figure 2.10. Plateau curve for ^{3}He well counter.

2.5.6 Pulse-height Spectrum

When operating a counter in pulse mode, each individual pulse amplitude carries important information regarding the charge generated by the neutrons interacting in the detector. Figure 2.11 shows the pulse height spectrum measured with the well counter. The multi-channel analyzer, with which the data in Figure 2.11 was obtained, was matched to within 4% to the counts from the scaler. The advantages of good resolution of the output pulse are a) efficient rejection of gamma-ray pile-up pulses, and b) high stability of the overall counting system.

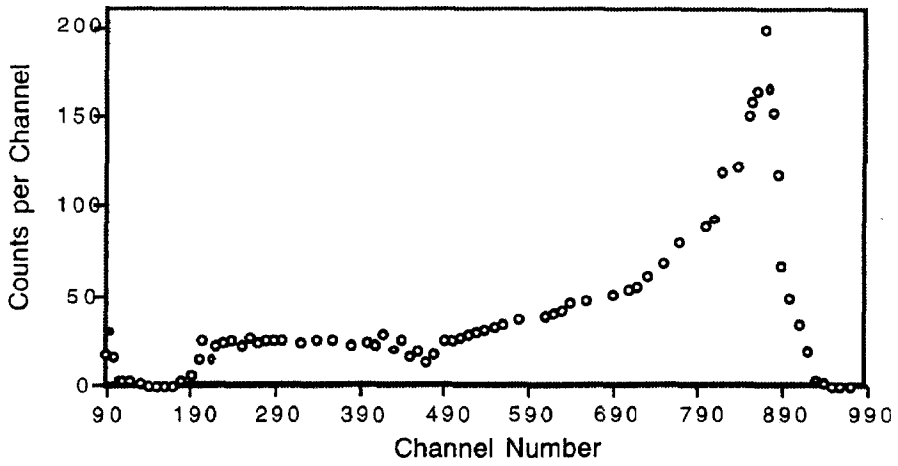

Figure 2.11. Pulse height distribution for thermal neutrons in well counter.

2.5.7 Dead Time Calculation

The dead time of the counting system was measured using the two source method. A 96.5 μCi Am/Be source and a 50 μCi Am/Li source were placed inside the cavity of the counter to provide counts, but were not close enough to interfere by scattering with each other. Because the measurement involves having two sources at one time, a dummy source with no activity was used to keep the scattering unchanged when one source alone was being utilized. The dead time in the well counter was found to be 0.14 ± 0.07 msec.

2.5.8. Position of the Source

The energy response of the detector depends upon the distance of the source from the effective center of the detector. The delayed neutron measurement requires the sample to be located at the same position after each shot. Therefore, we need to know the range over which the counter has a flat response. To investigate this effect, the efficiency of the detector was measured as a function of axial distance from the bottom of the cavity. The source was placed at the bottom of the detector cavity (40 cm long) and moved axially. The efficiency was measured as a function of source position. Figure 2.12 shows this relationship. The irradiated sample can be located within the first 10 cm of the cavity, and the response will be fairly flat.

2.5.9. Future Effort

The transfer system that satisfies the requirements for the experiment needs to be built and tested. Some additional equipment is also needed for the detection system. MCNP calculations are being performed to calculate the neutron background in Kiva 3 after a shot. Additionally, a trigger system that initiates the transfer of the samples needs to be designed.

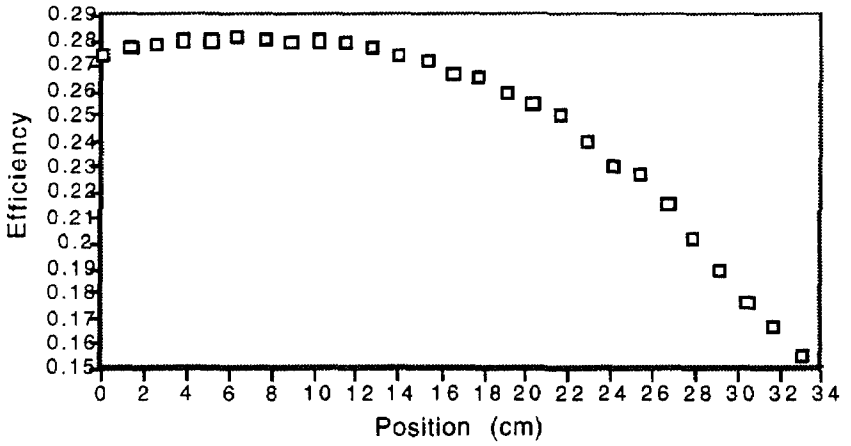

Figure 2.12. Counter efficiency as a function of source position.

3.0 SOLUTION ASSEMBLY PHYSICS

3.1. SHEBA Operating Experience

C. Cappiello, K. Butterfield, and R. Damjanovich

3.1.1. Entrained Radiolytic Gas

As part of the dosimetry workshop in June, SHEBA was operated four times in five days at power levels sufficient to produce radiolytic gases. The last two of these operations exhibited a phenomenon that had not been observed before. The assembly was put on an initial period and then, with no manipulation of the controls, the period gradually accelerated.

On examination of the data after the run, it was noted that while the period was accelerating, the level was also gradually dropping, and the usually quiet level sensor signal showed a significant amount of noise indicating radiolytic gas production at a lower power level than in other free runs.

Figure 3.1 is a plot of the reactor power and the fuel level during one of these operations.

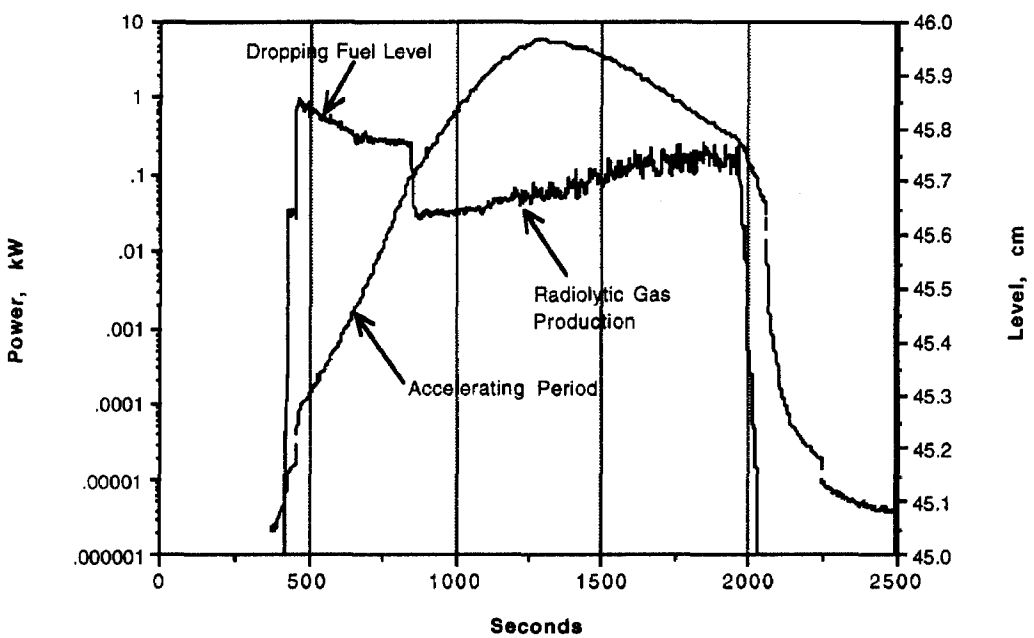

Figure 3.1. Reactor power and fuel level as a function of time for SHEBA.

One explanation for these observations is that some of the radiolytic gas remains entrained in the fuel following operation. If the system sits for several days between operations, the gas gradually escapes. But when the system is operated frequently, the initial fill of the reactor vessel initiates the release of some of the gas causing small bubbles to form throughout the solution (similar to pouring a carbonated beverage into a glass). These bubbles then migrate out of the solution causing an

increase in reactivity and a drop in the solution height. The migration of the bubbles also enables newly formed radiolytic gasses to escape more easily.

3.1.2. Temperature Coefficient

Throughout operations since 1993, the critical fuel height and temperature were recorded. These data were then plotted to determine the temperature coefficient of the SHEBA assembly. The measured temperature coefficient expressed as the change in critical height due to an increase in temperature was determined to be 0.1cm/°C.

However, during the spring of 1995, while operating SHEBA in the shielding pit, a significant and repeatable deviation from this temperature coefficient was measured. It appeared that below 15°C, the temperature coefficient increased by more than a factor of 3. Fig. 3.2 is a plot of the data through August 1995. The vertical offset between the data sets is due to the reflection of the pit.

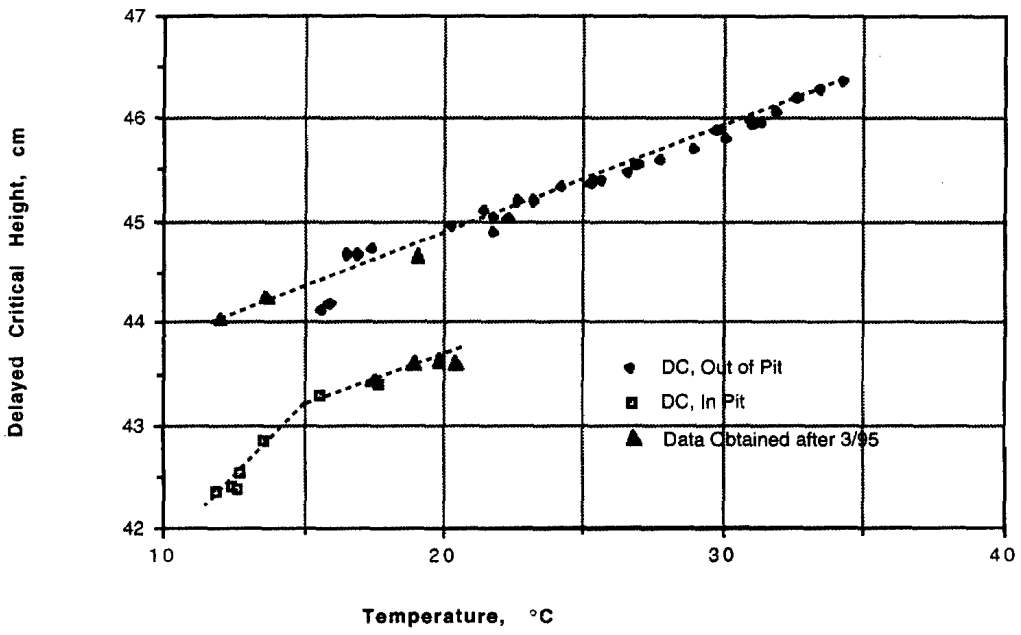

Figure 3.2. SHEBA data through August 1995 showing deviation from temperature coefficient.

Postulated causes of this shift included the following

- A hydration state change or phase change in the SHEBA fuel at this temperature. If this were the case, a similar shift should be seen in the temperature coefficient out of the pit at this temperature.
- This phenomenon is due to geometry effects when the critical height drops below 43 cm. To investigate this possibility, the fuel would have to be cooled to below 2°C to see if the phenomenon repeats out of the pit.
- This phenomenon was due to the pit itself or some type of change to the pit materials (concrete and dirt) at 15°C.

Because no data were available for SHEBA out of the pit at this low temperature, and SHEBA has no external cooling capability, two additional data points were obtained using the outside air temperature to cool the fuel. These data fell on the original temperature coefficient line of 0.1 cm/C°. Later in the summer, higher-temperature data were obtained in the pit and again, these data fell on the 0.1cm/C° line. The solid triangles on the Figure 3.2 plot are the data taken to investigate this phenomenon. It appears that this phenomenon is not due to a change in the fuel below 15 °C.

Beginning next fiscal year an inexpensive cooling system will be installed to cool the storage tanks to see if the phenomenon can be repeated out of the pit.

3.1.5. SHEBA Periscope Development

During the second half of FY95, we began developing a viewing device to visually observe radiolytic gas bubbles. The 3.5-in. diameter experiment port was fitted with a plexiglass flange. The initial attempt placed a small CCD camera and a high-intensity light directly on this flange. The picture quality at the beginning of the run was excellent in this configuration, but the neutron flux soon swamped the camera with "snow" long before we reached the power level required for gas production.

A periscope was then designed to allow the camera to operate outside the shielding pit. Figure 3.3 is a sketch of the periscope design showing the SHEBA tank and the lip of the shielding pit. A camera with a long zoom lens was used to peer down the tube, through the plexiglass flange, and into the tank. This new camera/lens arrangement requires a doubling of the light to get the same illumination in the picture from that of the small camera. Several different lighting schemes were tried, but because we have only one port for both lighting and viewing, we never achieved the same quality of picture we had seen with the camera and the light directly on the plexiglass flange.

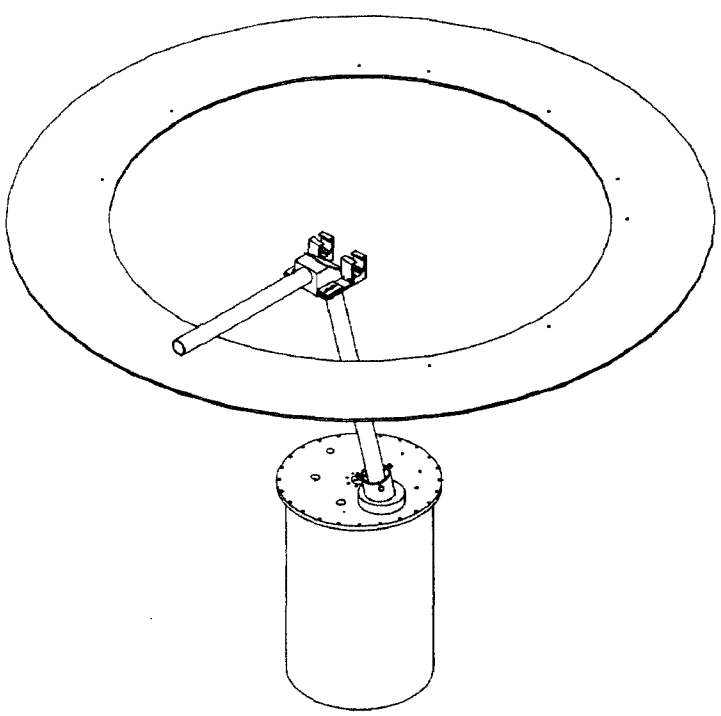

Figure 3.3. Periscope design showing the SHEBA tank and the lip of the shielding pit.

On July 12, 1995 we got our first video tape of radiolytic gas bubbles in the SHEBA assembly. The assembly was put on a 9-s period and allowed to free run. It hit a peak power of approximately 40 kW before the temperature and radiolytic gas production shut down the assembly. Following the peak of the free run, radiolytic gas bubbles could be clearly seen by the video camera. The solution appeared very viscous and the bubbles caused large surface disturbances as groups of bubbles overcame the fluid viscosity and burst to the surface at a frequency of about 10 - 15 seconds. Between these bursts of bubbles, the surface was relatively calm. The image was still plagued by neutron "snow" and poor lighting.

We have now purchased a Newvicon camera that should be less sensitive to the neutron flux. Several other lighting schemes are also being investigated to improve the picture quality.

3.2. Molybdenum Production Experiment Medical Isotope Production Summary

R. Lundberg, C. Cappiello, R. Paternoster, and R. Sanchez, LANL; D. Glen, DOE; R. Ball, B&W

Technetium-99m (^{99m}Tc) accounts for 80% of nuclear medicine procedures performed in the US today. Technetium-99m is obtained from ^{99}Mo that is a fission product in the ^{235}U fission chain. Currently, all of the ^{99}Mo is supplied by irradiating targets in a water reactor and then reprocessing the targets by dissolving them in nitric acid and running the solution through extraction columns. Only 1% of the fissions in the reactor are available as product and the reprocessing produces a significant quantity of radioactive wastes. In 1992, Babcock & Wilcox, combining the proven principles of the uranium-solution-fueled reactor, developed the idea of the Medical Isotope Production Reactor. The reactor would use the uranium solution as the fuel and the target, making 100% of the fissions available as product. A portion of the irradiated solution would be continuously circulated over extraction columns and the fuel returned to the reactor vessel. The advantages to this production method include reducing waste products, waste heat, and uranium consumption by a factor of 100. The reactor is small and can be designed to be passively safe. Such a reactor could also eliminate the dependence on foreign sources.

To provide a benchmark in the development of the MIPR, a small (41 ml) sample of 93% enriched uranyl nitrate fuel was irradiated in SHEBA to produce ^{99}Mo. The ^{99}Mo was then extracted from the fuel to investigate the feasibility of using a solution reactor to produce this isotope using an on-line, single-phase extraction process. The experiment also provided activities of the fuel solution and the extraction column which were used to validate calculations.

The sample was irradiated for 11 minutes while the SHEBA assembly produced 1.94×10^{13} fissions in the sample. The sample was left in SHEBA for three days to lower the dose rate. The sample was removed from SHEBA and measured for ^{99}Mo using gamma spectroscopy. The test yielded 0.3 mCi of ^{99}Mo.

The fuel was then split into two samples. One sample was mixed with alumina extraction media and the other sample with Reillex extraction media. The samples were agitated with the media for three hours and then the media and fuel were separated. The media were washed with the appropriate wash solution and the effluent was measured for ^{99}Mo and for impurities.

The alumina removed 93% of the ^{99}Mo from the fuel. The first rinse recovered 68% of the ^{99}Mo. The only contaminants to come off of the alumina in the rinse were tellurium and iodine. The Reillex did not perform as well, removing only 26% of the ^{99}Mo and transporting a number of contaminants with the ^{99}Mo through the rinse. A detailed description of this experiment and the results is included below.

This small-scale experiment demonstrated the feasibility of producing ^{99}Mo using a uranium solution and subsequently extracting it using a simple, convenient method. A larger scale production experiment is planned for which SHEBA's uranyl fluoride fuel will be replaced with a ~20% enriched uranyl nitrate fuel. SHEBA will then be used to evaluate the performance of a full-scale production reactor. The areas of investigation will include the following:

- Analytic and experimental characterization of reactivity effects of uranium concentration, solution temperature, and solution void;
- Radiolytic gas recombination;
- Volatile gas formation and removal;
- Heat transfer and removal;
- Evaluation of the ^{99}Mo strip fraction on alumina or other column;
- Evaluation of retention of other fission products on columns; and
- Evaluation of radiation damage on alumina.

Static Experiment for Production and Extraction of ^{99}Mo

(The following is from Chapter 4 of a Masters Thesis by Daniel Glen. He received an M.S. from the University of New Mexico, Department of Nuclear Engineering (Dr. Robert Busch, Advisor) while supported as a Graduate Research Associate at LACEF. It illustrates LACEF's continued support of higher education in the area of crtiticality safety and understanding of the basic physics of neutron chain reacting systems.)

3.2.1. Purpose of Experiment

The goal of this experiment is to irradiate small quantities of uranyl nitrate in a solution reactor to produce ^{99}Mo and to subsequently extract that ^{99}Mo from the fuel solution using a simplified and convenient method. Specifically this experiment plans to test the feasibility of using an on-line single-phase extraction process and determine some of these basic extraction efficiencies and product purity. In addition, the experiment will provide activities of the fuel solution and the extraction column, which will be used for comparing and validating calculations. This experiment is designed to allow the results to be directly applied to other associated MIPR research.

While the amounts of fuel and irradiation times do not support production levels, we could test the solution reactor processes. This experiment serves as a prototype and tests the overall feasibility for molybdenum produced in a solution reactor. As described in Chapter 3, molybdenum will be produced directly in the fuel solution as a result of reactor operation. Molybdenum will be separated from the fuel solution by an extraction column. This column will contain a specific material/resin that will selectively remove the molybdenum from the highly radioactive fuel solution as is passes through the column. Other radionuclides (contaminants) may also be captured by this extraction column, necessitating subsequent purification steps. The detailed chemistry reactions associated with the performance of the extraction columns are the subject of further research and will not be addressed by this experiment.

3.2.2. Description of Experiment

This experiment was conducted using the SHEBA reactor at the Los Alamos National Laboratory to model the methods for producing isotopes in a solution reactor. SHEBA (Solution High-Energy Burst Assembly) is a cylindrical, bare assembly, which uses a 5% enriched uranyl fluoride (UO_2F_2)

fuel solution that is stored in four criticality-safe stainless-steel tanks. It is located at Technical Area 18 of the Los Alamos National Laboratory. Operations are monitored and controlled by a digital control system. Reactivity is controlled by varying the solution level with a fuel pumping system. The assembly has a safety rod, which may be inserted in a thimble along the central axis of the Critical Assembly Vessel (CAV). Complete shutdown is accomplished by dumping solution through two parallel 1-in. scram valves. A 10-ft diameter, 10-ft deep pit has been dug into the floor of the SHEBA building to accommodate below-grade operation to minimize radiation exposure. SHEBA may be operated at ground level resting on a support plate or underground in the pit covered by shielding.

SHEBA has a critical mass of approximately 8.5 kg of ^{235}U and a critical volume of 85 liters. A typical burst releases 1.2 MJ of energy and creates 10^{16} to 10^{17} fissions. When operating at powers in the range of 2kW, radiolytic gas forms at the rate of approximately 1L/min. The assembly incorporates a cover gas system which collects the gases, maintains a non-combustible atmosphere, and allows the fission product gases to decay under confinement prior to release. The effects of the radiolytic gases are minimized by a catalytic converter to allow recombination of the hydrogen and oxygen. See Figs. 3.4 and 3.5 for schematic diagrams of the solution storage tanks, CAV, valves, pumps, and sensors used in SHEBA {Paternoster *et al.*, 1994}.

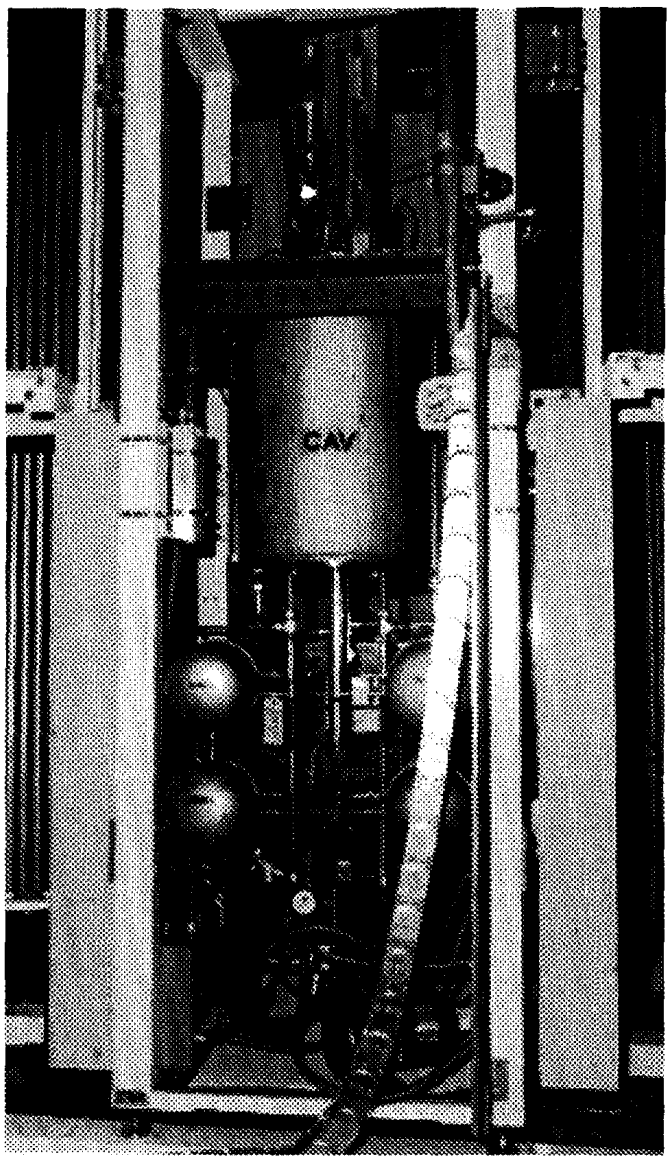

Figure 3.4. SHEBA assembly.

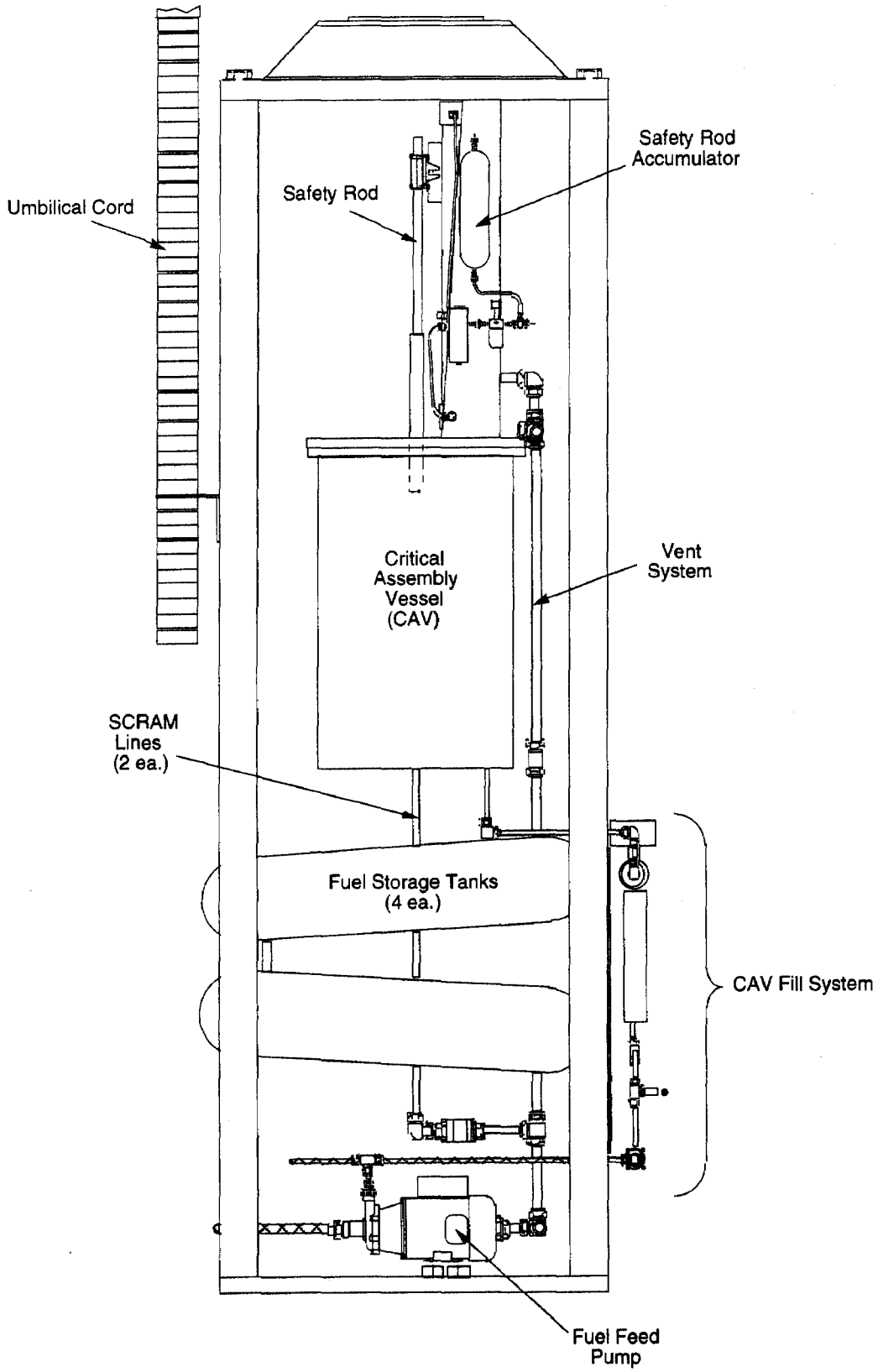

Figure 3.5. Schematic of the SHEBA critical assembly.

3.2.4. Sample Processing

The sample was removed from the reactor and transported to the counting facility (TA-48). The fuel sample was removed from the thimble and placed in a poly bottle. This phase of the experiment tested the extraction capability of two different substances: alumina and Reillex. This was done by mixing two 8-ml batches of the irradiated fuel sample with 0.54 g of alumina and 0.58 g of Reillex. The solution was agitated for 3 hours, then the extraction media was separated from the remaining fuel solution. Gamma spectroscopy was performed using a High Purity Germanium Counter (#64). Each sample was placed on shelf #10 and counted for thirty minutes. The efficiencies associated with this counter are shown in Table 3.3. The initial and final fuel solutions were counted to determine the removal characteristics of the extraction media. Following this, the Reillex was washed with water and the alumina was washed with a 0.1M NaOH solution in an effort to determine if the captured radionuclides could be readily removed from the media. This action, if successful, would facilitate any subsequent ^{99}Mo purification steps. The actual sequence of events for this experiment is shown in Table 3.4.

Table 3.3. HP Ge counter efficiencies.

Incident Gamma Energy	Counter Efficiency
122 keV	4.54×10^{-3}
165.88 keV	4.395×10^{-3}

Table 3.4. Sequence of experiment.

Step	Time	Action
Ia	1436 21-Jul	Reactor critical
Ib	1439 21-Jul	Reactor placed on 14-s period (Commence Free-run)
Ic	1450 21-Jul	SCRAM (Irradiation Complete)
II	21 thru 24 Jul	Allow decay period to lower dose rate
III	0800 24-Jul	Remove sample from SHEBA experiment port
IV	25-Jul	Transport fuel sample to counting facility
V	1030 26-Jul	Mix sample with extraction media
VII	1330 26 -Jul	Separate fuel sample from extraction media
VIII	26 thru 28-Jul	Perform gamma spectroscopy

Figure 3.3. SHEBA run.

3.2.5. Gamma Spectroscopy Results

Transient equilibrium between the ^{99}Mo parent and daughter ^{99m}Tc will occur within a couple days. Because of the better detection efficiency of the ^{99m}Tc 143-keV photon, the ^{99}Mo concentration was monitored by the ^{99m}Tc build-up instead of the β^- decay of ^{99}Mo. Because the counts were not performed until two days after the extraction, a transient equilibrium condition

existed. Therefore the 143-keV gamma gives a good indication of the amount of ^{99}Mo present before and after extraction was performed. The extraction and gamma spectroscopy were performed by R. Rundberg at TA-48. A summary of the experimental results of the two extraction media is detailed in Table 3.5.

Table 3.5 ^{99}Mo extraction data.

	Initial ^{99}Mo Counts in Fuel Solution (CPM/ml)	^{99}Mo Counts in Fuel Solution after Media Filtration (CPM/ml)	^{99}Mo Captured on Extraction Media (%)	Counts in Solution after a 5ml Wash (CPM/ml)	^{99}Mo Recovery from Extraction Media(%)
Reillex	$1.51 \times 10^4 \pm 62$	$1.11 \times 10^4 \pm 53$	26.5 ± 0.5	$2.02 \times 10^3 \pm 22$	31.6 ± 0.9
Alumina	$1.51 \times 10^4 \pm 62$	$1.09 \times 10^3 \pm 16$	92.8 ± 1	$1.52 \times 10^4 \pm 62$	67.8 ± 0.9

This data indicates that the Reillex did not suitably extract the ^{99}Mo from the uranyl nitrate fuel sample. The removal ability of the Reillex may depend on the pH value of the solution, which in this case was in the range of 0-1. Further analysis is required to determine if any pH dependency does exist and the effect it would have on the extraction efficiency.

The alumina did perform well in removing the ^{99}Mo from the fuel solution. This indicates that a mechanism, at least for this limited case, does exist to remove sufficient quantities of the ^{99}Mo through a direct extraction technique—providing encouraging data to demonstrate the feasibility of the extraction column concept.

Results indicated 71 μCiCi of molybdenum were present 6 days after irradiation (see calculation A.14). The amount of Moly predicted by the ORIGEN2 model was 161 μCi. This difference between the actual and calculated yield for ^{99}Mo is primarily due to the uncertainties associated with the neutron flux in the region of the target. Another significant simplification which may account for this difference in yield was using the thermal neutron cross-section library in the ORIGEN2 calculations with no epithermal constituent. Perturbation of the flux around the sample was expected due to introduction of a void above the fuel sample and the presence of the highly enriched uranyl nitrate. This lower yield is supported by the evidence (lower than expected reactor period) that the overall reactivity effect of the sample was negative in comparison to a SHEBA run without the sample.

3.2.6. Comparison to the FDA Molybdenum Purity Requirements

While the media did remove substantial quantities of ^{99}Mo, other radionuclides were also captured on the media. These radionuclides are considered contaminants and must eventually be removed to meet the Food and Drug Administration purity requirements for use of the ^{99}Mo in the production of radiopharmaceuticals. Table 3.6 gives the purity requirements for the current reactor-produced molybdenum production techniques {R.S. Mani, 1976}. The Reillex and alumina were washed with water and NaOH respectively in an effort to remove the ^{99}Mo so that it may be available for subsequent purity treatments. The identification of the contaminants and the results of the washes are contained in Tables 3.7 and 3.8. Because the irradiation and counting periods are short in comparison to a production mission cycle, the long-lived radionuclides such as Ru-106 and Cs-134 are not expected to be detected. In this experiment, only those radionuclide contaminants detected during the 30-minute counts are identified.

Table 3.6. FDA purity requirements for ^{99}Mo.

Radionuclidic purity (excluding Tc-99m)	Specification 99.5%
α activity	<0.1 nCi/mCi Tc-99m
Sr-90	<1.0 pCi/mCi Tc-99m
I-131	<0.1 nCi/mCi Tc-99m
Ru-106	<0.1 nCi/mCi Tc-99m
Cs-134	<0.1 nCi/mCi Tc-99m
Ag-110m	<0.1 nCi/mCi Tc-99m

Table 3.7. Purity of molybdenum using Reillex extraction media.

Contaminant	Gamma Energy Identifier (keV)	Initial Counts in Fuel Solution (CPM/ml)	Percentage captured on extraction column	Counts in Solution after 5 ml Wash (CPM/ml)	Purity
Ru-103	319	176	41	25	0.01 mCi/mCi Tc-99m
Te-132	228.5	7740	25.6	1130	0.5 mCi/mCi Tc-99m
I-131	364.5	2890	26	480	0.2 mCi/mCi Tc-99m
Ce-141	145.7	2620	18.7	372	0.15 mCi/mCi Tc-99m
Ce-143	293.4	1780	19.7	426	0.2 mCi/mCi Tc-99m
Zr-95	756.3	415	31.8	52	0.02 mCi/mCi Tc-99m

Table 3.8. Purity of molybdenum using alumina extraction media.

Contaminant	Gamma Energy Identifier (keV)	Initial Counts in Fuel Solution (CPM/ml)	Percentage captured on extraction column (%)	Counts in Solution after 5 ml Wash (CPM/ml)	Purity
Ru-103	319	176	100	0	<0.1 nCi/mCi Tc-99m
Te-132	228.5	7740	78	5380	0.3 mCi/mCi Tc-99m
I-131	364.5	2890	84.5	83	4.8 μCi/mCi Tc-99m
Ce-141	145.7	2620	0	0	<0.1 nCi/mCi Tc-99m
Ce-143	293.4	1780	0	0	<0.1 nCi/mCi Tc-99m
Zr-95	756.3	415	36.4	0	<0.1 nCi/mCi Tc-99m

The results from Tables 3.7 and 3.8 illustrate the need for additional purification steps in processing solution-reactor-produced molybdenum. Again the alumina performed better than the Reillex. All impurities detected were transported with the molybdenum using the Reillex resin, creating a solution containing significant amounts of impurities. The alumina, however only transported the tellurium and iodine radionuclides, greatly reducing the amount of unwanted radionuclide contamination.

3.2.7. Summary

The goal of this experiment, which was to irradiate small quantities of uranyl nitrate in a solution reactor to produce ^{99}Mo and to subsequently extract that ^{99}Mo from the fuel solution using a simplified and convenient method, was accomplished. The production of ^{99}Mo, directly from the fission yield of the uranyl nititrate fuel, occurred as expected. This short irradiation indicates that production is practicable, and an experimental reactor can produce small quantities.

The extraction process, modeled by this experiment, also shows that the capability to extract substantial quantities of the ^{99}Mo in a single step does exist. Even though the ^{99}Mo eluted from the extraction column does not meet the FDA purity requirements, isolation of the ^{99}Mo with minimal contaminants, as done with the alumina column, will allow for further processing. Subsequent purification steps should allow solution-reactor-produced ^{99}Mo to meet the FDA purity limits.

The alumina media performed substantially better than the Reillex. As shown in Table 3.5, the alumina was able to remove ~92% of the ^{99}Mo from solution whereas the Reillex only removed 26%. Each medium was then washed in an attempt to remove the ^{99}Mo. The alumina out-performed the Reillex again. The overall results of this experiment are that the alumina removed and isolated ~63% of the ^{99}Mo produced but contained Te-132 and I-131 contaminants. The Reillex removed and isolated ~8% of the ^{99}Mo produced, but contained Ru-103, Te-132, I-131, Ce-141, Ce-143 and Zr-95 contaminants.

Performance of the extraction medium probably depends on the associated pH of the fuel solution, and this experiment was conducted at a single extremely low pH level. Therefore additional tests should be conducted at various pH ranges before any final conclusions concerning the performance of the two media are made.

3.3. Tritium Production

Options are being considered to provide supplemental backup or peak tritium production capabilities using targets inserted in power reactors or DOE-owned test reactors. One such target uses helium-3 as the target material to produce tritium. The major concern with this concept is the large negative reactivity associated with helium-3 and the possible excursion that would occur if the helium-3 were suddenly lost during reactor operation. Using a borated insert to mitigate this excursion has been proposed.

The SHEBA assembly machine will be used to produce a thermal neutron flux to experimentally verify calculations for the design of this helium-3 target. Both tritium production and target worth will be verified. Experimental hardware has been designed and is in fabrication. Experiments should start the last week of September.

3.3.1. Reactivity Worth Analysis of Helium-3 Targets in SHEBA
(R. Kimpland)

As part of the light water reactor production of tritium (LWRPT) project, experimental targets containing helium-3 will be placed in the SHEBA critical assembly for irradiation. A set of transport calculations, using MCNP, was performed to determine the reactivity worth of the helium-3 targets and the SHEBA experiment well. Also, the reactivity worth of the helium-3 gas itself was calculated.

Two targets were examined, the first is a stainless steel canister (24.10 in. in length, 2-in. O.D., and 0.055-in. wall thickness) containing only helium-3 gas at 15 atms. The second target consists of a second similar canister filled with helium-3 gas at 15 atms and a neutron absorbing insert. The insert is an eight-finned stainless steel can containing B_4C powder enriched in Boron-10 (92%). In the MCNP model, this insert was simulated by a four-finned can, whose fins were twice as thick as the actual insert to conserve volume. The experiment well consists of a hollow stainless steel tube centered 4.19 in. from the inside wall of the SHEBA vessel. The experiment well has a 2.37-in. O.D. and a wall thickness of 0.34 in..

Three calculations were made for each target. The first calculation was a search for the critical height with the experiment well and target in place. The second calculation was done with the experiment well and target in place but without the helium-3 gas in the target. The third calculation was SHEBA minus the experiment well and target but with the critical height found in the first calculation adjusted for the displacement of the experiment well's volume. The ENDF-5 continuous energy cross-section sets were used for all the calculations. Each calculation used 10000 particles per generation and ran for 450 cycles, skipping the first 50 cycles.

For the first target, which had no insert, the reactivity worth of the experiment well and target was \$-2.71±0.09. The critical height of the fuel was approximately 49 cm. The reactivity worth of the helium-3 gas itself was \$-0.96±0.08, and the worth of the experiment well minus the target was \$-1.75±0.09.

For the second target, which had the insert, the reactivity worth of the experiment well and target was \$-3.16±0.08. The critical height of the fuel was approximately 50 cm. The reactivity worth of the helium-3 gas itself was \$0.12±0.08, and the worth of the experiment well plus insert alone was \$-3.04±0.08. For this target, an additional calculation was made in which the helium gas escapes and fuel floods the experiment well and target. The reactivity worth of this event was \$0.14±0.08. Tables 3.9 and 3.10 show the k_{eff} values and the fuel levels for each of the runs.

Table 3.9. First target (no insert).

Case	Fuel Level	k_{eff}
Well+Target	49.00 cm	1.00178±0.00042
Well+Target-Gas	49.00 cm	1.00853±0.00039
No Well	48.25 cm	1.02117±0.00042

Table 3.10. Second target (with insert).

Case	Fuel Level	k_{eff}
Well+Target	50.00 cm	1.00152±0.00040
Well+Target-Gas	50.00 cm	1.00071±0.00043
No Well	49.23 cm	1.02420±0.00038
Flooding	49.50 cm	1.00255±0.00038

4.0 EXCURSION PHYSICS

4.1. Dynamic Analysis of Nuclear Excursions In Underground Repositories Containing Plutonium

R. Kimpland

A recent study performed at the Los Alamos National Laboratory postulates that Pu-239 stored in underground repositories could lead to a nuclear explosion of up to a few hundred tons of TNT. The study suggests that plutonium originally contained in glass logs could escape its containment and disperse into the surrounding native rock of the repository. This dispersion would then lead to an autocatalytic process that ultimately would lead to a catastrophic nuclear explosion. A computer model that simulates this autocatalytic process has been developed at the Los Alamos Critical Experiments Facility. The model has been used to determine the fission yield of such an event and the effects of that yield on the repository. The goal of this work is to quantify the consequences of the autocatalytic process, not to determine the probability of such an event occurring.

4.1.1. Introduction

The recommended method for dealing with excess Pu-239 is to store this material in underground repositories, such as Yucca Mountain. The Pu-239 would be mixed with SiO_2 to form a glass log. This log would then be buried in the native rock of an underground repository. A recent report (Ref. 1) has postulated that this method of dealing with excess Pu-239 could lead to a catastrophic nuclear explosion of up to a few hundred tons in yield. This event is triggered by an autocatalytic process, which causes a critical system to drive itself automatically to a supercritical system.

This report presents the results of a dynamic analysis of the autocatalytic process proposed in the report referenced above. The goal is to simulate the autocatalytic process as accurately as possible and to determine its nuclear yield. No attempt was made to determine the probability of such an event occurring, or even if such an event is physically possible. The object of this study was to develop a dynamic model based on the scenario postulated in Ref. 1 and quantify its consequences.

4.1.2. Autocatalytic Process

The fundamental premise underlying the autocatalytic process is the fact that the plutonium is originally placed in an underground repository in an extremely undermoderated condition. Thus, if the plutonium can escape its confining glass log and spread out into the surrounding rock of the repository, which for the most part is quartz, it will become more moderated. Several mechanisms by which the plutonium may be spread out have been proposed, such as ground water finding its way into the repository and transporting plutonium into the surrounding rock, or earthquakes and volcanos disturbing the glass log and surrounding rock. Ground water seeping into the repository is assumed to carry away neutron poisons that were added to the glass log initially. Also, the ground water may cause steam explosions to occur, which would help to disperse the plutonium even more quickly. In addition to dispersing the plutonium, these events will crack and fracture the surrounding rock, allowing the plutonium to penetrate it. Given enough time and many such events, the plutonium could disperse into the surrounding rock until it reaches a critical configuration.

At this point, the power will begin to rise, causing the plutonium to heat up and eventually vaporize. It is assumed that all the energy of the fission fragments will be deposited into the plutonium only and not the surrounding rock. This assumption is made because it is believed that the plutonium will be gathered heterogeneously in the cracks of the surrounding rock and not be

homogeneously distributed throughout the rock. Thus, the plutonium will heat up quickly and vaporize while the surrounding rock may only heat up negligibly due to the energy of fission neutrons that escape from the plutonium. It should also be noted that the system should be pushed sufficiently far above critical to overcome the negative temperature feedback of $-1 \times 10^{-5} \Delta k_{eff}/C°$, which is given in Ref. 1. This negative temperature feedback will decrease reactivity \$5.00 for every 1000 C° increase in the plutonium. Assuming the plutonium vaporizes at 3000 K and starts out at 300 K, the system should start out at a reactivity greater than \$13.50. This would allow the system to still be critical at the point of plutonium vaporization.

Once the plutonium vaporizes, the autocatalytic process begins. This process is described in Ref. 2, which is a response prepared by the authors of Ref. 1 to an internal review of the draft of Ref. 1 performed by personnel at the Los Alamos National Laboratory. There it was assumed that the plutonium would vaporize at 3000 K, and the molecular velocity of the plutonium would be 45,000 cm/s. It was further assumed that the plutonium vapor would spread out through the surrounding rock at a velocity comparable to its molecular velocity. The worst-case scenario involves a glass log that initially contained 100 kg of plutonium. In spherical geometry, 100 kg of plutonium homogeneously distributed in SiO_2 and surrounded by a 1.0-m-thick reflector of quartz would go critical at a radius of approximately 75 cm. It is assumed that this is the point at which vaporization would occur and the autocatalytic process begin. This assumes that the glass log and surrounding rock are quartz (pure SiO_2) with a density of 2.2 g/cm^3. The plutonium vapor spreads out rapidly and reaches its maximum k_{eff} of 1.18 at a radius of approximately 150 cm. Then the plutonium vapor continues to spread until it reaches a subcritical configuration at a radius of approximately 250 cm. See Fig. 4 of Ref. 1. It is stated in Ref. 2 that the plutonium probably won't spread out through the surrounding rock unhindered, so it probably takes approximately 12 ms for the plutonium to spread from the critical radius, through supercritical, and back finally to a subcritical radius. It is during this 12 ms period of the autocatalytic process that the potentially catastrophic nuclear yield will be produced.

4.1.3. The Model

A computer model, which simulates the autocatalytic process described above, has been developed at the Los Alamos Critical Experiments Facility (LACEF). This model combines the neutron point kinetics equations with an equation of state for SiO_2 and energy, continuity, and momentum equations for SiO_2. It has been assumed that once the plutonium is vaporized, all the fission energy is deposited in the surrounding rock. Therefore, the model consists of a solid sphere of quartz with a radius of 150 cm. It is recognized that the actual scenario consists of a system whose radius increases from 75 cm all the way to 250 cm. For ease of computation a fixed geometry is assumed. This assumption is quite conservative, however, because testing of the model has shown that a negligible fraction of the total amount of energy generated is deposited into the system before it reaches maximum reactivity at 150 cm. Also, the model dumps all the energy produced into the system of 150 cm, whereas in the actual system most of that energy should be deposited into a much larger system with a radius of 250 cm. This will result in over-estimating any mechanical effects. The model also restricts the outward expansion of the quartz sphere until the pressure of the core exceeds the compressive strength of the hypothetical surrounding rock. This constraint on the model is extremely conservative because it has already been assumed that the surrounding rock is cracked and fractured, otherwise the plutonium vapor would not be allowed to disperse. Also, it has been assumed that the original glass log and some of the surrounding rock have been broken to allow ground water to seep in and carry neutron poisons away. All the events that were necessary to help disperse the plutonium out to 75 cm, such as steam explosions or earthquakes, must have turned the original glass log and surrounding rock to rubble. The significance of this is that the Pu+SiO_2 system will be extremely porous, and no condensed state pressure can build up until the system expands to a point

where the porosity has been eliminated. The model assumes a solid constrained sphere of SiO_2 because it best maintains the main theme of Ref. 1, which is that nuclear explosions can occur underground because of the confinement of the surrounding rock.

4.1.4. Neutron Point Kinetics Model

To calculate the power of the Pu+SiO_2 as a function of time, the point kinetics equations are used. These equations are given by

$$\frac{dN}{dt} = \frac{\beta}{\Lambda}\left[(R - 1)N + \sum_{i-1}^{6} \frac{\beta_i}{\beta} D_i\right] \tag{1}$$

and

$$\frac{dD_i}{dt} = \lambda_i (N - D_i) \tag{2}$$

where N is the fission power, R is the reactivity of the system in dollars, Λ is the mean generation time, and D_i is the relative precursor power. Because the reactivity of the autocatalytic process starts out near critical, moves to a maximum value, and then drops off to subcritical, a sine function is used to simulate the reactivity. An expression for the reactivity of this process is given by

$$R = 74.00\sin\left(\frac{t}{0.006}\frac{\pi}{2}\right) \tag{3}$$

where t is the time in seconds and 74.00 represents the maximum reactivity the system reaches in dollars. Figure 4.1 shows a plot of the reactivity as a function of time. After its minimum value is reached, the reactivity is held constant. Only the effect of the plutonium vapor spreading out through the surrounding rock is accounted for in the reactivity equation. No other reactivity feedback mechanisms are included in the kinetics model. For example, the effects of thermal-neutron-spectrum hardening and the negative reactivity feedback due to fuel density redistribution in a constrained assembly are not included.

The most important parameter in the calculation of the power is the mean generation time. The system being modeled is unique in that the size of the core is continually changing. The core starts out as a sphere of radius 75 cm and ends up as a sphere with a radius of 250 cm. The volume of the core starts out at $1.767\text{x}10^6$ cm^3 and ends up with a volume of $6.545\text{x}10^7$ cm^3, which is a remarkable change. One would expect the mean generation time to change quite dramatically during this change. By using ONEDANT, a set of calculations was made to determine the mean generation time at various points during the autocatalytic process. At a radius of 75 cm (time=0.0), the mean generation time is $7.3\text{x}10^{-5}$ s; at 150 cm (time=0.006 s), the mean generation time is $1.3\text{x}10^{-4}$ s; and at 250 cm (time=0.012 s), the mean generation time is $4.0\text{x}10^{-4}$ s. An expression for ß/Λ as a function of time is given by

$$\frac{\beta}{\Lambda} = 28.48 - 2268t + 28056t^2 \quad . \tag{4}$$

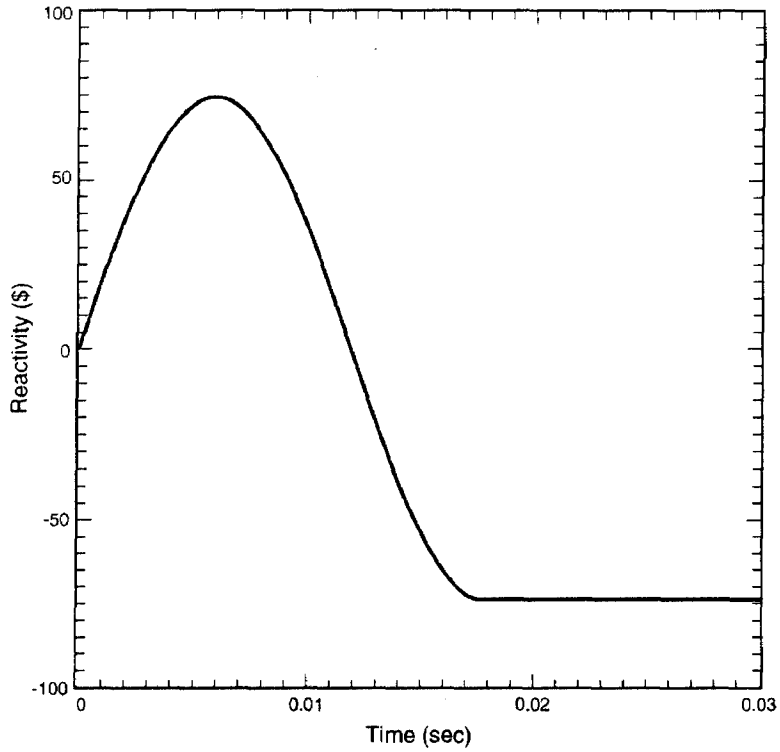

Figure 4.1. Reactivity insertion as a function of time in Pu +SiO_2 system.

This expression is simply an empirical fit that matches the known mean generation time with its corresponding reactivity in time. After the system becomes subcritical (time=0.012 s) the mean generation time stays constant at 4.0×10^{-4} s. The prompt alpha for the pulse, which is strongly dependent upon the mean generation time, is shown in Fig. 4.2 as a function of time. The mean generation times stated above are conservatively short because the model used to calculate them assumed that the plutonium was homogeneously distributed throughout the quartz. Again, it should be noted that the plutonium spreads out through cracks in the surrounding rock, which means that the plutonium is distributed more heterogeneously than homogeneously. This will cause the actual critical system to have a larger dimension than a system with the plutonium homogeneously distributed. Thus, a larger system will mean a longer mean generation time.

Another key parameter in the kinetics equations is the initial power of the system. For the autocatalytic process to occur, the plutonium must be completely vaporized. It is assumed that this vaporization occurs because of some event that causes the system to go supercritical initially. Because the history of the system is not known, in any detail, prior to the autocatalytic event, the model assumes that the initial power is 500 MW. This power should be conservatively high enough to ensure that the 100 kg of plutonium are completely vaporized in the time leading up to the autocatalytic event. The total amount of fission energy produced during the autocatalytic event is directly proportional to the initial power. It is believed that 500 MW is a very conservative upper limit for the initial power of any actual event.

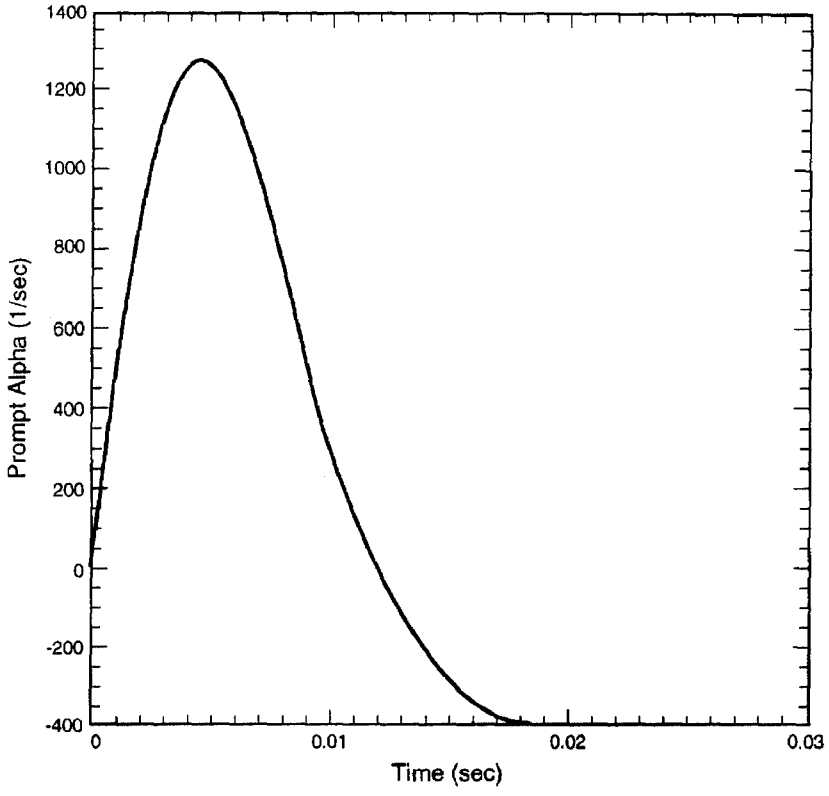

Figure 4.2. Prompt alpha for Pu +SiO_2 system calculated.

4.1.5. Equation of State

During the autocatalytic process, the fission energy generated will be deposited into the remains of the glass log and, later, in the surrounding rock. To determine the mechanical stresses produced by this energy deposition, an equation of state for SiO_2 has been developed. This equation is given by

$$\frac{dP}{dt} = \frac{\alpha}{\kappa}\frac{dT}{dt} + \frac{1}{\rho\kappa}\frac{d\rho}{dt} \tag{5}$$

where P is the pressure of the SiO_2, α is the isobaric compressibility of SiO_2 (5.5×10^{-7} $C^{\circ-1}$), κ is the isothermal compressibility of SiO_2 (2.74×10^{-5} MPa^{-1}), is the density of the SiO_2, and T is the temperature of SiO_2 (Refs. 3 and 4). An expression for the temperature of the SiO_2 as a function of time and position is given by

$$\frac{dT}{dt} = \frac{N}{MC_P}\frac{R}{r\pi}\sin\left(\frac{r\pi}{R}\right) \tag{6}$$

where M is the mass of the SiO_2, C_P is the specific heat of SiO_2 (7.5×10^{-4} MJ/kg/C°), r is the radial position, and R the radius of the SiO_2 sphere.

To determine the acceleration of the SiO_2 and its change in density, simple momentum and continuity equations are used. In spherical coordinates these equations are given by

$$\frac{\partial U}{\partial t} = -\frac{1}{\rho}\frac{\partial P}{\partial r} \tag{7}$$

and

$$\frac{\partial \rho}{\partial t} = -\frac{1}{r^2}\frac{\partial r^2 \rho U}{\partial r} \tag{8}$$

where U is the velocity of the SiO_2.

A multi-region model was used to simulate the SiO_2. The quartz sphere was split up into ten concentric shells of equal thickness. Each shell or region contains its own equation of state and its own energy, momentum, and continuity equations. These equations were made discrete and solved numerically on a dynamic system-simulation software package (Ref. 5).

4.1.6. Results and Conclusion

Figure 4.3 shows the model's predicted power pulse for the autocatalytic process. The spatially averaged peak power of the burst was 3.83×10^6 MW and the total fission energy yield for the prompt burst was 2.85×10^4 MJ or about 9.48×10^{20} total fissions. Figure 4.4 shows the core-averaged temperature of the quartz sphere and the pressure that was built up during the autocatalytic process. The fission energy generated caused the quartz to heat up an average of 1250 C° and it caused a pressure buildup of 24.6 MPa throughout the quartz.

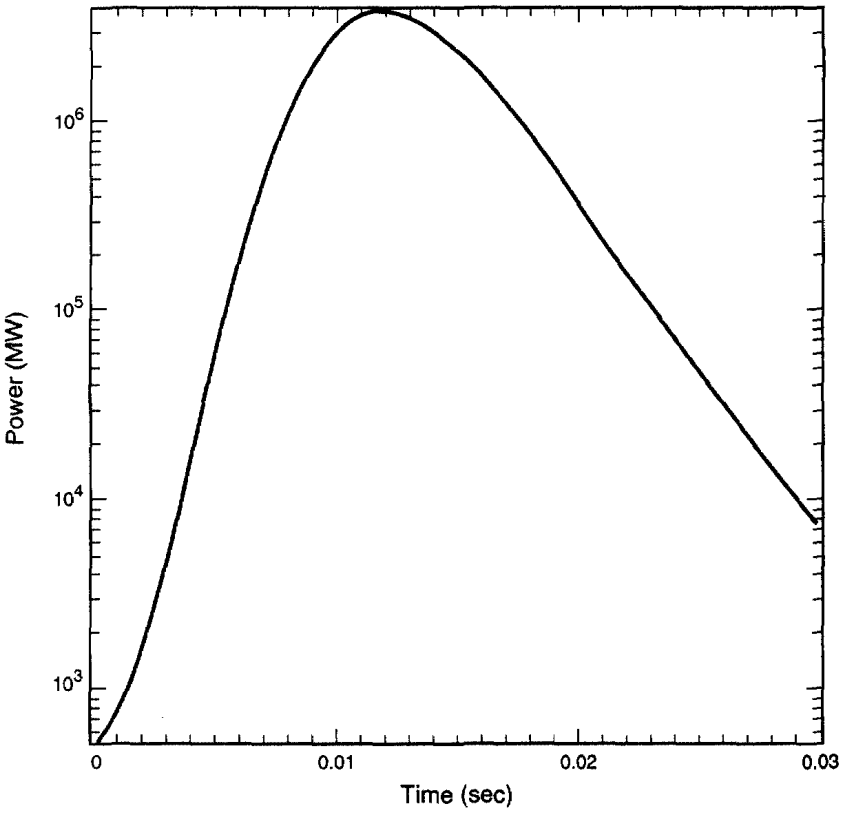

Figure 4.3. Calculated power transient in Pu +SiO_2 system.

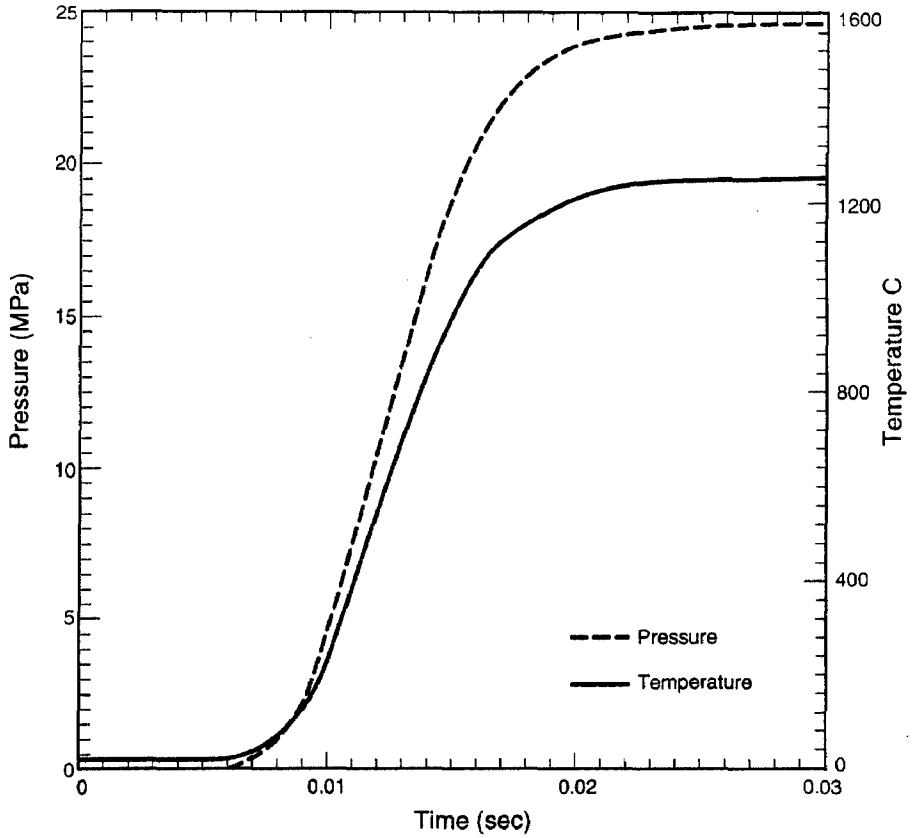

Figure 4.4. Calculated core-averaged temperature and pressure during excursion in SiO_2 system.

The computer model presented above attempts to simulate supercritical excursions of plutonium and SiO_2 in underground repositories. In particular, the model tries to simulate the "dry" autocatalytic process postulated in Refs. 1 and 2 as accurately as possible. The model's predicted total energy yield is at least two orders of magnitude less than the kinetic energy yield estimated in Ref. 1. The fact that the mean generation time continually changes as the plutonium vapor spreads out through the surrounding rock has a dramatic effect on the e-folding period during the autocatalytic process. The mean generation time increases by almost a factor of 6 during the course of the pulse. The effect of the mean generation time on the pulse can be seen from Fig. 4.2. As the mean generation time increases, the prompt alpha increases less with increasing reactivity.

Clearly, no significant kinetic energy was produced during the pulse. The only motion produced was a redistribution of core material from the center of the core outward. The fission energy generated only raised the temperature of the quartz a few hundred degrees, which produced a negligible pressure buildup of 24.6 MPa. Given a compressive strength for quartz of 1067 MPa, the surrounding rock can contain the quartz sphere without any difficulty (Ref. 4). Even if the quartz sphere was allowed to expand freely after the prompt burst, it would only generate 0.22 MJ of kinetic energy or about 0.11 lb of equivalent high-explosive yield. This calculation was made by giving the quartz sphere an initial pressure of 24.6 MPa and letting the outer boundary of the sphere expand against a vacuum. The model predicted a maximum dynamic pressure of 0.016 MPa. By multiplying the dynamic pressure by the volume of the quartz, the kinetic energy can be crudely approximated.

At a radius of 150 cm, the system contained over 31,000 kg of quartz, which provided a huge energy sink. It should be noted that at the 12 ms point during the burst, only 44% of the total fission yield had been generated. This means that in an actual system, over 50% of the 1.03×10^4 MJ yield should be deposited into a sphere at least 250 cm in radius, which would contain over 1.4×10^5 kg of

quartz. Due to the large thermal inertia of the quartz, no significant mechanical stresses were produced even with the extremely conservative constraints placed on the model. It is the opinion of the author that no kinetic energy could be produced by the autocatalytic process described in this report. The sheer size of the system considered, combined with the long mean generation time, makes it impossible for any significant inertial effects to occur. The integrity of an underground repository will not be compromised by the autocatalytic process postulated in Refs. 1 and 2.

References

1. C. D. Bowman and F. Venneri, "Underground Autocatalytic Criticality From Plutonium and Other Fissile Material," Los Alamos National Laboratory document LA-UR 94-4022 (Dec. 1994).
2. C. D. Bowman and F. Venneri, "Criticality Issues For Thermally Fissile Material in Geologic Storage," Los Alamos National Laboratory document LA-UR 95-504 (Jan. 1995).
3. R. H. Kimpland, "An Improved Multi-Region Computer Model For Predicting Nuclear Excursions in Aqueous Homogeneous Solution Assemblies," Ph.D Dissertation, University of Arizona, 1993.
4. R. C. Weast, *CRC Handbook of Chemistry and Physics*, 68th Ed. (CRC Press, 1987-1988).
5. G. A. Korn, *Interactive Dynamic System Simulation* (McGraw-Hill, Inc., 1989).

4.2. Development of the MRKJ One-Dimensional Reactor Transient Code for Study of Transient Nuclear Systems, Critical Experiments, and Criticality Accident Scenarios

W. Myers, S. Rojas, R. Kimpland, P. Jaegers, R. Sanchez, D. Hayes, R. Paternoster, R. Anderson, and W. Stratton

Due to the difficulty of porting the PAD code [5] to modern computing machines, the MRKJ One dimensional Reactor Transient code is being developed. It will be an improved version of the PAD code to use as a tool to analyze transient nuclear systems, critical experiments, and criticality accident scenarios. The recent interest in examining postulated dynamic nuclear systems created by long-term disposition of fissile material at Yucca Mountain [16]-[18] was the catalyst that accelerated this development.

4.2.1. History

The MRKJ Reactor Transient Code uses the calculational technique known generally as the "coupled neutronic-hydrodynamic method" [1]. This method was first proposed to assist in understanding and designing nuclear weapons explosions [2]. Development of the technique proceeded only as rapidly as reliable computers became available and it was not until the early 1950s under the guidance of Ernest W. Salimi and Conrad Longmire of the Los Alamos Scientific Laboratory* that working codes were created to couple together the differential equations for thermodynamics, materials motion, and neutron transport with rapidly changing reactivity.

The first nonweapon application of this technique was in 1957 subsequent to the accidentally large power excursion in the original Lady Godiva reactor [3] using the code referred to as the

* Now Los Alamos National Laboratory

"detailed method."** This code and a later version known as the RAC code [4] were replaced in the early 1970s by the Los Alamos Pajarito Dynamics code known by the acronym PAD [5].

The PAD code employed the coupled neutronic-hydrodynamics method in one dimension, with the neutronics provided by DTF-IV [6] transport calculations. The neutron transport calculations used a library of Hansen-Roach-16-energy group neutron cross sections [7] with a limited number of isotopes (about 16). PAD was originally written using FORTRAN IV and its options included three one-dimensional geometries; equations of state were created for a number of materials; and the DTF-IV transport calculations were incorporated for calculating the displacement reactivity feedback. The PAD code used a finite differencing scheme to solve for the state variables that describe the thermodynamics and hydrodynamics during a transient. The code was validated by calculation of the experiments Godiva [8], KIWI-TNT [9], the SNAPTRAN [10] series of experiments, and the KEWB [11] series.

4.2.2. Present

Due to the difficulties of running the PAD code running on more modern computers, the MRKJ Reactor Transient Code is being developed. The MRKJ code uses the same programming architecture as the PAD code but has some improvements. The MRKJ code is written in FORTRAN 77 which makes the code more portable to modern computing machines. It utilizes the one-dimensional discrete ordinance transport code ONEDANT [12] to perform the neutron transport calculations. The library of cross sections used in the ONEDANT calculations is a Hansen-Roach 16-energy-group cross section set with 167 isotopes. The larger library of isotopes increases the number of materials available to model different kinds of transient nuclear systems. (Note: Other cross section libraries compatible with ONEDANT could be used with some minor modifications of the MRKJ code.)

The ONEDANT discrete ordinate neutron transport calculations are done using a model that assumes spherical geometry and uses a discrete ordinance order of 32. Each defined coarse mesh region is modeled as a homogeneous material mixture. The coarse mesh region size and the number of fine mesh points used in each region can vary from problem to problem. The MRKJ code uses the time absorption calculation (alpha) option of the ONEDANT code and determines the power distribution of the system by extracting the regional fission rates from one of the ONEDANT output files.

The model and equations used by the MRKJ code to solve for the thermodynamic and hydrodynamic state variables during a transient are essentially the same equations used by the PAD code. The MRKJ code solves for the state variables by treating the analysis as an initial value problem. The thermodynamic/hydrodynamic model assumes no heat transfer between adjacent coarse mesh regions. This assumption is based on the fact that the rate of energy deposition due to fission is much, much larger than the rate of heat conduction between regions because the characteristic time scale for energy deposition from local fissions is much shorter than the characteristic time scale for heat conduction between regions. An equation can be solved for the power of the system as a function of time; an energy balance equation can be used to find the temperature of each region; an equation of state appropriate for the material(s) is used to relate the pressure and temperature in each region; equations of motion are used to determine the regional boundary movements due to pressure differences between adjacent regions. These equations are

** This code was created before the naming of codes was in vogue.

written as a system of first order ordinary differential equations and solved simultaneously using a fourth order Runge-Kutta [13] integration scheme.

The flow of calculations in the MRKJ code is very similar to the PAD code (see Fig. 4.5 for flow chart). Macroscopic material physical data (specific heat, bulk modulus, and nominal material densities, for example) and initial state variable values (temperature, pressure, power, boundary velocities, for example) for each region are read into the code for calculating the thermodynamic and hydrodynamic properties of the system during a transient. Geometric data (coarse mesh spacing and number of fine mesh points, for example) and microscopic physical data (constituent atom densities, for example) for each region are read in for the ONEDANT calculation. For calculational simplicity, the ONEDANT coarse mesh regions are defined to be the same as the thermodynamic/hydrodynamic coarse mesh regions. Initially, ten thermodynamic/ hydrodynamic calculational cycles are performed per time absorption calculation. The size of the code time step and number of thermodynamic/ hydrodynamic calculational cycles per time absorption calculation are adjusted depending on a differential magnitude change of a predetermined state variable (usually the volume) during a transient. Values for the state variables are conveniently written to output files for analysis and plotting.

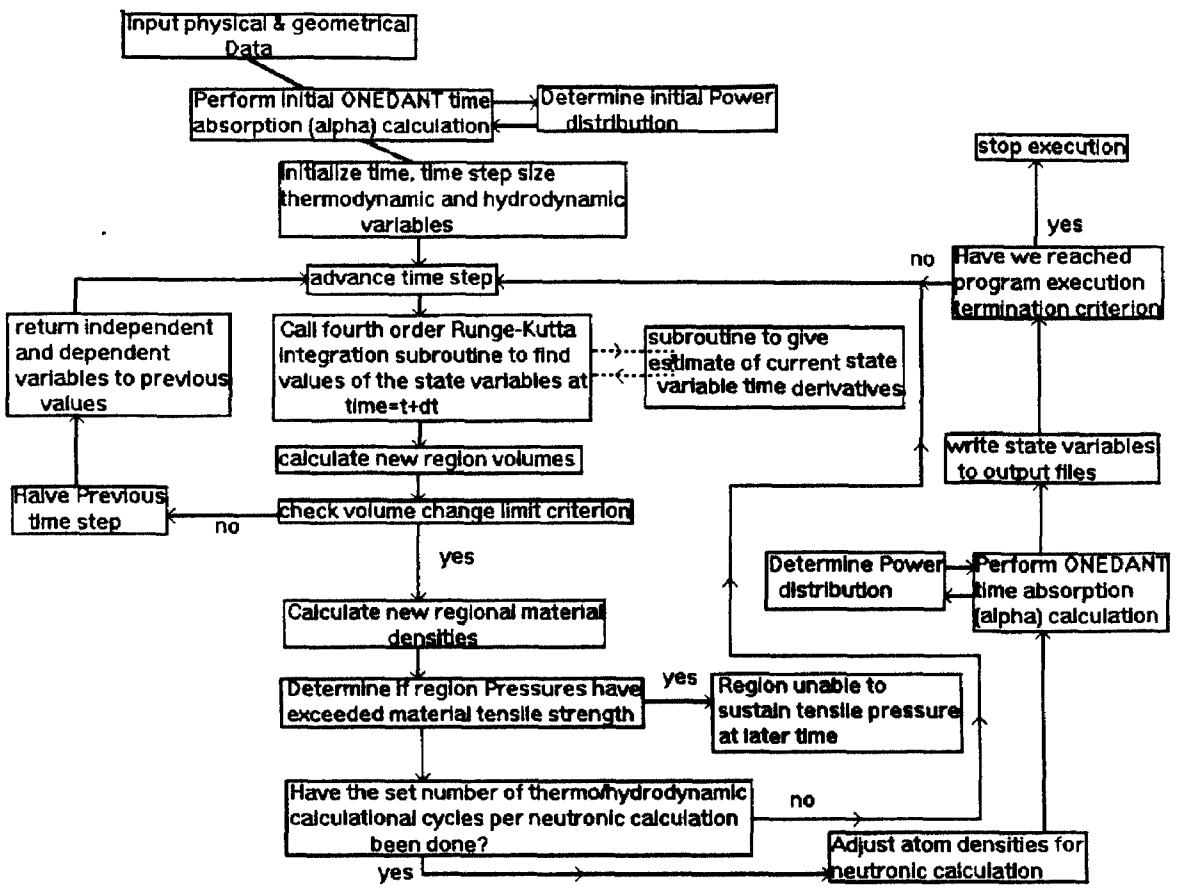

Figure 4.5. Basic flow chart of calculations in the MRKJ reactor transient code.

Similar to the PAD code, the MRKJ code gives estimates of the fission yield and the kinetic energy yield of a transient. The temperature, pressure, boundary location, and boundary velocity are calculated for each coarse mesh region for each time step until a predetermined code termination criterion is met. The values of the yields and state variables help determine if damage occurs to an assembly during the transient being analyzed. The MRKJ code results are consistent with previous PAD results predicted for the Lady Godiva assembly and are in good agreement with experimental results from the Lady Godiva assembly. Further development is underway for comparison with the KIWI-TNT excursion and other nuclear systems.

For analysis of the Lady Godiva assembly, the following equation of state was used [14]:

$$\rho = C_1(T - T_0) = C_2(\rho - \rho_0)$$

where

$$C_1 = \alpha B \text{ and } C_2 = \frac{B}{\rho}$$

and

T= Material temperature (T_0 = reference temperature)
ρ = Material nominal density (ρ_0 = reference density)
α = Material coefficient of expansion
B = Material bulk modulus

This equation of state is a function of the velocity of sound through the material by the relation

$$B = \rho V_s^2$$

where

V_S = velocity of sound through the material.

Some typical results from the MRJK code for a Lady Godiva type assembly are shown below in Figs. 4.6 through 4.11. This assembly was made of uranium metal enriched to 93.2 % U-235 with a radius of 8.8180 cm. A typical transient would be initiated with a step insertion of reactivity and an initial power level of 100 W. The initial alpha value for this transient was 1.15 x 10^5 gen/s. The power level would rise depositing energy into the system at a rate exponentially proportional to the time absorption (alpha) constant of the system. The temperature rise of the material would generate thermal stresses that cause the material to expand and contract. The material expansion is the reactivity displacement feedback mechanism that terminates the transient. If the thermal stresses exceed a material's tensile yield strength (or breaking pressure) in a region, the region is considered broken and this leads to an estimate of the kinetic energy generated during a transient. If during a transient no regions are broken, a ringing effect of the outer surface is predicted (see Fig. 4.11) that has been observed experimentally [15].

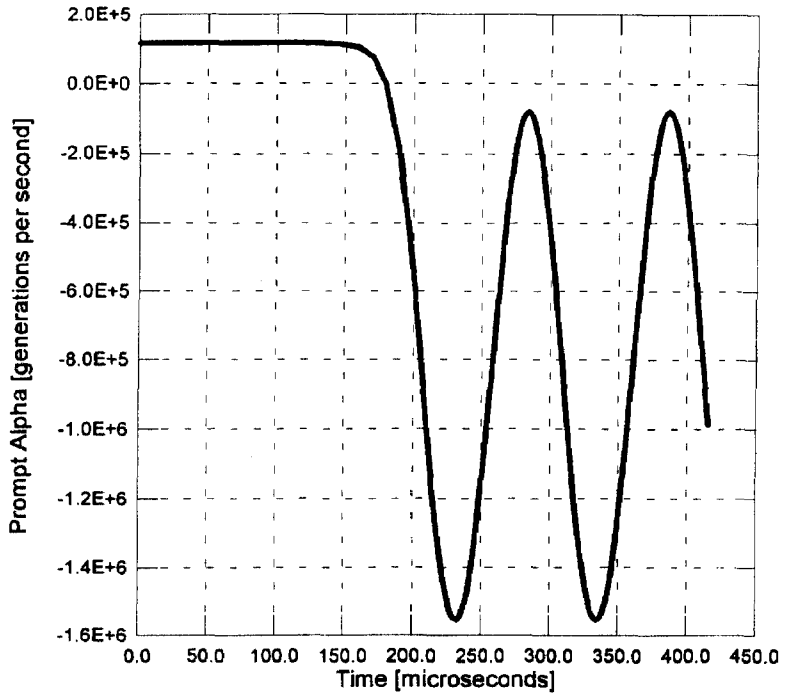

Figure 4.6. The prompt-alpha-versus-time behavior of a Lady Godiva assembly of radius 8.8180 cm and initial power level of 100 W as predicted by the MRKJ code.

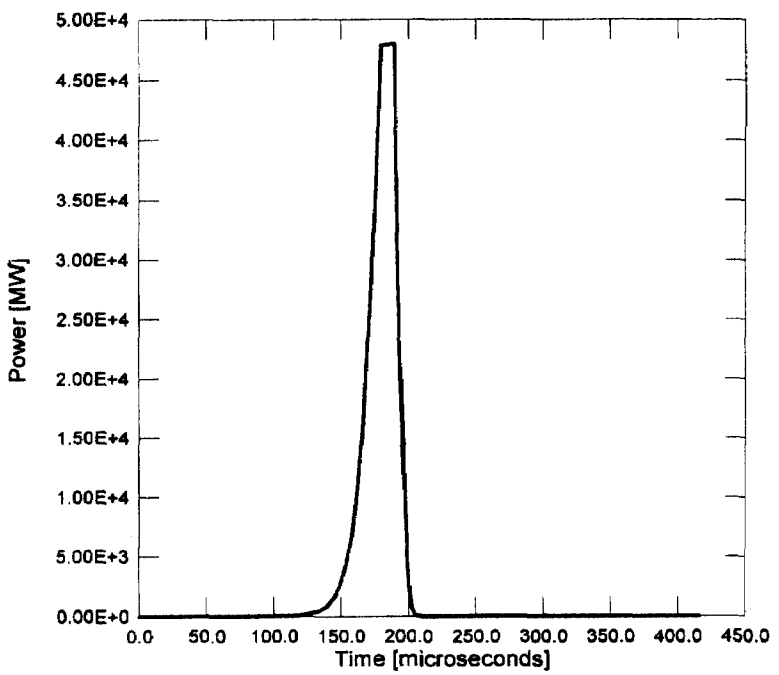

Figure 4.7. Power level versus time for a Lady Godiva assembly of 8.8180 cm and initial power level of 100 W as predicted by the MRKJ code.

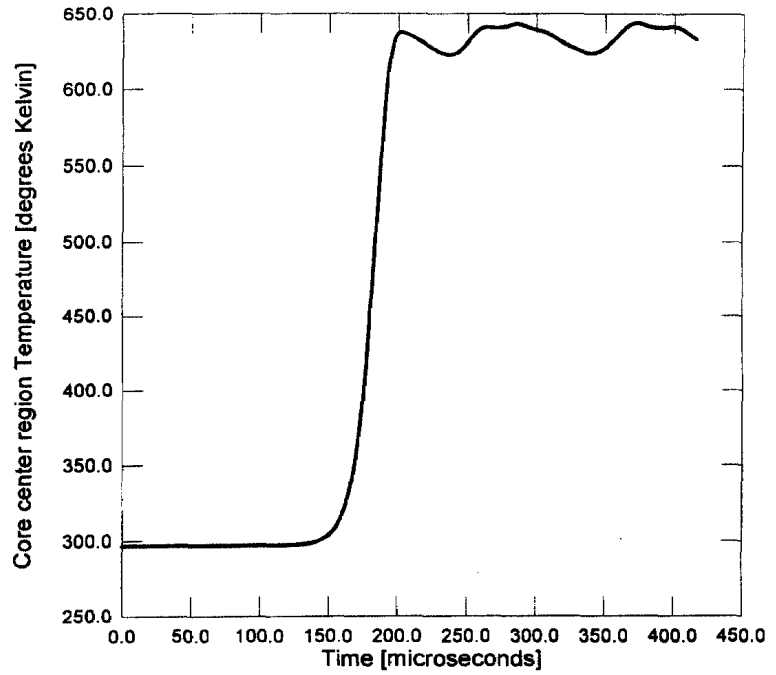

Figure 4.8. Center temperature versus time for a Lady Godiva assembly of radius 8.8180 cm and initial power level of 100 W as predicted by the MRKJ code.

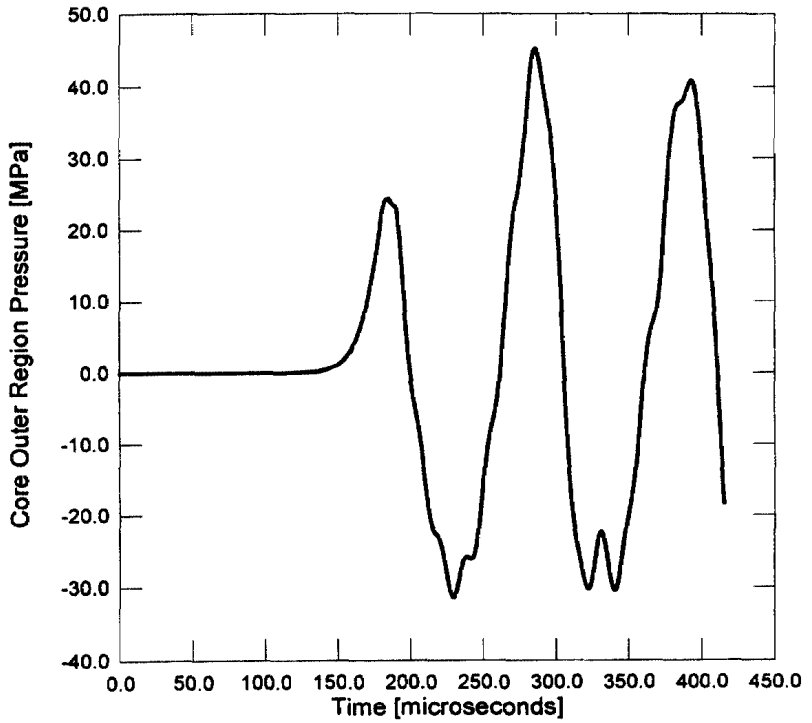

Figure 4.9. Outer region (near surface) condensed pressure versus time for a Lady Godiva assembly of 8.8180 cm and initial power of 100 W as predicted by the MRKJ code.

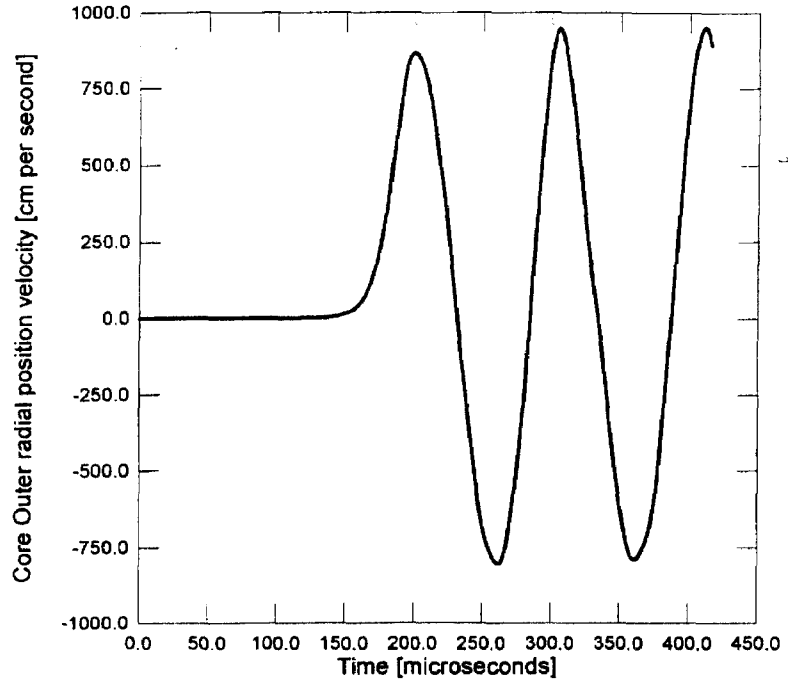

Figure 4.10 Outer radial position (core boundary) velocity versus time for a Lady Godiva assembly of radius 8.8180 cm and initial power level of 100 W as predicted by the MRKJ code.

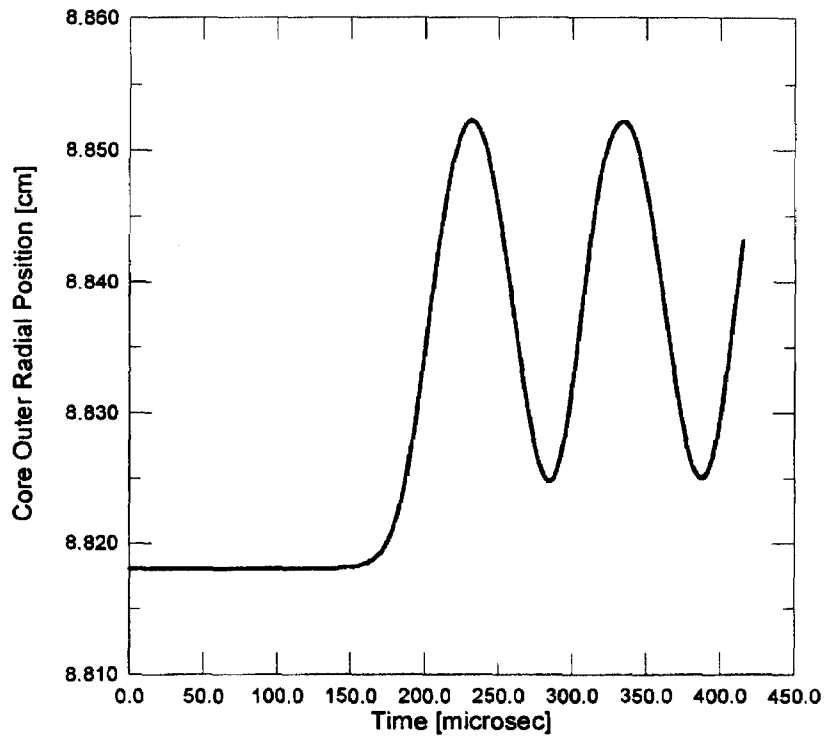

Figure 4.11. Outer radial position (core boundary) versus time for a Lady Godiva assembly of radius 8.8180 cm and initial power level of 100 W as predicted by the MRKJ code.

A similar model was used to study the dynamics of critical homogeneous mixtures consisting of plutonium and silicon dioxide or plutonium and Nevada Tuff ("dry" cases, no water). Worst case scenarios as identified by Sanchez et al., [19] were analyzed to determine total fission energy generated and kinetic energy yield during an excursion. Preliminary results for the total fission yield of such systems are being examined, but essentially no kinetic energy yield is being found. Further development is underway to examine the dynamics of the postulated three component autocatalytic systems (fissile material, diluent, silicon dioxide or Nevada Tuff, and water) [16]-[18].

References

1. R.B. Lazarus, W.R. Stratton, and T.H. Hughes, *Computing Methods in Reactor Physics* (Gorden and Breach, NY, 1968) p. 513.
2. R.D. Richtmeyer, "Radiation Hydrodynamics," Los Alamos Scientific Laboratory report LA-591-MS (July 22, 1947).
3. R.E. Peterson, "Lady Godiva: An Unreflected Uranium-235 Critical Assembly," Los Alamos Scientific Laboratory report LA-2029 (April 1956).
4. C.G. Chezem and W.R. Stratton, "RAC, A Computer Program for Reactor Accident Calculations," Los Alamos Scientific Laboratory report LA-2920 (January 1963).
5. D.M. Peterson, W.R. Stratton, and T.P. McLaughlin, "PAD: A One-Dimensional Coupled Neutronic Thermodynamic-Hydrodynamic Computer Code," Los Alamos Scientific Laboratory report LA-6540-MS (December 1976).
6. K.D. Lathrop, "DTF-IV, A FORTRAN-IV Program for Solving the Multigroup Transport Equation with Anisotropic Scattering," Los Alamos Scientific Laboratory report LA-3373 (1965).
7. G.E. Hansen and W.H. Roach, "Six and Sixteen Group Cross Sections for Fast and Intermediate Critical Assemblies," Los Alamos Scientific Laboratory report LA-2543-MS (December 1961).
8. T.F. Wimett, " Time Behavior of Godiva Through Prompt Critical," Los Alamos Scientific Laboratory report LA-2029 (April 1956).
9. Roy Reider, "Kiwi-TNT Explosion", Los Alamos Scientific Laboratory report LA-3351 (July 1965).
10. R.R. Johnson, "Snaptran 10A/2 Kinetics Testing and Destruct Reactor Experiments," North American Aviation report NAA-SR- 11906 (July 15,1966) .
11. M.S. Dunenfield and R.K. Stitt, "Summary Review of the Kinetics Experiments on Water Boilers," American Aviation report NAA-SR-7087 (1963).
12. R.E. Alcouffe, R.S. Baker, F.W. Brinkly, Jr., D. R. Marr, R.D. O'Dell, and W.F.Walters, "DANTSYS: A Diffusion Accelerated Neutral Particle Transport Code System," Los Alamos National Laboratory report LA-12969-M (June, 1995).
13. M.K. Jain, *Numerical Solution of Differential Equations*, 2nd ed. Halstead Press, a division of John Wiley & Sons, Inc., New York, 1984 p. 31.
14. W.R. Stratton, L.B. Engle, and D.M. Peterson, "Energy Release from Meltdown Accidents," *Trans. Am. Nucl. Soc.*, **17**, 362 (1973).

15. T.F. Wimett, "Dynamics and Power Prediction in Fission Bursts," *Nuclear Science and Engineering* **110**, 209-236 (1992).

16. C.D. Bowman and F. Venneri, "Nuclear Excursions and Eruptions from Plutonium, and Other Fissile Material Stored Underground," Los Alamos National Laboratory, November 22, 1994, draft report.

17. C.D. Bowman and F. Venneri, "Criticality Issues for Thermally Fissile Material in Geologic Storage," Los Alamos National Laboratory document LA-UR-95-504 (January 1995).

18. C.D. Bowman and F. Venneri, "Underground Autocatalytic Criticality from Plutonium and Other Fissile Material," Los Alamos National Laboratory document LA-UR-95-4022 (January 1995).

19. R. Sanchez, W. Myers, D. Hayes, R. Kimpland, P. Jaegers, R. Paternoster, S. Rojas, R. Anderson, and W. Stratton, "Criticality Characteristics of Mixtures of Plutonium, Silicon Dioxide, Nevada Tuff, and Water," Los Alamos National Laboratory document LA-UR-95-2130 (1995).

5.0 DOSIMETRY

5.1. Characterization of Neutron Spectra Produced by Godiva and SHEBA for Dosimetry Applications

W.H. Casson, R. E. Anderson, K. B. Butterfield, C. C. Cappiello, R. R. Paternoster, and R. G. Sanchez

There is a continuing erosion of available facilities in the United States where the capability of producing neutron fields, which have characteristics different from the commonly available isotopic based sources, are available to all types of users. From 1960 to 1987, the Health Physics Research Reactor(HPRR) in Oak Ridge provided a series of standard fields which were reproducible and which adequately mimicked radiation fields found in work environments such as those around nuclear power reactors, weapons production facilities, storage facilities, and experimental areas. This facility was used not only by U.S. organizations but was known world-wide for excellence in neutron calibrations. The Oak Ridge program was generously supported at that time by DOE-OHER. The essential components of this facility have been reproduced and expanded at the LACEF facility.

The Godiva assembly, which has the same fuel geometry as HPRR, is capable of producing several of the spectra used in that program. In addition, the SHEBA assembly provides a unique neutron field applicable to the many process facilities that handle fissile materials in solution. The immediate application of these capabilities is in the area of accident dosimetry. Reference fields have been characterized with respect to both absorbed dose rate and neutron spectra produced by four shielding configurations using Godiva and the free field of SHEBA giving the LACEF facility five unique standard fields for dosimetry testing. These shielding configurations use the shields that were used at the Oak Ridge facility. Shields are available for at least four additional configurations.

Neutron spectra were measured using a set of nine Bonner spheres based on a spherical ^{3}He detector system. The use of multi-sphere spectroscopy is difficult because the solutions to the unfolding algorithms are not unique. It is difficult to ascertain whether the convergence is toward a reasonable spectrum related to the actual one or if the system converged to a false solution. In this situation, the problem was avoided by using spectra derived for HPRR and verified through many years of accumulated experimental data. The resulting spectra, Fig. 5.1, deviated from the HPRR spectra in ways that were expected, i.e., there was a slightly increased high-energy neutron distribution due to the smaller size of the Godiva device. The intermediate neutron energy population was increased at energies expected due to increased scatter from the kiva structure. HPRR was housed in a light metal, low-scatter facility. These factors provided a high level of confidence in the derived results.

The SHEBA neutron spectrum is not similar to the HPRR or any other well-characterized and published spectrum. The starting spectrum was chosen to be a modified fission spectrum. Several modifications to that spectrum were required before a consistent picture started to emerge. Even so, the final spectrum, Fig. 5.2 does not have the same high level of confidence. To ensure that the spectrum resulted in a reasonable absorbed dose calculation, the absorbed dose was measured using a tissue-equivalent proportional counter which is optimized for health physics measurements. Also independent measurements were taken with TLDs and an electronic dosimeter system. In all cases the results were consistent with the derived spectrum. It should be noted that the Bonner sphere system does not have high resolution in the region from about 3 to 5 MeV and above. Because the absorbed dose calculation is not very sensitive to the neutron energy distribution in this region, the resulting error in the spectrum, the response of most activation foils and dosimeters, and the conversion to absorbed dose or dose equivalent can be considered insignificant relative to the error in the response functions or conversion factors. Due to the possibility that some application may need detailed

information in this region, and to the desire to have a complete knowledge of the spectrum, NE213 measurements are to be conducted to provide a more detailed and complete spectrum.

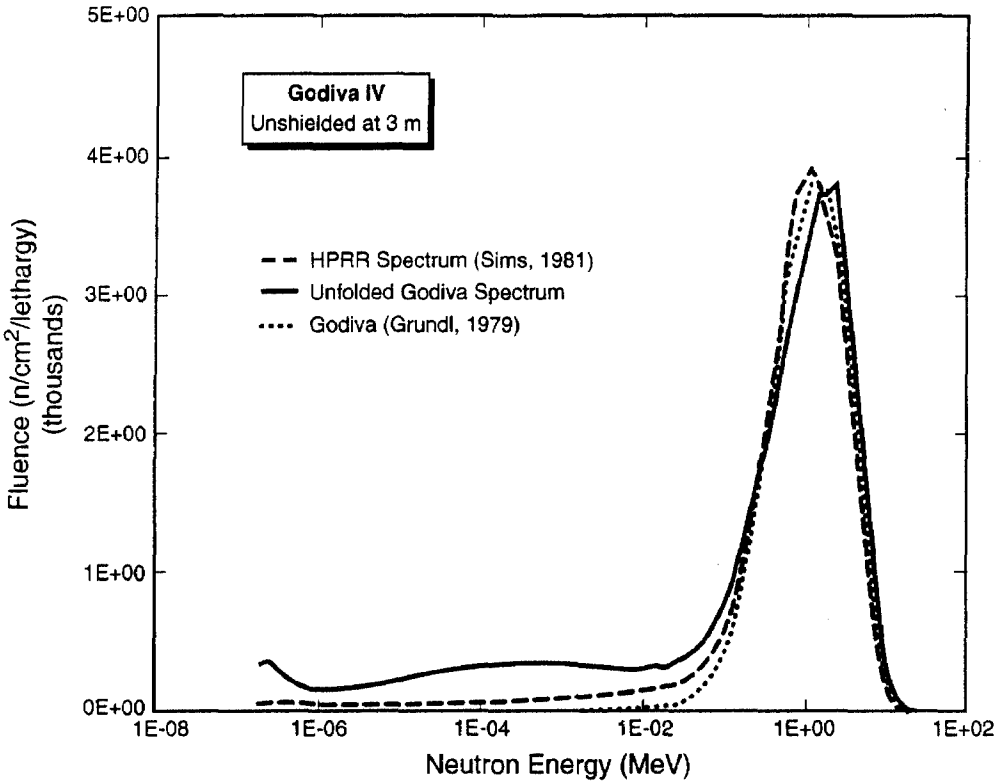

Figure 5.1. Bare Godiva and HPRR neutron spectrum.

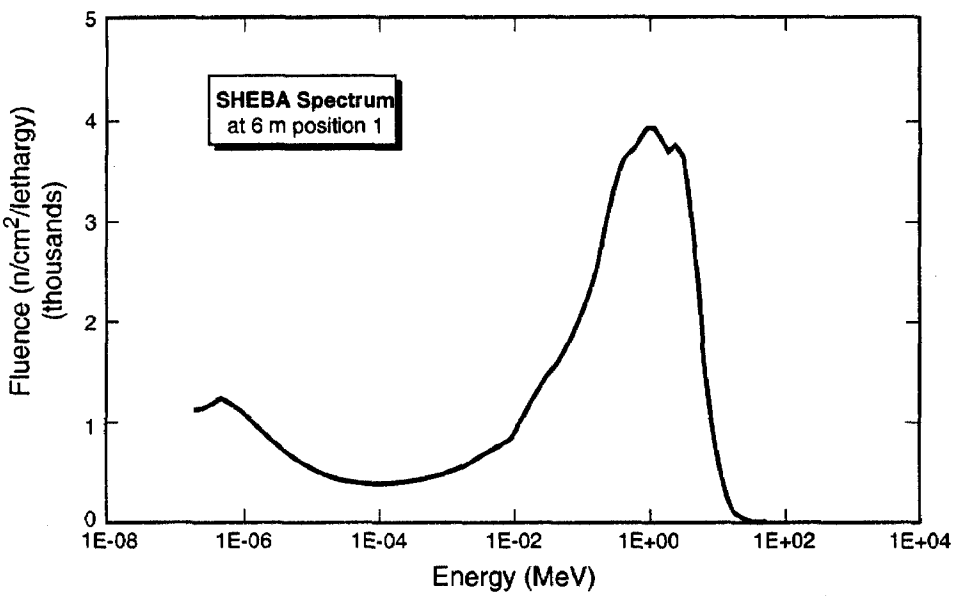

Figure 5.2. SHEBA neutron spectrum at 6 m.

Measurements of the neutron spectrum using Bonner spheres or any other available spectroscopy system requires operation at low power levels. The spectrum at high power or burst mode should be the same according to theory and previous operating experiences. However, this can be crudely verified by using threshold detectors and activation foil techniques. A threshold detector set has been requested from Oak Ridge which was used extensively with the HPRR and at the Nevada Test Site. The response of this system will be recalculated using MCNP and other appropriate techniques. This system will then be used to verify the neutron spectrum from a high-level burst and to provide additional verification of the calculated absorbed dose delivered during a burst as a function of ΔT and additional verification of the reference sulfur pellet system which has been installed on both machines for dosimetry purposes. This effort should have implications for the Hiroshima dosimetry, since this system was used to derive the transport equations used to determine doses to individuals in all the dose studies.

5.2. Conduct of the 23rd Nuclear Accident Dosimetry Intercomparison Study

W. H. Casson, R. E. Anderson, K. B. Butterfield, C. C. Cappiello, R. R. Paternoster, and R. G. Sanchez

Nuclear accident simulations were conducted using the HPRR at Oak Ridge for approximately 25 years. The last Oak Ridge study was conducted in 1985, just prior to the shutdown of that facility. Los Alamos National Laboratory has recognized the value of these studies and has supported the resumption of the studies at LACEF using the Godiva IV and SHEBA II assemblies. Significant work was accomplished toward this end through the cooperative efforts of the Environmental, Safety and Health Division (ESH) and NIS-6. A successful proposal was then submitted to EH to conduct a DOE internal intercomparison. The study was scheduled and invitations were made to appropriate facilities. Delays in the restart of the Godiva assembly resulted in a very short schedule for initial startup tests and the dosimetry measurements described in the previous section. Thanks to the dedicated efforts of several individuals, all the required measurements and calculations were completed along with meeting all operational requirements in time for the first day of the intercomparison. There were 17 individual participants from 9 facilities in the intercomparison. A staff of about eight was required to conduct the study along with many other support and facility personnel. Major potential problems with security and radiation protection were addressed during this study. Each issue was identified and addressed thanks to the outstanding efforts of a few of the support personnel involved. All scheduled operations took place as planned without any reduction in security, personnel safety, or experimental intent.

During the intercomparison study, seven operations were conducted, four using Godiva and three with SHEBA. All the SHEBA (see Fig. 5.3) runs were conducted without any shielding or other neutron field modifiers. The first run with SHEBA was a relatively low-power run, which gave the participants an opportunity to set up and test the equipment and become familiar with the operating procedures. The second run was identical to the first except the delivered dose was increased by a factor of 10. This was treated by the participants as an accident scenario. Equipment was set up in the NIS "schoolhouse" so that the activation foils and other activated materials could be measured without removing the material from the site. All the participants were provided with the neutron spectrum and the delivered absorbed dose so that they could evaluate their techniques and algorithms during the process. The next operation, conducted with Godiva in a free-field configuration (see Fig. 5.4), provided a large absorbed dose with a nearly unmodified fission-type spectrum. The remainder of the operations used some method or technique to alter the spectrum or field characteristics to more accurately simulate probable accident scenarios. For example, the next operation used Godiva with a 20-cm concrete shield. This simulated a typical facility wall between the accident and the victim. Next SHEBA was operated in a long period free-run condition, which resulted in a longer exposure time. This removed an effective time mark from the analysis, which makes some algorithms dysfunctional due to the dependence on decay correction calculations.

AN IMAGE IS NOT AVAILABLE FOR THIS PAGE, THE COMPLETE DOCUMENT IS AVAILABLE IN THE LIBRARY

AN IMAGE IS NOT AVAILABLE FOR THIS PAGE, THE COMPLETE DOCUMENT IS AVAILABLE IN THE LIBRARY

Table 5.2. Summary of results for NAD-23 giving reported doses in RAD with error from reference shown in parentheses.

Assembly	Lab A	Lab B	Lab C	Lab D	Lab E	Lab F	Lab G
SHEBA	12 (9)	15.7 (43)	10.4 (5)	11.35 (3)	13 (18)	11.9 (8)	14 (27)
SHEBA	114 (5)	107 (1)	92 (15)	133 (23)	162 (50)	83.1 (23)	127 (18)
Godiva	272 (36)		196 (2)	166 (17)	284 (42)	211 (5)	84 (58)
Godiva	32 (6)	32.9 (3)	31 (9)	47 (38)	39 (15)	47.5 (40)	35 (3)
SHEBA	104 (11)	126 (34)	102 (8)	106 (13)	130 (38)	91 (3)	101 (7)
Godiva	32 (23)	30 (15)	24 (8)	35 (35)	30 (15)	28.5 (10)	40 (54)
Godiva	48 (19)	49 (17)	119 (102)	34 (42)	52 (12)	77.6 (31)	22 (63)
Average Errors	18	9*	27	31	27	22	39

Averages of the errors are shown in parentheses for all seven reported participants for the given configuration. Average errors, for each participant, of the results from the second SHEBA run and all Godiva runs.

* The first Godiva result was not available due to an operational delay.

As a result of the intercomparison study, facilities required to maintain the capability of assessing the personnel absorbed dose in the event of a criticality accident were given an opportunity to test their systems, fine-tune the algorithms, and train personnel in the complex data analysis required. Most of the participants had not participated in an exercise of this type. This is strongly reflected in the results (Note: DOE requires the capability of reporting personnel neutron absorbed doses within ±30%). The data from the previous intercomparison indicates that the ability to perform this type of assessment improves with experience and only meets the DOE requirements after several such exercises. It is for this reason that it is planned to continue the NAD studies at LACEF and hoped that DOE recognizes the value and continues its support.

6.0 TRAINING

6.1. Training Activities

Nuclear Criticality Safety Classes

R. E. Anderson, J. A. Bounds, K. B. Butterfield, C. C. Cappiello, T. P. McLaughlin (ESH-6), R. R. Paternoster, R G. Sanchez, and S. Vessard (ESH-6)

The Nuclear Criticality Safety Class has been offered slightly more often than once a month since the facility restart in June 1991. Listings of the personnel who have attended the training between April 1 1995, and Sept. 30, 1995, are presented in Table 6.1. This training is intended primarily for nuclear materials handlers and supervisory personnel in the DOE complex, with occasional participation by persons from outside the DOE. To maintain a high level of instructional quality, attendance is limited to an enrollment of approximately 15 persons per class.

During the class, the students engage in hands-on manipulation of nuclear material and build a stack of uranium foils and Lucite plates to achieve a multiplication of approximately 4. The students then continue to add to the stack, which is assembled by remote control, until a multiplication of approximately 125 is achieved. Finally, the students observe a critical assembly operation (currently this is done with the Flattop assembly) and are allowed to operate the assembly under direct supervision of LACEF personnel.

This training is a highly effective demonstration of the principles used to determine the safe handling procedures for nuclear materials in real-world situations.

Table 6.1. Attendance at Nuclear Criticality Safety Courses March 1995 - October 1995.

	Dates	Format	LANL Participants	Non-LANL Participants
1.	May 23-25, 1995	3-day	2	15
2.	June 20-21, 1995	3-day	0	17
3.	Aug. 21-22, 1995	5-day	0	13
4.	Sept. 12-14, 1995	3-day	2	10
5.	Sept. 26-28, 1995	3-day	2	12
	Totals		6	67

7.0 DOCUMENTATION

7.1. Documentation

7.1.1. Completion of Draft TSRs

In accordance with DOE Order 5480.22, a set of draft Technical Safety Requirements was submitted on February 25, 1995. The document was issued as a Los Alamos controlled publication: LA-CP-95-11. When reviewed and approved by the DOE, these will replace the current Technical Specifications contained in LA-6016-SOP, Rev. 2 (October 1987). The new TSRs provide a broad envelope for operation of the LACEF and the Hillside Vault consistent with the new SAR. The new TSRs bring new capabilities and new requirements. Some of these are as follows:

- Specifications for entering radiological control areas surrounding the kivas during critical operations,
- Specifications to operate assemblies outside,
- Reduced requirements for assembly operations, and
- Additional requirements for surveillance procedures.

During the second half of FY95 initial comments on the draft TSRs were received from DOE/AL. Comments were resolved and a revised draft was submitted to DOE/AL on September 26, 1995.

7.1.2. Updates to LACEF Training Plan

LACEF has come a long way in operator training implementation, formalization and refinement in 1995. The LACEF Training Plan has been revised to meet the requirements of revised DOE Order 5480.20A and a Training Implementation Matrix (TIM) has been submitted to DOE/AL for approval. Working closely with the Laboratory Training and Development office, job/task analysis has lead to the design of individual training plans for each position in LACEF, including LACEF-specific support positions. These training plans have been assigned to appropriate personnel and each plan has been completed.

1995 has seen the development of a LACEF Training Reference Manual to document implementation of the learning objectives in lesson plans for LACEF training. It was consequently used as a self-study guide for training that meets DOE Order 5480.20A for certifying eleven critical assembly operators (Crew Members) and 4 senior critical assembly operators (Crew Chiefs) in July 1995.

A more formalized oral testing board has been established and the oral boards are documented. OJT for operating specific critical assembly machines has become more formalized as a documented qualification method that is implemented after the individual is certified to be an operator by written examination and oral testing. All of the Crew Members are qualified on the Flattop Assembly, and 10 are qualified to operate Comet as well. 7 are qualified to operate Big Ten, 5 to operate SHEBA, 5 to operate Godiva, 3 to operate Skua, 2 to operate Mars, and 1 to operate Planet (Mars and Planet are not being operated at this time).

The final step for implementation of the LACEF Operator Training process is to complete development of a test question bank with expected answers. LACEF personnel has been asked to submit questions that will be evaluated by subject matter experts at the site for support of the learning

objectives for the training. Questions that meet the criteria will be placed in a test question bank for generation of a test with randomly chosen questions. Questions on some topics will be weighted to be certain that those more important topics appear on the test each time it is presented. The test question bank will be validated by Laboratory Training and Development before it is used to certify operators. Completion of this activity is expected by September 1996.

The Los Alamos Critical Experiments Facility Receives the Donald G. Summers LANL QA Award

This has been a very exciting year for the Los Alamos Critical Experiments Facility (LACEF). LACEF is finally reaping rewards from a journey we embarked upon from the low of a shutdown in 1990, to receiving noteworthy practices in QA during the 1995 DOE Pilot Audit and winning the Don Summers LANL QA Award in 1995. During this year LACEF has also been able to issue a new, approved SAR and the accompanying Technical Safety Requirements.

Dramatic changes in DOE during the late 1980's resulted in increased regulatory compliance issues. This change came suddenly to LACEF with a shutdown order to address informality of operations having safety implications.

One of Group Management's responses to this problem was to hire a full-time Quality Assurance Engineer with expertise in regulatory compliance and documentation of compliance activities who would report directly to the Group Leader and whose informal job description was "Get the Group out of trouble, and then keep the Group out of trouble".

After a survey of current conditions, the first step to correcting the problems at the facility was for the Group to write and approve a Quality Assurance Plan. The generation of several detailed administrative QA procedures followed closely to provide guidance for implementation of formality of operations in areas such as document control, design control, configuration management, nonconformance and occurrence reporting, and formal training for critical assembly operators as well as general facility specific ES&H Training. These procedures were based on how the work was actually being done and were generated by the personnel in LACEF and the NIS-6 Engineering Support Team who were responsible for the work. Facility personnel attended several training sessions on quality assurance, regulatory compliance, formality of operations and the implementation of the plan. Several databases were designed and operated to track progress on the action items that were the results of the implementation of the plan.

Implementation of this plan and the associated administrative procedures was enhanced when facility personnel began to see results in the form of reduced assessment findings where activities were formally described and documented. Additional focus on compliance activities and fine-tuning of management plan implementation has been the result of hiring a very capable Facility Manager in August of 1994.

The operating philosophy of the group is now based on success in being proactive in implementing formality of operations by thoroughly documenting how they implement DOE Orders and Rules, use National Standards, and comply with national and state environmental laws. Strict compliance to Group procedures and policies is supported and expected by line management.

When DOE converted their regulatory compliance orders into Code of Federal Regulation rules, and 10 CFR 830.120, "Quality Assurance" was approved, the quality assurance plan and administrative procedures were fully implemented and operating at TA-18. The Quality Assurance

Plan has evolved into the "NIS-6 Management and Conduct of Operations Plan" to reflect the real nature of a QA plan where excellent management of an operation is the bottom line.

LACEF participated in the Laboratory's "rule compliance" self-assessment exercises for DOE/AL and issued a matrix showing that LACEF had fully implemented their Quality Assurance Plan and is continuing to improve and refine management and conduct of operations at the facility. The activities described in this matrix were assessed by DOE/AL in December of 1994 and the matrix was approved by DOE/AL in June 1995. In addition, a similar matrix addressing group implementation DOE Order 5480.19, "Conduct of Operations" was submitted to DOE by ESH-IO in February of 1995.

In the future, LACEF is looking to expand and enhance their experimental capacity by taking on new challenging experiments for their critical assembly machines and research personnel. This means that the "Management and Conduct of Operations Plan" and associated administrative procedures will necessarily have to be constantly reviewed and improved to accommodate those changes in mission and processes. Meanwhile, the proactive philosophy of the LACEF Team and Engineering Support Team, the support of NIS-6 Management, and the efforts of everyone involved in making sure that work at TA-18 is done right and documented, have made it possible for LACEF to be named the Donald G. Summers QA Award winners at Los Alamos National Laboratory for 1995.

Appendix

Criticality Characteristics of Mixtures of Plutonium, Silicon Dioxide, Nevada Tuff, and Water

R. Sanchez, W. Myers, D. Hayes, R. Kimpland, P. Jaegers,
R. Paternoster, S. Rojas, R. Anderson, and W. Stratton

EXECUTIVE SUMMARY

The major objective of this study has been to examine the possibility of a nuclear explosion (and evaluate this event if it is possible) should fifty to one hundred kilograms of plutonium be mixed with SiO_2, vitrified, placed within a heavy steel container, and buried in the material known as Nevada tuff. To accomplish this objective, we have created a survey of the critical states or configurations of mixtures of plutonium, SiO_2, tuff, and water and examined these data to isolate those configurations that might be unstable or autocatalytic. The survey of critical data now exists and is published herein. We identify regions of criticality instability with the possibility of autocatalytic power behavior (the existence of such autocatalytic phenomena is not new). Autocatalytic power behavior is possible but improbable, for a very limited range of wet systems. A quantitative and conservative evaluation of the fission power behavior of these autocatalytic mixtures shows that no explosion should be expected.

Three basic modes of mixing plutonium, tuff, SiO_2, and water were postulated in Refs. 1, 2, and 3. These are as follows

1. Expansion of the plutonium into a larger mass of Nevada tuff (or SiO_2) under dry conditions,
2. Movement of water into a volume of plutonium tuff (or SiO_2) mixture of nearly any atom ratio of silicon to plutonium, and
3. Plutonium moving into a stratum of tuff (or SiO_2) that contains an appropriate amount of water.

Each of these scenarios requires a breach of the original container, disintegration of the vitreous log, and for cases 1 and 3, further movement and mixing of the plutonium into tuff (SiO_2).

Case 1 requires more plutonium to be stored than has been suggested; and if sufficient plutonium should be available, an extraordinary or impossibly rapid expansion of PuO_2 molecules at high velocity through large solid masses of tuff or SiO2 is also required. Criticality is possible, but highly improbable, given realistic assumptions for masses and compositions; autocatalysis requires additional unphysical assumptions. No explosion should be expected. It is specifically shown in a companion paper that no explosion results even with these assumptions for the only detailed scenario described in Refs. 1, 2, and 3.

Case 2 requires that the vitreous log disintegrates and that water enters the system. Mixing with more tuff (SiO_2) may or may not have occurred. This case would be the plutonium equivalent of the Oklo phenomenon of two or more billion years ago (Ref. 4). A critical system is possible, but autocatalysis is not possible, and an explosion is not possible.

Case 3 requires disappearance of the container, disintegration of the vitreous log, and movement of PuO_2 with or without SiO_2 into a stratum of tuff (SiO_2) that contains an appropriate amount of water. This process could lead to critical configurations that could be unstable with the possibility of an autocatalytic power response. Criticality constraints and constraints based on the amount of fissile mater-ial and water content of the tuff (SiO_2) severely limit the possibilities. Those remaining configurations have been examined for a worst case. A critical system is possible, and autocatalysis is possible, but no explosion should be expected.

This study has adopted highly conservative positions with respect to both nuclear and geologic assumptions. A more realistic treatment of nuclear assumptions is expected to severely constrain the

possibilities for criticality and autocatalytic behavior. The probabilities and even the possibilities of the several geologic and chemical phenomena and actions that must occur before a criticality study is even appropriate are not evaluated in this paper. These chemical and geologic considerations (studies underway, see Ref. 5) may eliminate the problem and the need for a criticality and dynamic study completely.

I. INTRODUCTION

The nuclear criticality characteristics of mixtures of plutonium, silicon dioxide and water (Part A) or plutonium, silicon dioxide, Nevada Yucca Mountain tuff, and water (Part B), have become of interest due to the appearance of recent papers on the subject (Refs. 1, 2, and 3). These papers postulate that if excess weapons plutonium is vitrified into a silicate log and buried underground, a self-sustaining neutron chain reaction may develop given sufficient time and interaction with the burial medium. Moreover, given specific geologic actions resulting in postulated configurations, the referenced papers state that nuclear explosions could occur with multi-kiloton yields (Ref. 1) or yields equivalent to hundreds of tons of TNT (Ref. 3). (References 1 and 2 are draft documents that were distributed widely; Ref. 3 has been submitted to a professional journal for publication.)

The objectives of this paper (and the companion papers on dynamics) are as follows:

1. To examine the possibility of a nuclear explosion (and evaluate this event if it is possible) should several kilograms of plutonium be mixed with SiO_2, vitrified, placed within a heavy steel container, and buried in the material known as Nevada tuff;
2. To establish the parameters (density, moderation, reflection, poisons, and dilution with non-fissile material) that determine when mixtures of Pu-239, SiO_2, and water (Part A) and mixtures of Pu-239, Nevada tuff, and water (Part B) are critical, i.e., are capable of sustaining a continuing neutron chain reaction without change of fission power;
3. To examine these data to find those configurations that may be unstable or "autocatalytic" (the critical state in which an increase in fission power leads automatically to a further increase of reactivity and, hence, greater fission power); and
4. To establish the restrictions or constraints on these data that are required by criticality physics, the amount of plutonium postulated to be stored, and possible water content in the Nevada tuff.

Given these conditions, the companion paper on dynamics will examine possibilities for and possible consequences of an uncontrolled fission power transient, using calculational methods that have been developed to study power transient dynamics of pulsed assemblies or reactors and criticality accidents.

Part A of this paper will concentrate on the pure SiO_2 diluent, while in Part B, criticality computations have been completed using the actual elemental composition of Nevada Yucca Mountain tuff (see Ref. 6). Tuff contains many elements, including neutron poisons, which place additional constraints on the postulated situations in Refs. 1, 2, and 3.

The calculations presented in this paper assume homogeneous spherical distributions with pure Pu-239 as the fissile material. This is a conservative assumption when dealing with static or near-static criticality phenomena because the critical masses for pure Pu-239 are substantially lower than those for U-235 and also lower than for weapons-grade plutonium. In addition, any significant heterogeneity of the plutonium is expected to reduce the reactivity of the system significantly (even enough to preclude criticality in some cases).

By critical, or the critical state, we mean that the system can just maintain an existing fission rate or power without change; by supercritical, we mean that the fission rate would be increasing; and by

subcritical, we mean that the fission rate, if it exists, would be decreasing to zero power or to a near-zero power if an intrinsic source were present in the material.

Additional critical mass data have been included for clarity and understanding.

Most of the computations in this paper have been completed by use of the ONEDANT neutron transport computer program (Ref. 7), a modern version of the classic system created by Bengt Carlson (Ref. 8). More details of models and computational methods are given in the Appendix.

II. NUCLEAR CRITICALITY—SIMPLE SYSTEMS

To introduce the discussion of nuclear criticality parameters for a three-component system, it is useful to begin with illustrations of the criticality properties of a simple two-component system that is more familiar than mixtures of plutonium, SiO_2 or tuff, and water. Thus, in Fig. 1, the critical mass of plutonium metal mixed with water is illustrated as a function of the density of plutonium in the water (Ref. 10). The mixture is idealized to be only metal and water; actual solutions of plutonium compounds would differ but little. Both water-reflected (20-cm thickness) and unreflected (bare) systems are shown. The general characteristics illustrated are similar for nearly all diluents of fissile material: U-235, U-233, or Pu-239. The initial effect of the diluent (water in this case) is to reduce the density of the plutonium, thus allowing greater neutron leakage and requiring a larger mass of fissile material to achieve the critical state. A maximum critical mass (about 9 kg for the reflected case) can be seen at a plutonium density of ~6 g/cm^3 (kg/L) where the moderating property of the hydrogen dominates the loss of neutrons due to leakage or absorption. As still more diluent is added, the moderating power of hydrogen causes the critical mass to decrease to a minimum value (about 500 grams at a plutonium density of 0.03 kg/L for the reflected case) at which point a balance is reached between the moderating and absorptive properties of the diluent. With more dilution, the absorption cross-section of hydrogen dominates, and the mass required for criticality increases until finally an asymptote is reached, which establishes the limiting density for dilution; both the mass and volume are unbounded. The limiting value of the density is an important property that will be useful in later discussions. For plutonium-water mixtures, the asymptote is at about 0.007 kg/L and, obviously, both the bare and reflected cases converge to this same value. These data are very well established by experiment (Ref. 13) and the computational scheme is well established by comparing calculational results with experimental results (Ref. 12).

The presence of water has a significant effect on the critical mass. It is this sharp dependence of the Pu-239 critical mass on the moderator content (in this instance, the hydrogen content) of the system that makes the analyses of criticality phenomena so complex. A wide variety of results are possible. For example, the critical mass of a plutonium metal ball with a water reflector is given in Table I as about 5.2 kg, while the critical mass of a plutonium solution with the same water reflector is about 0.5 kg. Under more unusual and extraordinary circumstances, (non-absorbing diluents and cryogenic temperatures) the critical mass might be significantly lower.

Illustrating the critical masses of fissile metals mixed in water in this manner is well established; to our knowledge, data similar to these were first calculated in late 1942 by J. Robert Oppenheimer (Ref. 14). In the 1950s nuclear criticality data were summarized and published by H. Paxton of Los Alamos and D. Callihan of Oak Ridge (the two architects of the science of criticality physics and safety, see Ref. 13), and this manner of presentation became common usage. These same data, however, can be presented in different formats to illustrate different criticality properties. In Fig. 2, the critical volume of Pu-239 in water is illustrated as a function of the plutonium density (the critical volume increases monotonically with decreasing plutonium density) and in Fig. 3, the critical mass is shown as a function of the critical volume. The data for Figs. 1, 2, and 3 are given in Table I.

Each representation is useful in understanding the influence of various parameters and in establishing conditions of nuclear criticality stability or possible instability. For example, if a slightly supercritical Plutonium-H_2O mixture should be created at a density just below the low-density asymptote (choose about 10 kg and a density of about 0.008 kg/L) the solution would heat and lose water, thus decreasing the volume and increasing the plutonium density. Given only these two effects, the system would now be at a very high reactivity and power would increase. However, any decrease of volume caused by water loss would be balanced by boiling and expansion, thus reducing

reactivity. The net result is boiling, just maintaining criticality. This would continue until the system is dry enough to be subcritical. An example is given in the Appendix of the companion paper on dynamics. This condition is often referred to as "unstable" or "autocatalytic." Another example of an interesting, although not unstable condition, is the region in Fig. 1 between densities of about 1.0 and 0.08 kg/L. If water, which is a diluent, moderator, and absorber, is added, a supercritical state is created. This same situation can be seen in Fig. 3 between volumes of about 3 and 8 liters where, if the volume should be increased by the addition of water, a supercritical state is created. However, this is not autocatalytic like the first example; thermal expansion, possibly with boiling, would reduce reactivity to return the system to subcriticality; little change of composition would occur.

Part A: Criticality Data
Plutonium, Silicon Dioxide, and Water

III. NUCLEAR CRITICALITY — OTHER MATERIALS

As was mentioned above, the general characteristics of Figs. 1, 2, and 3 can be seen when other materials (some good moderators and some indifferent moderators) are used as a diluent. Examples are illustrated in Fig. 4 in which the critical masses of plutonium diluted with SiO_2 and reflected by 100 cm SiO_2[†] and plutonium diluted with and reflected by 20 cm of water are presented. The critical mass data for U-235 diluted with and reflected by graphite (Ref. 15) are added for comparison. The numerical data for Plutonium-SiO_2 are given in Table II.

The general characteristics of these data are qualitatively similar, but the maximum and minimum critical masses differ by large factors as do the low-density asymptotes caused by water and graphite (a factor of 70). The importance of the asymptote is emphasized because its existence is independent of material but its value (in terms of the fissile material density) is very dependent on the material and its density and helps to limit the possibilities of underground critical states for the problem being investigated. The data describing U-235 diluted with graphite are included to illustrate the wide range of criticality possibilities.

For reference below, Fig. 5 presents the critical mass data of plutonium when mixed with and reflected by 100 cm of SiO_2 as a function of the critical volume. This figure is the analog of Fig. 3 for plutonium and water.

No experimental critical data are available to assure the correctness of the calculations for the Plutonium-SiO_2 system, except for the end point of unreflected plutonium metal. There are no integral tests of the silicon cross sections. In addition, for dry silicon and plutonium mixtures, many fissions take place primarily in the intermediate energy range (between 0.1 eV and 100 keV), where no integral tests for the plutonium fission cross sections exist. Thus, for these dry systems, calculations should be treated with some caution. However, because of the abundance of other experimental critical data for both fast and thermal plutonium systems (Ref. 13), the calculations for these wet plutonium-SiO_2 systems are expected to be reliable. We note that the study is, nevertheless, internally consistent and relative values of critical parameters are reliable. Critical radii, obtained by a different computer program, and cross sections are presented for comparison in the Appendix.

[†] These data, and later Pu-H_2O-Tuff data, are new and were taken for this study.

IV. CRITICAL DATA FOR PLUTONIUM-SiO_2-H_2O, —A THREE-COMPONENT SYSTEM

In Fig. 6, the reflected critical-mass data for Plutonium-H_2O and Plutonium-SiO_2 are reproduced from Fig. 4 along with the addition of critical data for Plutonium-SiO_2 mixtures in which water has been mixed in equal amounts in both the core and 100-cm reflector. The model for adding water assumes that the volume of water added displaces an equal volume of SiO_2 and plutonium. For this model, the densities of the plutonium and SiO_2 decrease with the addition of water. This is the three-component material postulated in Refs. 1, 2, and 3 that we wish to study in detail. (The plutonium-tuff-water systems will be discussed in Part B. In this latter discussion the displacement model and a "porosity" model will be considered.) The top curve describes dry Pu-SiO_2 mixtures reflected by 100-cm-thick dry SiO_2. The bottom curve is plutonium mixed with and reflected by a 20-cm-thick layer of water, while the intermediate curves are Pu-SiO_2 cores mixed with successively greater weight fractions of water and reflected by 100-cm-thick SiO_2 with the same weight fraction of water. The powerful moderating property of water is evident. The atom ratio of silicon to plutonium for each of the "wet" curves is indicated in Fig. 6 and this same ratio is held constant as more water is added. Thus, in this model, plutonium density decreases steadily as water is added.

For relatively low atom ratios of silicon to plutonium, e.g., 183, 752, and 1570, the initial addition of water decreases the critical mass and critical volume very sharply, or, one can say that this 3-component material has significantly greater reactivity. For each ratio of silicon to plutonium, however, a minimum critical mass is reached as water is added, comparable to the minimum seen in the two-phase mixtures. For still larger weight fractions of water, the hydrogen in the water becomes a poison (a neutron absorber) and a water (hydrogen) induced asymptote is seen; its location is a unique function of the plutonium density, the atom ratio of silicon to plutonium, and water content. As examples, for Si/Pu = 752 the asymptotic plutonium density is 0.0045 kg/l; for Pu/Si = 2812, it is 0.0025 kg/l. For very large Si/Pu atom ratios, greater than about 6000, the addition of water (hydrogen) acts invariably as a poison, and the critical mass increases regardless of the amount of water introduced.

The complexity of the criticality characteristics of this three-component system can be illustrated by a different scheme of data presentation. In Fig. 7, the critical mass of plutonium is illustrated as a function of the atom ratio of silicon to plutonium. The atom ratio for the asymptote is readily seen. Note that the ordering of the several critical mass functions is reversed between ratios of silicon to plutonium of 10^3 and 10^4. As will be clear later, this is the region of interest for the problem being studied. The data for these mixtures of plutonium, SiO_2, and water are listed in Table III.

Data similar to these for Pu-SiO_2-water have been obtained elsewhere for mixtures of U-235-graphite-water. The general characteristics are similar. See, for example, Refs. 10 and 13.

These data can be examined in another way that is useful in understanding the constraints on the problem at hand. In Figs. 8 and 9, the critical masses of plutonium taken from Figs. 6 and 7 (and Table III) are illustrated as functions of the weight percent of water; the dry critical mass from Fig 6 (Table III) is the starting point on the left ordinate and water content increases to the right. The critical volume and mass decrease with additional water moderation (except for the very high Si/Pu atom ratios) until a minimum is reached. With additional water content, the critical mass and volume increase until an asymptotic value is achieved. For each Si/Pu atom ratio, the weight percent water at the low-plutonium-density asymptote is readily seen or can be estimated with reasonable confidence. For example, for Si/Pu= 2812 it is 11.2% and for 5513 it is 3.0%. Thus, for a fixed Si/Pu ratio the water content must be less than the asymptote or criticality cannot occur. Or if the water content is fixed, the possible Si/Pu ratio and plutonium mass for criticality are readily seen.

V. CONSTRAINTS ON THE POSSIBLE CRITICAL CONFIGURATIONS

The set of necessary data for mixtures of plutonium, SiO_2, and water is now nearly complete, and constraints can be applied that limit the number of cases that need to be examined in more detail. Not all configurations are of interest. To develop these constraints, a few specific cases must be chosen. It is necessary to assume specific details to avoid generalities that cannot be checked. To proceed, we assume 75 kg of plutonium in a silicon dioxide log of 50-cm radius and 100-cm length reflected by pure SiO_2. The Si/Pu ratio of this log is about 90:1 and the density of plutonium in the log is about 0.1 kg/l. In addition, we must make assumptions relating to the physical and geological situation. These assumptions, postulated in Refs. 1, 2, and 3 are accepted for purposes of discussion and calculation, but only for these purposes.

The situations or processes postulated in Refs. 1, 2, and 3 involve at least the following:

1. Seventy five kilograms are to be vitrified into silicate "logs." These logs are to be placed within a massive container and buried in a SiO_2 medium. The initial Si/Pu ratio for these logs is about 90:1 and the plutonium density is about 0.1 kg/l. This log is identified (by an X) as safely subcritical on Figs. 4, 5, 6, and 7.
2. Over sufficient time, the containment in which this log is placed disintegrates and the plutonium diffuses into a spherical mixture of Pu-SiO_2 with the possibility of some water content.

Three specific scenarios have been postulated. Others are mentioned in Refs. 1, 2, and 3 but are only variations of these three. The scenarios are as follows:

a. The volume of plutonium and SiO_2, initially subcritical, slowly expands and mixes with more SiO_2, eventually reaching a critical state and finally a supercritical state caused by the increased moderation of SiO_2. This is the "dry" scenario.

b. The SiO_2 "log" cracks or disintegrates and water enters the region containing plutonium. The amount of SiO_2 mixed with the original log may or may not have increased. This is one "wet" scenario: water moves into the volume containing plutonium.

c. The plutonium and SiO_2 separates (Ref. 2 postulates that some or all of the SiO_2 dissolves and moves elsewhere.) and the plutonium remains behind in the form of particles that are free to move. These particles then slowly move into a stratum of SiO_2 that has some water. The plutonium may exist as a dry powder, most likely PuO_2, or may be mixed with water, or carry some silicon with it. This is another "wet" scenario during which plutonium moves into a wet stratum.

Discussion of Postulates

a. The Dry Scenario—Expansion of the initial volume of dry SiO_2 mixture into more dry SiO_2. By referring to Fig. 5, M_C(Pu) vs V_C, the initial mass of 75 kg in a Pu-SiO_2 log (now taken to be a sphere) is identified at an initial volume of 785 liters. If the mixing and expansion should take place as postulated, a critical state for the 75 kg could be achieved at a volume of about 2000 liters. Reference 1 further assumes that this expansion would increase to the maximum supercriticality state at a volume of about 9000 liters (where the critical mass is only 34 kg) before a neutron chain reaction would begin. No mechanism for this phenomenon is known and it is considered in these papers only to show that even these assumptions would not lead to an autocatalytic state with the

potential for an explosion. Reference 1 argues that the time scale for these actions may be geologic, later references (Refs. 2 and 3) add possibilities that take place on a much faster time scale, a millisecond expansion of PuO_2 vapor through solid tuff at molecular velocities, This hypothesis is nonphysical. Even if the PuO_2 could be preferentially heated to high temperatures, the mean free path for collisions with SiO_2 molecules is very, very short. At this stage of examination, and accepting the assumptions in Refs. 1, 2, and 3, a critical state is possible, but a supercritical state or autocatalytic state or both is impossible* The dry scenario will be re-examined again in Part B for the plutonium-tuff mixtures.

b. The Wet Scenario—Mixing of the water with the Pu/SiO_2 mixture, either with or without mixing with more SiO_2. Should sufficient water mix with the 75-kg mass at some volume below the 2000 liter dry-critical-level case, the effect could be to create a small, low-power critical system or reactor. This scenario is the plutonium analog to the Oklo "reactor" of two billion years ago (Ref. 4) as recognized in Refs. 1, 2, and 3. The fission power could vary widely, given sufficient freedom of postulates. The behavior of such a system is controlled primarily by the flow rate of the water, which is reported to be extremely slow through tuff (Ref. 16). Too much water or too little water would stop the reaction. It is difficult to achieve significantly higher reactivities than delayed critical on geologic time scales (or any time scale) because these higher reactivities lead to higher powers, higher temperatures, and evaporation of the water. No explosion would be expected because the $Pu\text{-}SiO_2\text{-}H_2O$ system would have sufficient time to adjust to the addition of water by removing water through boiling. This is a self-regulating process.

c. The Movement of Plutonium into a Wet Stratum—The movement of dry or damp plutonium, or PuO_2, with or without SiO_2, into a stratum containing an arbitrary amount of water. This case is more complicated and requires very careful examination because it is the only scenario so far identified (and believed to be unique) that could lead to an unstable or possibly autocatalytic power transient. In effect, the assumption states that a set of cracks (equivalent to drill holes) exists, which could allow a slow penetration of plutonium particles into a wet stratum, creating what is assumed to be a uniform mixture of the three components. The possible critical states of this three-component mixture have been illustrated in Figs. 6, 7, 8, and 9.

One constraint on the critical configurations that needs to be examined is the water-poisoning asymptote (Figs. 8 and 9) for each Si/Pu ratio. For example, if the water concentration is more than 3 wt %, criticality is not possible for ratios of silicon to plutonium greater than 5513, regardless of how much plutonium is involved. As another example, for a Si/Pu ratio of 1570, no criticality is possible for a water concentration greater than 21 wt %. This constraint, based on the water-induced asymptote is illustrated in Fig 10; for a given Si/Pu ratio, the water content must be less than the uppermost line on the figure for criticality to be achieved. For some mixtures of plutonium, SiO_2, and water, a configuration that is found just on or very near this line on Fig. 10 can be unstable and possibly could be "autocatalytic," i.e., if water leaves the system and the volume does not change, the system reactivity and fission power could increase.

A second constraint is found by further examination of the functions in Fig. 8. Examples make this easier. Referring to Fig. 8, Table III, and the Si/Pu ratio of 5513, the dry critical mass is about 84 kg. The minimum of this function is about 70 kg at 0.5 wt % water. At higher concentrations of water, the critical mass increases continuously up to the asymptote corresponding to about 3 wt %

---

* Nevertheless, the calculational assumptions relating to the expansion of plutonium at hot molecular velocities half a meter or more into surrounding solid SiO_2, are examined in a companion paper.

water. Between 0.5 wt % and 3 wt % water, an unstable or possibly autocatalytic region exists. Autocatalysis is impossible between 0.0 wt % and 0.5 wt % water; it is possible only between 0.5 wt % and 3.0 wt %. On the same figure, for a Si/Pu ratio of 2812, the unstable region exists only between 4.0 wt % and 11.2 wt % water. The minimum of each of these Si/Pu critical functions is plotted on Fig. 10 as the lower curve. The unstable or possibly autocatalytic region lies only between these two curves on Fig. 10. The lower limit function is modest; it represents the water content for no instability. A somewhat higher water content would be barely autocatalytic and trivial in results.

A third constraint is, of course, the available mass of plutonium, which has been taken to be 75 kg. If this amount is assumed to move into a wet stratum of SiO_2, the Si/Pu ratio will slowly decrease. The following examples are instructive. If the water content were, e.g., 0.5% by weight (see Fig. 8), criticality is possible for Si/Pu atom ratios of 7350 or 6785, but the required masses are 1000 kg and 300 kg, respectively; only 75 kg are available. If the water concentration were 1.0 wt %, 75 kg could be critical at an Si/Pu ratio of 5513. Proceeding to lower Si/Pu ratios at 75 kg on Fig. 8, this mass could be critical for 4.0 wt % water at Si/Pu = 4376 and for 10.0% at Si/Pu = 2812. The locus of these points is plotted on Fig. 10 as the middle function. The region of autocatalysis is now restricted to the region between the lowest and the middle-function of Fig. 10.

The final constraint to be discussed in this section is the assumed amount of water in the SiO_2 surrounding the Pu-SiO_2 mixture. The only guidelines on water content of the soil or rock are the actual measurements and analyses by geologists. A reasonable upper limit is 5% by weight (Ref. 5). Both 5.0 wt% and 10.0 wt % water content will be examined to be conservative. These constraints are illustrated by vertical lines on Fig. 10.

The full picture of all these constraints can be seen on Fig. 10 as triangles shaded on the semi-log plot. The defining corners for 75 kg and 5 wt % water are as follows: Si/Pu = 5800, %H_2O = 0.5; Si/Pu = 3900, % H_2O = 5.0; Si/Pu = 2400, % H_2O = 5. If the limiting amount of water is 10.0%, the defining points on Fig. 10 are 5800 and 0.5 wt %; 2800 and 10.0 wt %; and 1600 and 10.0 wt %. Configurations with compositions outside these limits are of no interest for the reasons just developed.

A question can be raised for a special class of configurations such as the following. Assume, for example, that plutonium penetrates into a moist layer of rock containing 6 wt % water and the penetration is sufficient to achieve a total of 75 kg in the appropriate spherical volume (see Fig. 8). No criticality is possible at Si/Pu = 4376 because of too much water. However, if the climate of the region should enter a drying phase, the water content could be reduced to 3.8 wt % and the system could become critical, unstable, and possibly autocatalytic, but the constraints discussed above would remain operative.

The appropriate constraints on plutonium and water concentration have been defined and the (now more limited) possibilities for supercritical configurations will be considered. This case, the movement of plutonium into a wet stratum, raises the possibility of unstable configurations and the possibility of an autocatalytic reactivity power transient. This is the situation of most interest.

VI. REACTIVITY (k_{eff}) CALCULATIONS

The previous section defined the possibilities for critical conditions, given certain constraints. This section will examine the possibilities for supercritical configurations that might be created and developed as a result of the movement and mixing of plutonium, silicon, and water. As an example, if a critical state is achieved at a water concentration of 4.0 wt %, a plutonium mass of 90.1 kg (ignoring for the moment the mass-loading limit of 75 kg for each log), and at a Si/Pu ratio of 4376 (see Fig. 8 and Table III), the resulting fission power could heat the volume and transport water out of the volume, thus reducing the weight percent of water and increasing the reactivity of the mixture. Note that this process does not change the volume or the mass of plutonium so that this change in composition does not follow the critical mass function of Si/Pu = 4376 in Fig. 8; it has become supercritical. This process could continue and reactivity could rise creating a faster reaction rate. Reference 3 postulates that this autocatalytic process will result in an explosion of "hundreds of tons of TNT equivalent." The criticality aspects of the unstable regions defined above will be examined, quantitatively, in this section, and the postulated explosion aspects will be examined in Part B (for tuff) and in the companion papers on dynamics.

Given the initial assumptions of Refs. 1, 2, and 3, the critical state, i.e., a self-sustaining neutron chain reaction, is not impossible; thus the magnitudes of the possible reactivity and power transients must be examined.

The first step in the analysis of a postulated criticality event is to examine the magnitude of the neutron multiplication factor, often referred to as k_{eff}. This has been done for several functions (with different Si/Pu ratios) for the appropriate amounts of water and for several different masses of plutonium. Typical results are illustrated in Fig. 11 (Table IV) for two cases in which the k_{eff} is plotted against water content for different Si/Pu atom ratios and plutonium masses. For example, 90.1 kg of plutonium with Si/Pu = 4376 is just critical with 4 wt % water. As the water content is decreased, with the mass of plutonium and volume remaining constant, the k_{eff} rises to a maximum of 1.071, where the water content is 1.06 wt %, and drops to 1.031 for the dry case. The same Si/Pu ratio with a fissile mass of 32.5 kg is just critical with 2 wt % water. In this case the k_{eff} decreases monotonically to 0.902 as the water content is reduced.

A second set of examples is illustrated on Fig. 12. The Si/Pu ratio is 2812, the plutonium masses and water contents are 84.4 kg and 10 wt %, 35.8 kg and 9.0 wt %, and 16.0 kg and 7.0 wt %. The data for these functions are taken from Table IV, the starting point (k_{eff} =1.000) can be identified on Fig. 8 and in the tables. In this case the largest mass could reach a k_{eff} of 1.178 and remain critical even when dry. Each of the lesser plutonium masses is subcritical when dry and the maximum k_{eff} is lower.

These data show that calculated neutron multiplication factors for some cases range up to as much as about 1.18. Other (not illustrated) data show excess reactivities up to 1.3, but these are not considered because the plutonium mass or soil water content is outside the constraints given above. Some of these reactivity functions have the appearance of being very large and significant. Others are much less significant. It is not obvious that all examples need to be examined in detail. The intent is to pick those that are reasonably typical or are approaching what might be a severe case. Cases showing the possibility of supercriticality and an autocatalytic power response will be examined quantitatively in the following Part B for tuff and in a companion paper on dynamics.

Part B: Criticality Data
Plutonium, Tuff, and Water

VII. NUCLEAR CRITICALITY, PLUTONIUM-TUFF

The tuff composition used in these calculations is taken from Ref. 6 and differs from SiO_2 in that the SiO_2 content is only 77% by weight with the difference made up primarily by oxides of aluminum, potassium, and sodium, for example, with a number of minor constituents, some of which are neutron poisons. The composition is given in Ref. 6 and reproduced in the Appendix. The treatment of the Pu-tuff-H_2O data parallels the treatment of the Pu-SiO_2-H_2O data with the addition of pertinent comparisons. To allow easy comparison between Pu-SiO_2 data and Pu-tuff data, the Si/Pu ratio for tuff will be multiplied by 1/0.77 and denoted by Si/Pu*; densities are comparable.

In Fig. 13 (Table V) the calculated reflected critical masses for plutonium mixed with Nevada tuff are shown as a function of the plutonium density along with the comparable critical masses for plutonium mixed with pure SiO_2. The latter data are reproduced from Fig. 4. The model used for mixing the plutonium with tuff is the volume displacement model discussed earlier, i.e., the volume occupied by the plutonium displaces a comparable volume of tuff. Significant differences can be noticed immediately. 1) The low-density asymptote is increased from 0.001 to 0.003 g/cm^3. Thus, the number of highly diluted cases requiring consideration is further restricted. 2) The moderating/absorbing effects of SiO_2 that decrease the critical mass from 95.7 kg at a plutonium density of 0.184 kg/l to 35.1 kg at a density of 0.0048 kg/l (seen in Fig. 13) very nearly disappear when the diluent has the composition of tuff. With tuff as a diluent, the maximum and minimum critical masses are 112.6 kg and 85.6 kg; the ratio of the maximum and minimum critical masses in the region of this dip in the critical mass functions drops from 2.7 to 1.3. The potential for the postulated dry autocatalytic behavior (as postulated in Refs. 1 and 2) depends on the presence of this "dip." Substantial reduction in the magnitude of the "dip" constrains the conditions that must be met to achieve autocatalytic behavior. This increased minimum mass when Nevada tuff is the diluent eliminates the need to consider the "dry critical" problem that was postulated in Ref. 1 and in Section V of this paper; 75 kg would never become critical in dry tuff. Including the Pu-240 or allowing for decay of Pu-239 to U-235 would increase the critical masses even more.

Figure 14 illustrates the data of Table V in a plot of critical mass vs critical volume for Pu-tuff and Pu-SiO_2. This figure is the analog of Figs. 3 and 5. The differences are evident immediately and are significant. The potential for dry criticality of 75 kg, and even much more, is eliminated under these conditions as well.

VIII. CRITICAL DATA FOR Pu-TUFF-H_2O, A THREE COMPONENT SYSTEM

The critical data for Pu-SiO_2-H_2O mixtures were presented in Fig. 6 and Table III. The comparable data for Pu-Tuff-H_2O are given in Table VI and illustrated in Fig. 15 . The changes that derive from the increased plutonium density at the asymptote at 0.003 kg/l are more apparent, as is the ultimate poisoning by hydrogen. The model used for the mixing of water with the Pu-tuff is the displacement model: a given mass of water displaces the appropriate volume of Pu-tuff. However, a different model is possible. This derives from the observation that tuff has a porosity of several percent by volume. Five percent to eleven percent porosity (i.e., void) has been reported (Refs. 5 and 16). This model has been considered and some results are reported in the Appendix. The calculated critical masses differ somewhat from those determined by using the displacement model, but these differences do not affect the final conclusion.

Pu-tuff-H_2O critical mass data are presented in Fig. 16 as a function of the weight percent of water. The increased effect of the neutron absorbers in tuff is clearly seen in the more restricted range of the functions in this figure. To compare these data with the data of Figs. 8 and 9, the Si/Pu ratios for tuff are multiplied by 1/0.77 and denoted by Si/Pu*.

IX. DISCUSSION OF POSTULATES

a. The Dry Scenario. The postulated slow geologic expansion of the Pu-SiO_2 log into surrounding (in this case) tuff is unchanged compared to the pure Pu-SiO_2 case. As mentioned above, the significant difference is that the "dry critical" state is not created because of the criticality characteristics of the Pu-tuff mixtures (Figs. 13 and 14, Table V). The minimum critical mass of plutonium in tuff is greater than 75 kg. The "dry supercriticality" is eliminated for Pu-tuff mixtures. Nevertheless, the dynamic behavior of the Pu-SiO_2 system will be examined in a companion paper on dynamics for the case of pure Pu/SiO_2 mixtures.

b. The Wet Scenario. The postulate of mixing water with the Pu-SiO_2 is unchanged for the Pu-tuff system. A water-induced criticality remains possible, even if improbable, and the comparison to the Oklo phenomenon remains valid. The power level would be determined by the flow and amount of water. As with pure SiO_2, no explosion should be expected.

c. The Movement of Plutonium into a Wet Stratum. The postulated mechanism is unchanged. By postulate, much of the SiO_2 in the original log (which fixes the plutonium in place) disappears, allowing the plutonium to be mobile and penetrate slowly into a stratum of wet tuff. The addition of plutonium would start at a very high Si/Pu ratio and progress to smaller ratios as more plutonium migrates into the stratum. One constraint is defined for each Si/Pu ratio by the water-poisoning asymptote seen on Fig. 16. The locus of these asymptotes is plotted as the upper line on Fig. 17; the water content must be less than this value for criticality to occur. This figure is the analog of Fig. 10 for pure SiO_2 diluent.

Referring again to Fig. 16, the minimum of each function is the lowest water concentration above which instability or autocatalysis is possible. A lower water concentration cannot lead to instability. The locus of these points is plotted on Fig. 17 as the lower line, providing another constraint on the amount of water to be considered.

The limitation set by the mass loading limit of 75 kg can be read from the functions for each Si/Pu* atom ratio on Fig. 16. The locus of these points is plotted on Fig. 17 as the middle line, comparable to Fig. 10 for SiO_2.

The final constraint is the amount of water that would actually be found in the tuff. This has been estimated to be about 5 wt % (Ref. 5). However, twice this amount will be considered to assure conservatism. These constraints are illustrated on Fig. 17 as vertical lines at 5% and 10% water content.

The full picture of the constraints for Pu-tuff-H_2O can be defined as was done for Pu-SiO_2-H_2O. On Fig. 17, a triangle is defined by the coordinates for 5 wt % water and 75 kg. These are a Si/Pu* ratio of 2700 and 0.4 wt % water; 1850 and 5 wt %; and 1450 and 5 wt %. For 10% water and 75 kg, the coordinates are 2700 and 0.4 wt %; 1500 and 10.0 wt %; and 1100 and 10 wt %. Configurations of Pu-Tuff-H_2O that lie outside these boundaries are not of interest because, as discussed earlier, criticality or autocatalytic behavior or both are not possible.

X. REACTIVITY (k_{eff}) CALCULATIONS FOR Pu-TUFF-H_2O MIXTURES

Reactivity calculations have been completed in the same manner as those for the Pu-SiO_2-H_2O mixtures. The general characteristics are similar, but details differ significantly. The cases of most interest are the data for a Si/Pu* atom ratio of 1570. These data are illustrated on Fig. 18 and are presented numerically in Table VII. The masses of plutonium and the initial water content are as follows: Case (1) 404.7 kg and 11.2 wt % water; Case (2) 108.3 kg and 10.0 wt % water; Case (3) 63.8 kg and 9 wt % water; Case (4) 45.5 kg and 8 wt % water; and Case (5) 36.4 kg and 7 wt % water. These data cluster in the upper right hand corner of the permissible triangle on Fig. 17. This "corner" (10.0 wt % water, 75 kg and Si/Pu* ratio of 1500) is the condition that will lead to the highest k_{eff} and the largest integral of k_{eff} as a function of weight percent of water. The reactivity functions of Fig. 18 are almost precisely at the correct spot to examine the most severe limiting case. Case (1) on Fig. 18 has too much plutonium and water; Case (2) exceeds the mass limit but has the correct limiting amount of water. The other three are all within permissible constraints. The maximum k_{eff} for 75 kg of plutonium is about 1.06 (by interpolation) when approximately three-fourths of the water is forced out of the system (see Fig. 18).

By examining the data of Figs. 17 and 18, it is apparent that an estimate for the total energy release can be reached without the aid of a computer program designed to calculate dynamic behavior. In fact, the mixture or assembly defined by 10% water in tuff, 75 kg of plutonium, and a Si/Pu* ratio of about 1500 is close to the most severe test of whether or not an explosion could develop. The configuration most closely approximating this assembly is defined by the data in Table VI for a Si/Pu* of 1570 and Table VII-D and is illustrated in Fig. 18 for the case labeled by 108.3 kg. The mass of 108.3 kg is greater than the constraint of 75 kg, but this merely introduces an extra measure of conservatism.

We assume that the configuration has been created and, as stated, it is just critical with 10 % water by weight and 108.3 kg of plutonium. From Table VI and using a density of 2.38 kg/l, the total mass of the "core" is 5.85×10^4 kg. For the accuracy needed here, the mass of water is taken to be 5.85×10^3 kg.

The assumptions for the power transient are as follows: initially, and during the period of rising power, all the fission energy is deposited into boiling water, with no change in temperature or generation of pressure. This decrease in water content will increase reactivity to a maximum k_{eff} of 1.080 where the water content is only 2.38 % by weight. The steam is assumed to vanish, an assumption that should increase the energy of the postulated transient. In fact, a significant pressure would be generated by steam, and this pressure would cause expansion and reduction of reactivity; also, should the temperature rise, the temperature coefficient of reactivity for neutrons would be negative.

By reference to Fig. 18, the system would be subcritical even before all the water evaporated. However, for ease of analysis this effect is ignored and the energy required to evaporate all the water is 1.3×10^{10} joules. After this change, the system becomes subcritical, and the reactivity decreases very rapidly. The energy generated after this boiling process and while the power is dropping will be smaller (or certainly not greater) than that generated during the power rise.

If this energy is now used to heat the mass of tuff, the temperature rise would be about 220 °C.

No kinetic energy, dynamic behavior, or explosion will occur.

The energy generation cannot be judged definitively on the basis of static criticality calculations alone. We have, however, reached conclusions for the upper limit of the energy generation in one case. The companion papers on dynamics will examine further the generation of fission energy and the possibility of explosive energy release.†

XI. SUMMARY AND CONCLUSIONS

This paper has examined the static criticality aspects of mixtures of plutonium and SiO_2; plutonium, SiO_2, and water; plutonium and Nevada tuff, and plutonium, Nevada tuff, and water.

A conservative approach was taken by assuming the plutonium was pure Pu-239, homogeneously distributed within the moderator/absorber material in a spherical form. Any deviation from these criteria, e.g., substitution of weapons-grade plutonium (about 5% Pu-240, 95% Pu-239) for pure Pu-239 results in lower neutron multiplication factors and higher critical masses than those calculated in this work. Inclusion of elements found in the Nevada tuff also lowers the calculated neutron multiplication factors. These effects can be significant, especially for the dry criticality case discussed above. All reactivity calculations have included the assumption of uniform, fine-grain mixing of all components throughout.

The several chemical and geologic assumptions taken in Refs. 1, 2, and 3 are accepted in this study for purposes of calculation only, in spite of the extraordinarily low probability and long time scale they imply; no credence is given to these assumptions because of their application herein.

The general characteristics of fissile systems diluted with a moderator/absorber material were summarized. The qualitative features of the plots of the critical masses of such systems versus the fissile density are generally similar. All exhibit a maximum critical mass with small amounts of diluent, followed by a minimum caused by the moderating effect of the diluent, and finally a low-density unbounded critical mass and critical volume asymptote caused by the neutron absorbing effect or neutron capture of the diluent. Configurations near the asymptote can display instability and possible autocatalytic behavior. The quantitative features, such as the values for the critical masses, the location of the maximum and minimum critical masses, and the location of the asymptote depends on the fissile material and the moderator/absorber materials present.

The postulates of Refs. 1, 2, and 3 were characterized as falling into one of the following three cases:

1. expansion of the plutonium into a larger mass of SiO_2,
2. water entering the volume of SiO_2 that contains the plutonium, and
3. plutonium, as a metal or oxide, entering a wet stratum of rock,

These three cases were repeated using Nevada tuff in place of the pure SiO_2.

---

† In the final stages of preparation of this paper, the authors became aware of the work done in this field by B. F. Gore, U. P. Jenquin, and R. J. Serne of the Pacific Northwest Laboratories. Their publication is identified in Ref. 17. We apologize for the lack of comparisons of comparable criticality situations. This fault will be remedied in a future publication.

These cases were then examined for the potential for autocatalytic behavior. We obtained the following results:

1. The system consisting of pure Pu-239 with pure SiO_2 as a diluent exhibits the classic dependence of the critical mass on the fissile material density. Thus, a critical system is possible, but very improbable, and autocatalytic behavior is judged to be possible only if assumptions regarded as impossible are accepted. The calculations reported in Ref. 3 will be examined further in a companion paper on the dynamics of these systems. When Nevada tuff is the diluent, nuclear criticality and autocatalytic behavior are not possible for log loadings of less than approximately 84 kg of Pu-239. Pu-239 masses greater than about 84 kg or a substantial variation in the composition of the tuff or a mechanism for "purification" of the tuff will be necessary if criticality is to be achieved. If weapons-grade plutonium (5% Pu-240) is considered, the requirements are much more stringent. No explosion is possible.

2. For geologic time scales or for processes that add water, criticality is possible for both SiO_2 and Nevada tuff diluents. However, no autocatalytic behavior is expected because the system has sufficient time to respond to the reactivity increases (which occur as a result of the addition of water) by ejection of water (e.g., through boiling), which reduces reactivity. A behavior similar to the Oklo phenomena (Ref. 4) is expected, and the total fission energy generated depends on the length of time such a system operates. No explosion is possible.

3. For plutonium entering a wet stratum of SiO_2 or Nevada tuff, criticality and autocatalytic behavior are possible, but the Si/Pu ratios for which this can occur are constrained by the total amount of plutonium present and by the water content of the strata. These constraints limit the amount of insertion of reactivity when water is removed from the system. The behavior of these wet systems will be examined in a companion paper on dynamics, but an upper limit estimate based only on criticality data shows no kinetic, dynamic, or explosive energy.

Acknowledgments

The authors would like to thank Randi L. Bagley, Barbara F. Milder, Paul Henriksen, and Carey Parish for their assistance in the typing of the manuscript and preparing tables and figures. We thank A. Petschek, G. E. Hansen, T. F. Stratton, P. Whalen, and H. J. C. Kouts for reviewing this document and suggesting improvements.

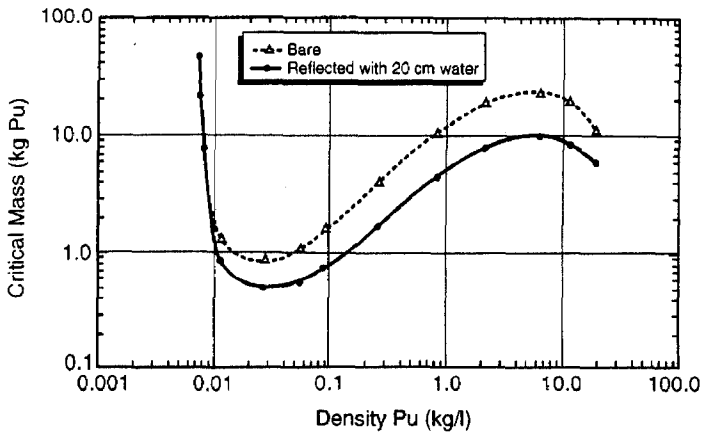

Figure 1. Critical mass of plutonium metal as a function of plutonium density when mixed with water. The plutonium is idealized to be a sphere with a fine grain powder and mixed uniformly with the water. The data defining the low-density asymptote are new for this study. The major body of data was taken from Ref. 9 and is reproduced in Table I. An important characteristic to note is the minimum critical mass at a plutonium density of about 0.03 kg/l.

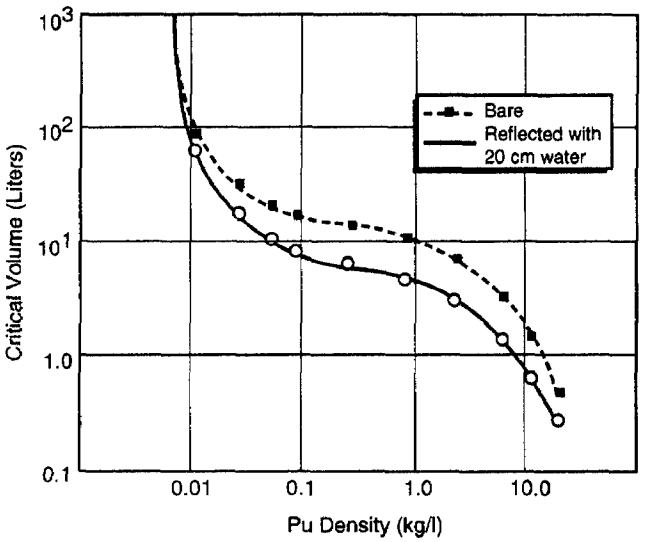

Figure 2. Critical volume of plutonium-water mixtures as a function of the plutonium density.

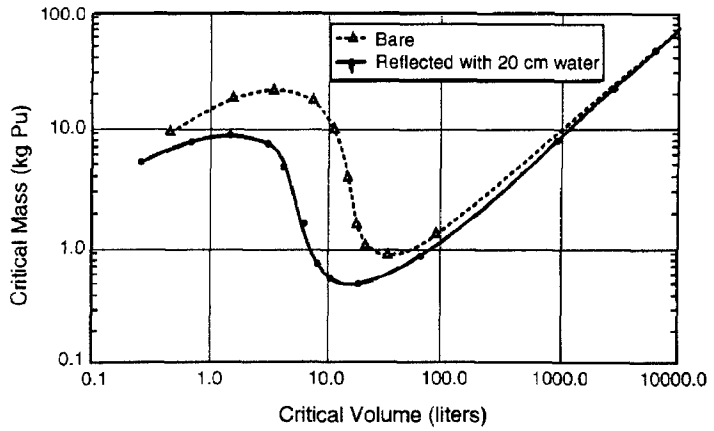

Figure 3. Critical mass of Pu-H_2O mixtures as a function of the critical volume of the mixture.

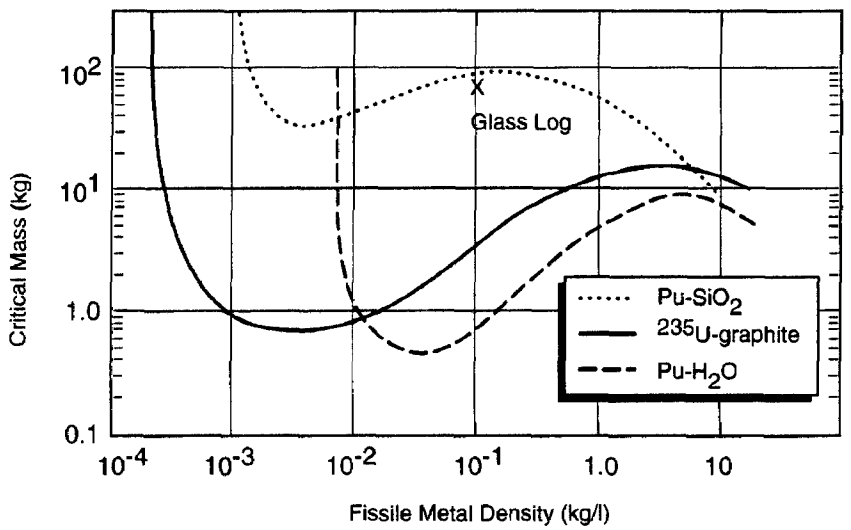

Figure 4. Critical masses of Pu-H_2O mixtures reflected by water, Pu-SiO_2 mixtures reflected by SiO_2, and U-235-graphite mixtures reflected by graphite. The wide range of the maximum and minimum critical masses and the wide range of the low-density asymptotes are of interest. Each function displays a minimum mass at densities slightly higher than the asymptote. The low-density asymptote in each case is caused by the neutron absorption in the diluent.

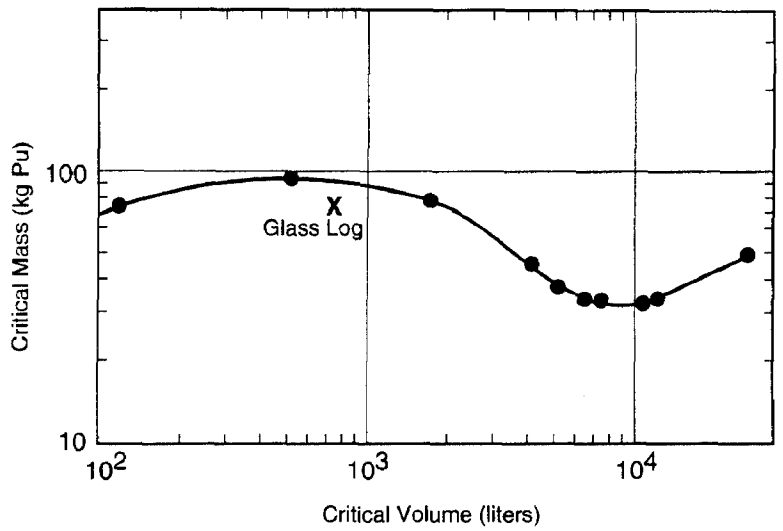

Figure 5. Critical mass of plutonium mixed with and reflected by SiO_2 as a function of the critical volume.

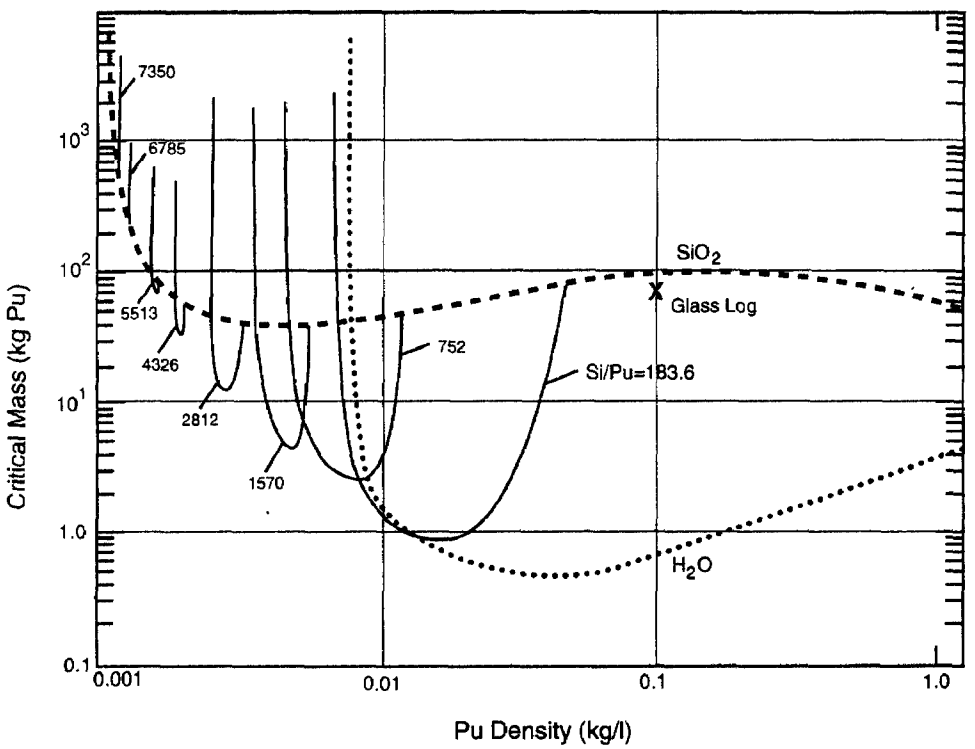

Figure 6. Critical data for mixtures of plutonium, SiO_2, and water plotted as a function of plutonium density. The upper function is for Pu-SiO_2 reproduced from Fig. 4 (and Table II); the lower function is for Pu-H_2O reproduced from Fig. 1 and Table I. The three-component data from Table III illustrate the dramatic effect of the addition of water. Note that the low-density asymptote is different for each Si/Pu atom ratio. These data will be used to establish limits on the configurations of interest.

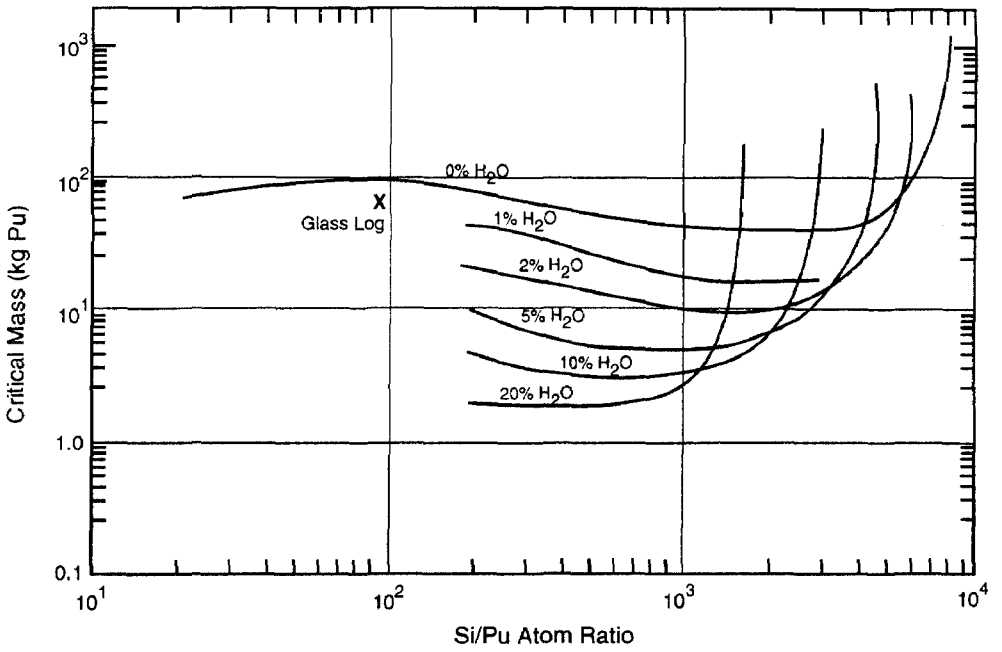

Figure 7. Critical mass of plutonium vs the Si/Pu atom ratio for a few weight percent water in the core and reflector. This figure illustrates a part of the complexity of the criticality of three component systems.

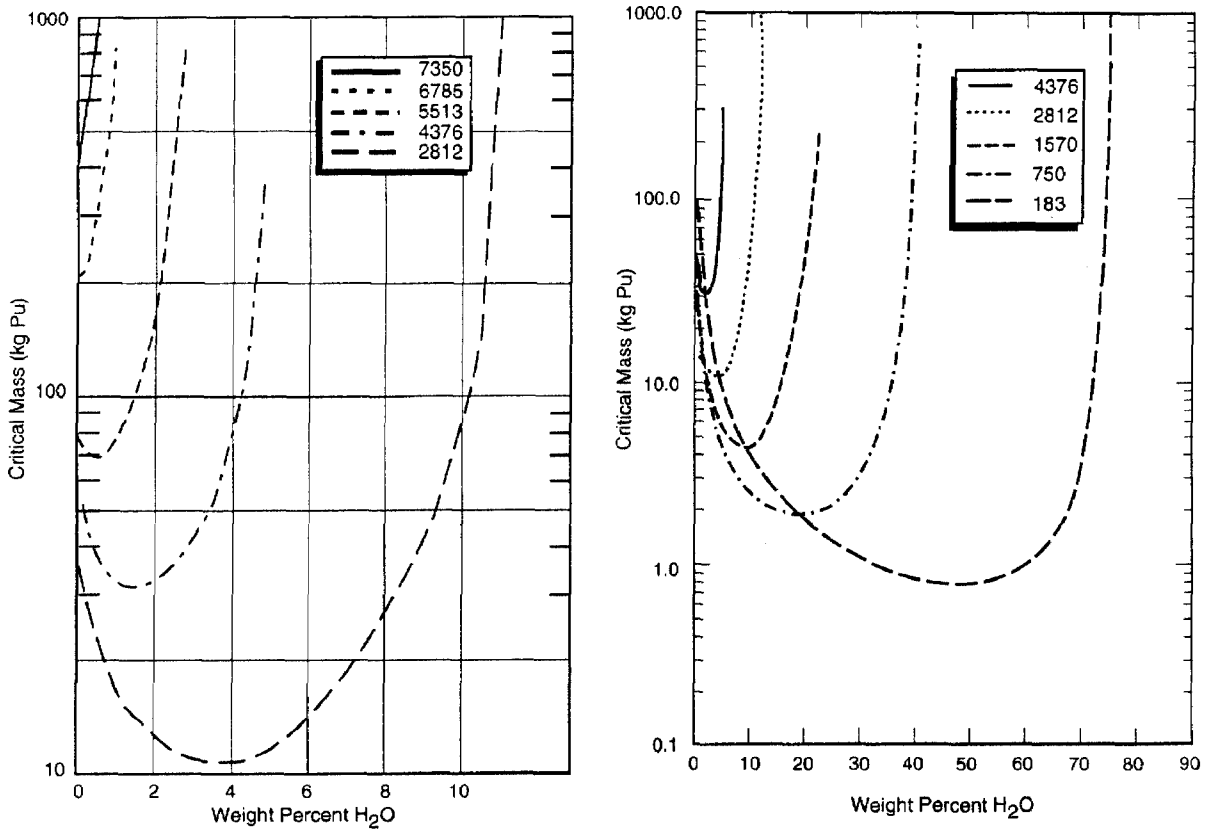

Figures 8 and 9. The critical mass Mc of plutonium as a function of the weight percent of water for various Si/Pu atom ratios. These critical mass data are the same as those illustrated in Fig. 6 but shown as a function of the weight percent of water. Note that for each Si/Pu atom ratio the asymptote establishes an upper limit on the amount of water for the critical state. In addition, for each Si/Pu ratio, the minimum of the function establishes a lower limit to any possible unstable condition. The loci of these two limiting conditions are plotted on Fig. 10.

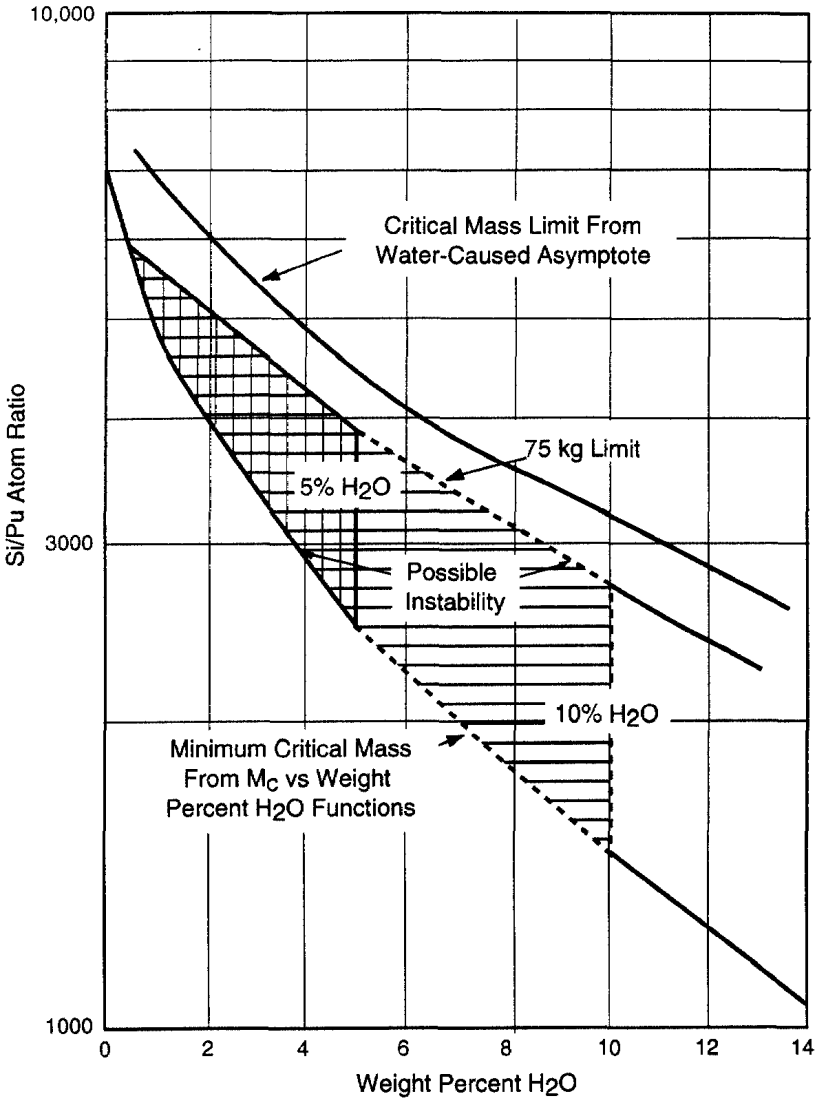

Figure 10. Limiting values of water content as a function of Si/Pu ratio. The limiting loci described for each Si/Pu ratio in the caption for Figs. 8 and 9 are illustrated as the top and bottom lines. The intermediate line reflects the limit of 75 kg of plutonium and is also derived from Figs. 8 and 9. A vertical line is drawn at 5 and 10 wt% water to show the limit based on the accepted maximum water content and twice this amount. The region within the triangular areas represents the only region of possible autocatalytic behavior.

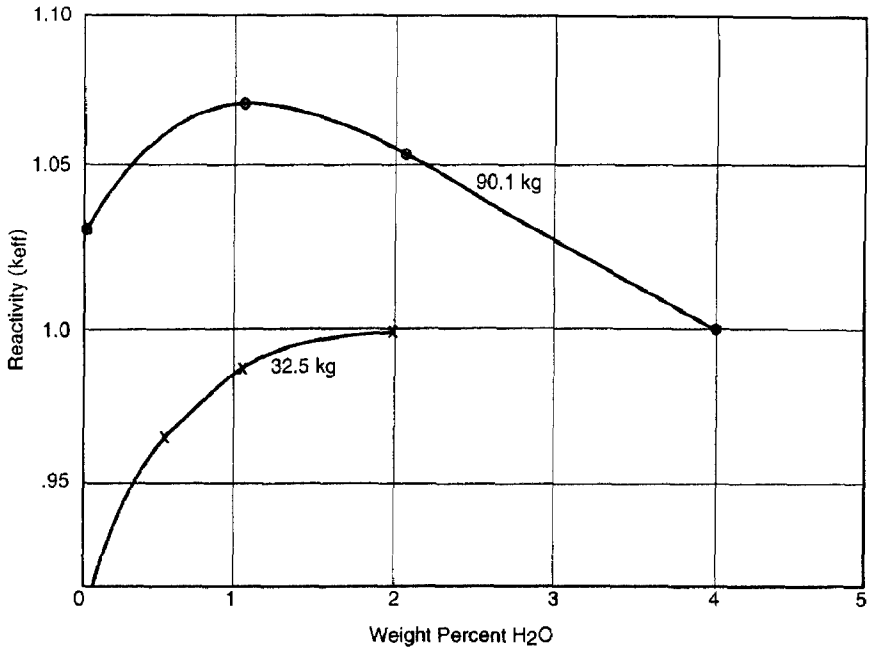

Figure 11. Plot of k_{eff} vs water content for several Si/Pu ratios. The reactivity (k_{eff}) is for two plutonium masses of 90.1 kg and 32.5 kg, each taken from the critical mass curve in Fig. 8 with Si/Pu=4376. The critical point (90.13 kg or 32.49 kg) is taken from the function in Fig. 8 and k_{eff} is calculated by step-wise removal of the water. The upper function (for 90.1 kg) exhibits autocatalytic behavior as water evaporates and leaves the system. The mass, however, is above the allowed limit. The lower curve (32.5 kg) is taken from Fig. 8 at a point first expected to show the same instability. However, as water content decreases, the reactivity steadily decreases.

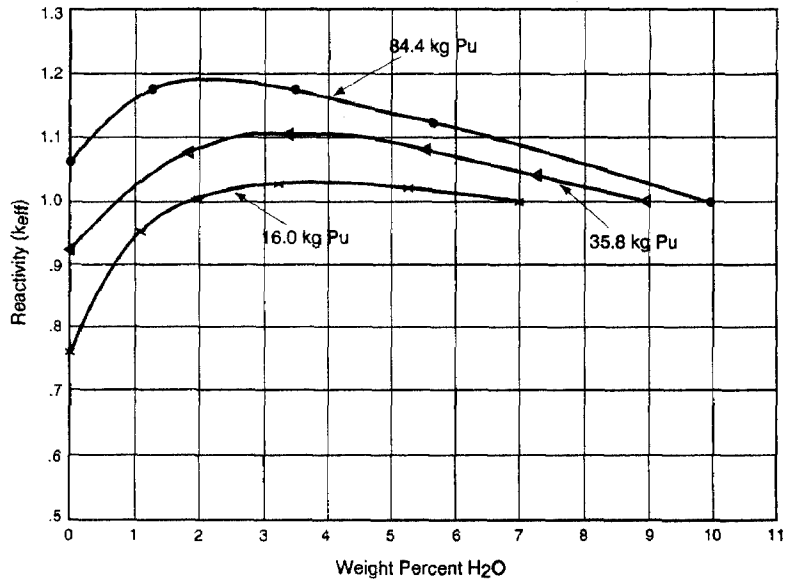

Figure 12. Reactivity (k_{eff}) for three plutonium masses, each taken from the critical mass curve in Fig. 8 with Si/Pu=2812. In this case, each of the k_{eff} functions would be unstable and autocatalytic. The one for 84.4 kg is outside the 75-kg limit of Fig. 10, but the other two satisfy the constraints.

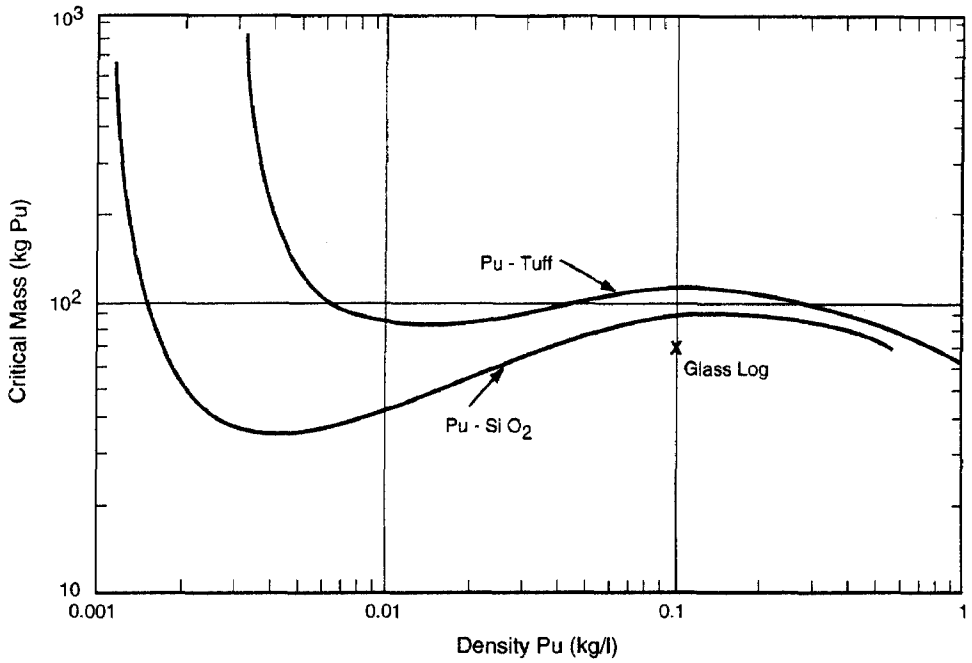

Figure 13. Reflected critical mass of plutonium metal mixed with tuff or SiO_2 vs plutonium density. This figure is analogous to Figs. 1 and 4. However, the function for Pu-tuff shows a much increased minimum critical mass (85 kg at 0.015 kg/l, compared to 35 kg at 0.004 kg/l), thus eliminating the need to consider the dry criticality as postulated in Ref. 1. The increased value of the minimum critical density asymptote should be noticed.

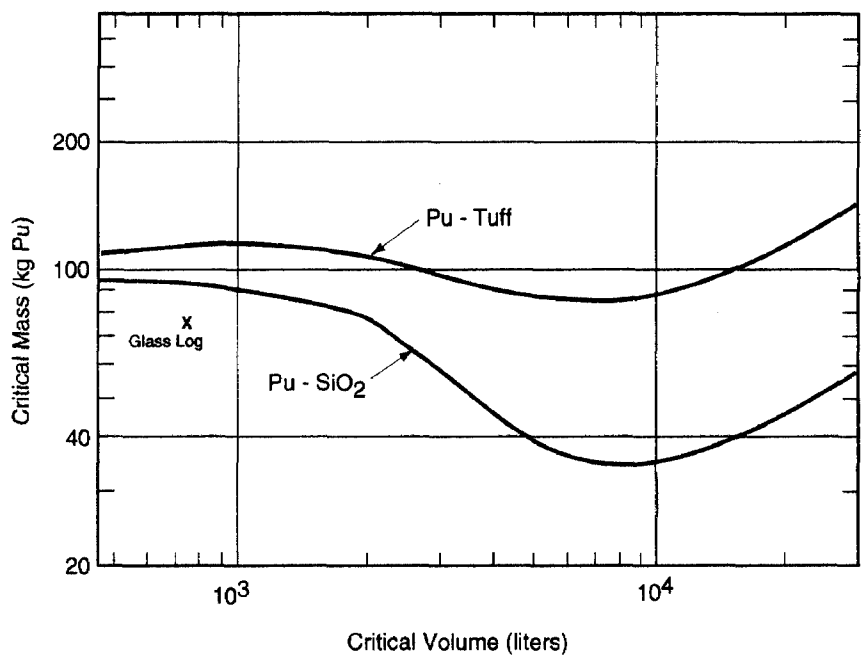

Figure 14. Reflected critical mass of plutonium mixed with tuff or SiO_2 vs critical volume. This figure is analogous to Figs. 3 and 5. Criticality of 75 kg of plutonium in dry tuff is not possible.

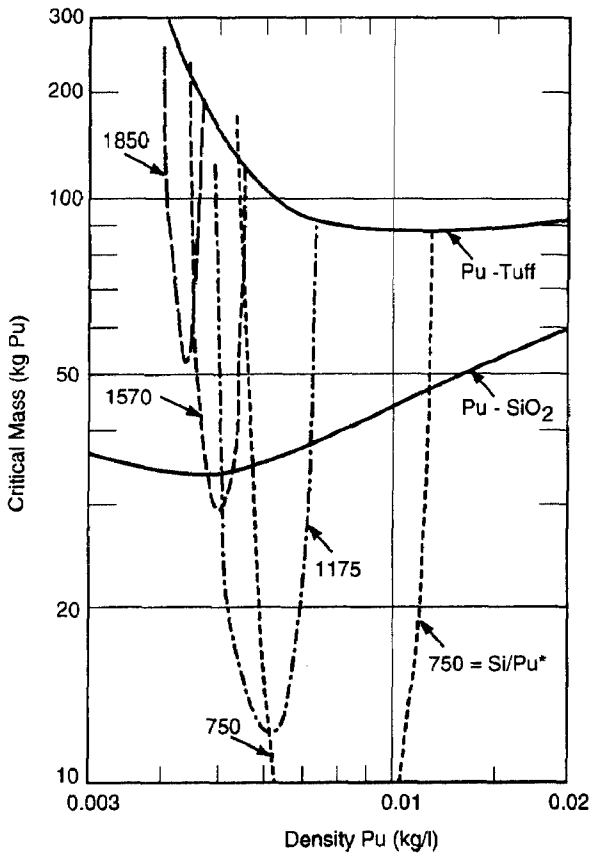

Figure 15. Reflected critical mass of plutonium mixed with tuff and water vs density of plutonium. This figure is analogous to Fig. 6 for plutonium mixed with SiO_2 and water.

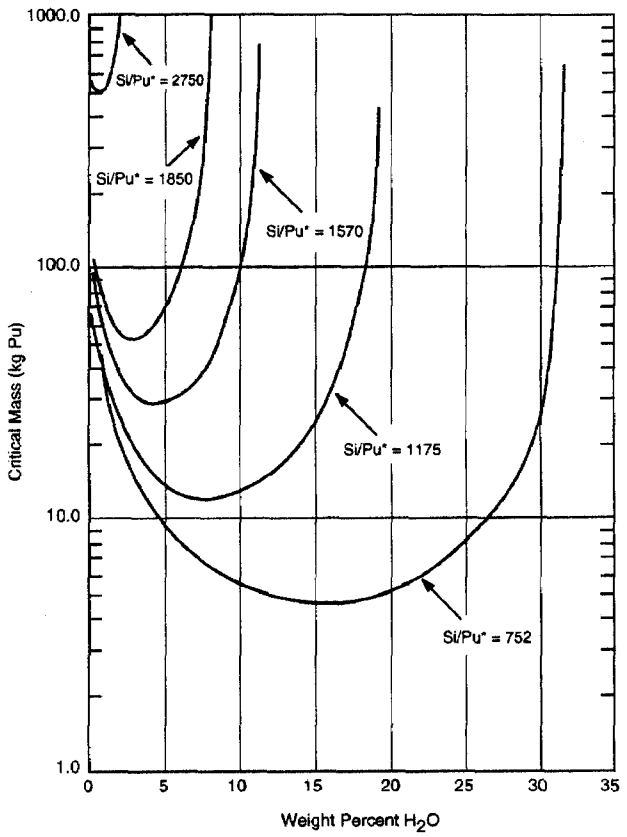

Figure 16. Reflected critical mass of plutonium metal mixed with tuff and water vs weight percent water. This figure is analogous to Figs. 8 and 9 for Pu-SiO_2 and water.

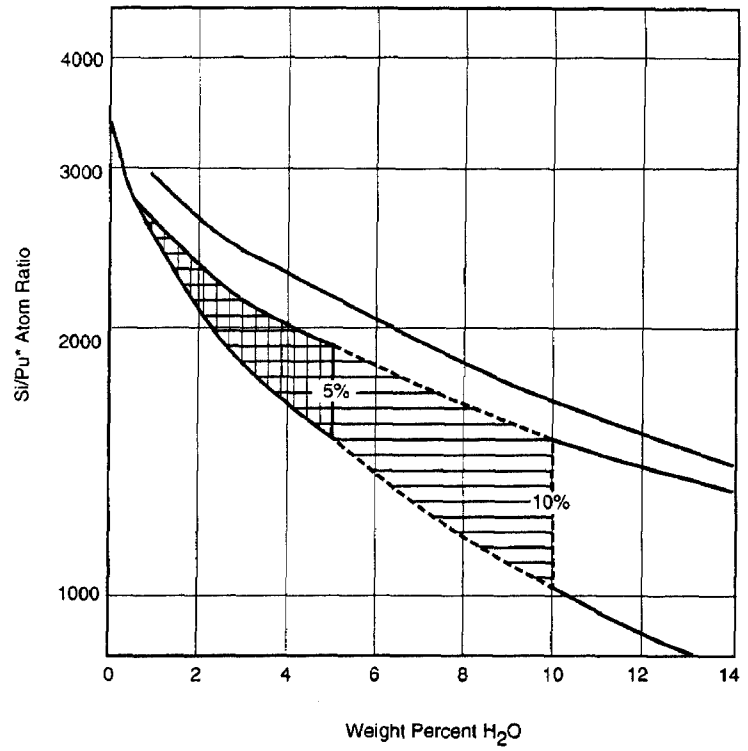

Figure 17. Silicon/plutonium ratio in tuff multiplied by 1/0.77 (and denoted by Si/Pu vs weight percent water. This figure is analogous to Fig. 10 for SiO_2. The lower, intermediate, and upper limits are derived in the same manner as for Fig. 10. Configurations outside these limits are not of interest. The configurations within the shaded triangles may be unstable. The most severe unstable or autocatalytic mixture is expected to be at Si/Pu*=1570 and 10 wt % H_2O.*

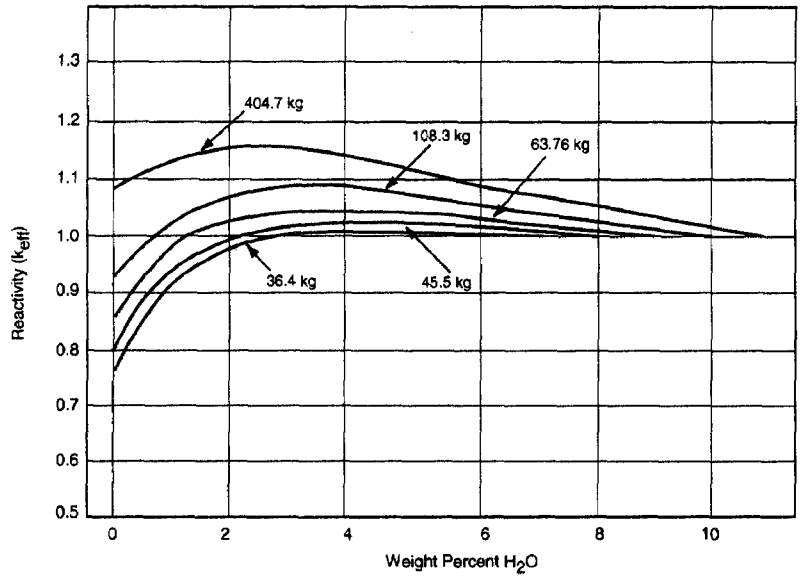

Figure 18. Reactivity (k_{eff}) vs weight percent water for Si/Pu=1570 (tuff) and 404.7, 108.3, 63.76, 45.5, and 36.42 kg of plutonium. These functions lie very close to the most severe configuration defined in Fig. 17. The uppermost function is outside the constraints for both mass of plutonium and weight percent water. The second curve (for 108.3 kg of plutonium) is satisfactory for the water content, but beyond limits for the mass of plutonium. The lower three functions all lie within the derived limits.*

Table I. ^{239}Pu Metal-Water Mixtures:
Critical Parameters for Bare and Water-Reflected Spheres

	Unreflected				Water Reflected		
H/^{239}Pu (Atom ratio)	Pu Density (kg/l)	Radius (cm)	Volume (liter)	Mass (kg)	Radius (cm)	Volume (liter)	Mass (kg Pu)
0.0	1.97×10^{1}	4.90	0.49	9.71	3.98	2.64×10^{-1}	5.20
1.00×10^{0}	1.13×10^{1}	7.15	1.53	17.3	5.48	6.89×10^{-1}	7.79
3.00×10^{0}	6.11×10^{0}	9.38	3.46	21.1	7.04	1.46×10^{0}	8.93
1.00×10^{1}	2.34×10^{0}	12.2	7.61	17.8	9.06	3.12×10^{0}	7.29
3.00×10^{1}	8.46×10^{-1}	14.1	11.7	9.93	10.5	4.85×10^{0}	4.10
1.00×10^{2}	2.62×10^{-1}	15.1	14.4	3.78	11.4	6.21×10^{0}	1.63
3.00×10^{2}	8.81×10^{-2}	16.1	17.5	1.54	12.5	8.18×10^{0}	0.72
5.00×10^{2}	5.29×10^{-2}	17.0	20.6	1.09	13.5	1.03×10^{1}	0.55
1.00×10^{3}	2.65×10^{-2}	19.8	32.5	0.86	16.4	1.85×10^{1}	0.49
2.00×10^{3}	1.33×10^{-2}	28.1	92.9	1.23	24.7	6.31×10^{1}	0.84
3.32×10^{3}	8.00×10^{-3}				61.05	9.53×10^{2}	7.62
3.54×10^{3}	7.50×10^{-3}				87.2	2.78×10^{3}	20.8
3.64×10^{3}	7.30×10^{-3}				113.47	6.12×10^{3}	44.7
3.74×10^{3}	7.10×10^{-3}				198.3	3.27×10^{4}	232.0

Table II. ^{239}Pu Metal-SiO_2 Mixtures: Critical Parameters for SiO_2 Reflected Spheres

Si/^{239}Pu (Atom ratio)	Density (kg/l)	Radius (cm)	Volume (liters)	Mass (kg Pu)
0.00	$1.96x10^{1}$	4.02	$2.71x10^{-1}$	5.3
$0.87x10^{0}$	$1.0x10^{1}$	6.17	$9.86x10^{-1}$	9.9
$1.75x10^{0}$	$5.0x10^{0}$	9.75	$3.88x10^{0}$	19.4
$2.75x10^{0}$	$3.17x10^{0}$	12.83	$8.86x10^{0}$	28.1
$4.41x10^{0}$	$1.98x10^{0}$	16.78	$1.98x10^{1}$	39.3
$8.75x10^{0}$	$1.00x10^{0}$	24.12	$5.88x10^{1}$	58.8
$1.47x10^{1}$	$5.96x10^{-1}$	30.97	$1.25x10^{2}$	74.2
$4.72x10^{1}$	$1.84x10^{-1}$	49.74	$5.15x10^{2}$	95.7
$1.836x10^{2}$	$4.77x10^{-2}$	73.98	$1.70x10^{3}$	80.9
$7.528x10^{2}$	$1.16x10^{-2}$	98.95	$4.06x10^{3}$	47.2
$1.175x10^{3}$	$7.40x10^{-3}$	108.26	$5.32x10^{3}$	39.6
$1.578x10^{3}$	$5.54x10^{-3}$	115.80	$6.51x10^{3}$	36.1
$1.839x10^{3}$	$4.76x10^{-3}$	120.77	$7.38x10^{3}$	35.1
$2.812x10^{3}$	$3.11x10^{-3}$	140.93	$1.17x10^{4}$	36.5
$4.376x10^{3}$	$2.00x10^{-3}$	183.81	$2.60x10^{4}$	52.0
$5.513x10^{3}$	$1.58x10^{-3}$	232.47	$5.26x10^{4}$	83.6
$6.783x10^{3}$	$1.29x10^{-3}$	338.17	$1.62x10^{5}$	209.0
$7.351x10^{3}$	$1.19x10^{-3}$	438.21	$3.53x10^{5}$	419.8
$8.019x10^{3}$	$1.09x10^{-3}$	801.25	$2.15x10^{6}$	2352.2
$8.167x10^{3}$	$1.07x10^{-3}$	1095.7	$5.51x10^{6}$	5906.9

Table III. ^{239}Pu-SiO_2+H_2O Mixtures:
Critical Parameters for Spheres Reflected with SiO_2+H_2O Mixtures

Si/^{239}Pu (Atom ratio)	Water (wt%)	Density (kg/l)	Radius (cm)	Volume (liters)	Mass (kg Pu)
183	0.0	$4.77x10^{-2}$	73.98	$1.70x10^{3}$	80.9
183	2.0	$4.56x10^{-2}$	49.85	$5.19x10^{2}$	23.7
183	5.0	$4.26x10^{-2}$	38.21	$2.34x10^{2}$	10.0
183	10.0	$3.83x10^{-2}$	30.35	$1.17x10^{2}$	4.5
183	20.0	$3.07x10^{-2}$	24.50	$6.16x10^{1}$	1.9
183	30.0	$2.45x10^{-2}$	22.51	$4.78x10^{1}$	1.2
183	40.0	$1.93x10^{-2}$	22.40	$4.71x10^{1}$	0.91
183	50.0	$1.48x10^{-2}$	24.08	$5.85x10^{1}$	0.87
183	60.0	$1.10x10^{-2}$	28.98	$1.02x10^{2}$	1.1
183	70.0	$7.70x10^{-3}$	48.36	$4.74x10^{2}$	3.7
183	75.0	$6.20x10^{-3}$	354.22	$1.86x10^{5}$	1166.8
752	0	$1.16x10^{-2}$	98.95	$4.06x10^{3}$	47.2
752	5.0	$1.04x10^{-2}$	47.93	$4.61x10^{2}$	4.8
752	10.0	$9.34x10^{-3}$	40.92	$2.87x10^{2}$	2.7
752	15.0	$8.37x10^{-3}$	39.21	$2.52x10^{2}$	2.1
752	20.0	$7.48x10^{-3}$	40.27	$2.73x10^{2}$	2.0
752	25.0	$6.70x10^{-3}$	43.71	$3.50x10^{2}$	2.3
752	30.0	$5.98x10^{-3}$	51.46	$5.71x10^{2}$	3.4
752	35.0	$5.32x10^{-3}$	70.62	$1.48x10^{3}$	7.9
752	40.0	$4.71x10^{-3}$	278.99	$9.10x10^{4}$	428.7

Table III. ^{239}Pu-SiO_2+H_2O Mixtures:
Critical Parameters for Spheres Reflected with SiO_2+H_2O Mixtures (continued)

Si/^{239}Pu (Atom ratio)	Water (wt%)	Pu Density (kg/l)	Radius (cm)	Volume (liters)	Mass (kg Pu)
1570	0.0	$5.58x10^{-3}$	116.82	$6.68x10^{3}$	37.2
1570	1.0	$5.45x10^{-3}$	86.97	$2.76x10^{3}$	15.0
1570	5.0	$5.00x10^{-3}$	63.96	$1.10x10^{3}$	5.5
1570	8.0	$4.68x10^{-3}$	61.76	$9.87x10^{2}$	4.6
1570	10.0	$4.48x10^{-3}$	62.83	$1.04x10^{3}$	4.7
1570	15.0	$4.02x10^{-3}$	74.54	$1.74x10^{3}$	7.0
1570	18.0	$3.76x10^{-3}$	95.74	$3.68x10^{3}$	13.8
1570	20.0	$3.60x10^{-3}$	132.56	$9.76x10^{3}$	35.1
1570	21.0	$3.52x10^{-3}$	182.20	$2.53x10^{4}$	89.2
2812	0.0	$3.11x10^{-3}$	140.93	$1.17x10^{4}$	36.5
2812	1.0	$3.04x10^{-3}$	110.00	$5.58x10^{3}$	16.9
2812	3.0	$2.91x10^{-3}$	96.92	$3.81x10^{3}$	11.1
2812	4.5	$2.82x10^{-3}$	97.76	$3.91x10^{3}$	11.0
2812	5.1	$2.78x10^{-3}$	99.67	$4.15x10^{3}$	11.5
2812	7.0	$2.67x10^{-3}$	112.59	$5.98x10^{3}$	16.0
2812	9.0	$2.55x10^{-3}$	149.50	$1.40x10^{4}$	35.8
2812	10.0	$2.50x10^{-3}$	200.47	$3.38x10^{4}$	84.4
4376	0.0	$2.00x10^{-3}$	183.81	$2.60x10^{4}$	52.0
4376	0.5	$1.98x10^{-3}$	164.23	$1.86x10^{4}$	36.7
4376	1.0	$1.95x10^{-3}$	157.56	$1.64x10^{4}$	32.0
4376	2.0	$1.91x10^{-3}$	159.44	$1.70x10^{4}$	32.5
4376	3.0	$1.87x10^{-3}$	177.99	$236x10^{4}$	44.2
4376	4.0	$1.83x10^{-3}$	227.28	$4.92x10^{4}$	90.1

Table III. ^{239}Pu-SiO_2+H_2O Mixtures:
Critical Parameters for Spheres Reflected with SiO_2+H_2O Mixtures (continued)

Si/^{239}Pu (Atom ratio)	Water (wt%)	Pu Density (kg/l)	Radius (cm)	Volume (liters)	Mass (kg Pu)
5513	0.0	1.58×10^{-3}	232.47	5.26×10^{4}	83.6
5513	0.5	1.57×10^{-3}	220.22	4.47×10^{4}	70.3
5513	1.0	1.55×10^{-3}	226.65	4.88×10^{4}	75.6
5513	1.5	1.54×10^{-3}	247.87	6.38×10^{4}	98.0
5513	2.0	1.52×10^{-3}	294.56	1.07×10^{5}	162.7
6785	0.0	1.290×10^{-3}	338.17	1.62×10^{5}	209.0
6785	0.10	1.287×10^{-3}	340.36	1.65×10^{5}	212.6
6785	0.25	1.283×10^{-3}	349.56	1.79×10^{5}	229.6
6785	0.50	1.275×10^{-3}	382.42	2.34×10^{5}	302.9
6785	0.60	1.272×10^{-3}	404.13	2.76×10^{5}	352.0
6785	0.70	1.270×10^{-3}	430.96	3.35×10^{5}	425.9
7350	0.0	1.191×10^{-3}	438.21	3.52×10^{5}	419.8
7350	0.10	1.188×10^{-3}	457.96	4.02×10^{5}	478.0
7350	0.25	1.184×10^{-3}	506.19	5.43×10^{5}	643.3
7350	0.50	1.178×10^{-3}	701.26	1.44×10^{6}	1701.4
7350	0.60	1.175×10^{-3}	913.38	3.19×10^{6}	3751.8
7350	0.70	1.173×10^{-3}	1935.6	3.04×10^{7}	35620.4

Table IV. ^{239}Pu-SiO_2+H_2O Reflected Spheres: Reactivity (k_{eff}) For Several Si/^{239}Pu Ratios, Masses of Plutonium, and Water Contents

A. Si/^{239}Pu = 183
Mass Pu = 3.7 kg
Density Pu = 7.70×10^{-3} kg/l
Volume = 474 liters

% Water by wt	k_{eff}
70	1.00
65	1.040
49	1.028
34	0.825
0.0	0.008

B. Si/^{239}Pu = 752
Mass Pu = 7.9 kg
Density Pu = 5.30×10^{-3} kg/l
Volume = 1.476×10^{3} liters

% Water by wt	k_{eff}
35	1.000
25	1.081
16.25	1.080
0.0	0.220

C. Si/^{239}Pu = 1570
Mass Pu = 35.1 kg
Density = 3.60×10^{-3} kg/l
Volume = 9.76×10^{3} liters

% Water by wt	k_{eff}
20.0	1.000
16.42	1.068
12.12	1.143
6.79	1.199
0.0	0.779

D. Si/^{239}Pu = 1570
Mass Pu = 89.2 kg
Density = 3.52×10^{-3} kg/l
Volume = 2.53×10^{4} liters

% Water by wt	k_{eff}
21.00	1.000
20.31	1.014
14.58	1.137
12.36	1.184
6.94	1.278
0.0	0.982

E. Si/^{239}Pu = 2812
Mass Pu = 16.0 kg
Density = 2.67×10^{-3} kg/l
Volume = 5.98×10^{3} liters

% Water by wt	k_{eff}
7.00	1.000
5.30	1.023
3.26	1.029
1.14	0.955
0.0	0.773

F. Si/^{239}Pu = 2812
Mass Pu = 35.8 kg
Density = 2.55×10^{-3} kg/l
Volume = 1.40×10^{4} liters

% Water by wt	k_{eff}
9.00	1.000
7.28	1.041
5.52	1.079
3.40	1.109
1.19	1.075
0.0	0.922

Table IV. ^{239}Pu-SiO_2+H_2O Reflected Spheres
Reactivity (k_{eff}) For Several Si/^{239}Pu Ratios, Masses of Plutonium, and Water Contents (continued)

G. Si/^{239}Pu = 2812
Mass Pu = 84.4 kg
Density = 2.50×10^{-3} kg/l
Volume = 3.38×10^{4} liters

% Water by wt	k_{eff}
10	1.000
5.64	1.122
3.47	1.173
1.21	1.178
0.0	1.066

H. Si/^{239}Pu = 4376
Mass Pu = 32.5 kg
Density = 1.913×10^{-3} kg/l
Volume = 1.70×10^{4} liters

% Water by wt	k_{eff}
2.0	1.000
1.01	0.988
0.51	0.962
0.0	0.902

I. Si/^{239}Pu = 4376
Mass Pu = 90.1 kg
Density = 1.832×10^{-3} kg/l
Volume = 4.92×10^{4} liters

% Water by wt	k_{eff}
4.000	1.000
3.060	1.024
2.085	1.053
1.060	1.071
0.0	1.031

J. Si/^{239}Pu = 5513
Mass Pu = 162.7 kg
Density = 1.519×10^{-3} kg/l
Volume = 1.07×10^{5} liters

% Water by wt	k_{eff}
2.0	1.000
1.039	1.039
0.516	1.052
0.0	1.049

Table V. ^{239}Pu Metal - Nevada Tuff Mixtures
Critical Parameters For Tuff-Reflected Spheres

(Si/^{239}Pu)1/0.77 (Atom ratio)	Pu Density (kg/l)	Radius (cm)	Volume (liters)	Mass (kg Pu)
0.87×10^{0}	1.0×10^{1}	6.27	1.04×10^{0}	10.4
1.75×10^{0}	5.0×10^{0}	9.94	4.12×10^{0}	20.6
2.75×10^{0}	3.18×10^{0}	13.13	9.49×10^{0}	30.1
4.41×10^{0}	1.98×10^{0}	17.25	2.15×10^{1}	42.6
8.75×10^{0}	1.0×10^{0}	24.93	6.49×10^{2}	64.9
1.47×10^{1}	5.96×10^{-1}	32.16	1.39×10^{2}	83.1
4.72×10^{1}	1.85×10^{-1}	52.53	6.07×10^{2}	112.6
1.83×10^{2}	4.77×10^{-2}	81.03	2.22×10^{3}	106.2
7.53×10^{2}	1.16×10^{-2}	120.68	7.36×10^{3}	85.6
1.175×10^{3}	7.40×10^{-3}	144.39	1.26×10^{4}	93.3
1.578×10^{3}	5.54×10^{-3}	170.81	2.08×10^{4}	115.7
1.839×10^{3}	4.76×10^{-3}	192.78	3.00×10^{4}	142.9
2.736×10^{3}	3.20×10^{-3}	361.34	1.97×10^{5}	632.4
2.812×10^{3}	3.11×10^{-3}	398.70	2.65×10^{5}	825.7
2.919×10^{3}	3.00×10^{-3}	466.90	4.26×10^{5}	1279.2

Table VI. ^{239}Pu Metal, Tuff, and H_2O Mixtures
Critical Parameters for Spheres Reflected With Tuff - H_2O Mixtures

(Si/^{239}Pu)1/0.77 (Atom ratio)	Water (wt %)	Pu Density (kg/l)	Radius (cm)	Volume (liters)	Mass (kg Pu)
752	0.0	$1.16x10^{-2}$	120	$7.36x10^{3}$	85.6
752	1.0	$1.14x10^{-2}$	88.43	$2.90x10^{3}$	32.9
752	2.0	$1.11x10^{-2}$	75.49	$1.80x10^{3}$	20.0
752	3.0	$1.08x10^{-2}$	68.11	$1.33x10^{3}$	14.3
752	5.0	$1.03x10^{-2}$	59.83	$8.97x10^{2}$	9.3
752	7.0	$9.88x10^{-3}$	55.38	$7.11x10^{2}$	7.0
752	10.0	$9.22x10^{-3}$	52.13	$5.93x10^{2}$	5.5
752	13.0	$8.61x10^{-3}$	51.02	$5.57x10^{2}$	4.8
752	15.0	$8.23x10^{-3}$	51.34	$5.66x10^{2}$	4.7
752	20.0	$7.67x10^{-3}$	53.14	$6.28x10^{2}$	4.8
752	25.0	$6.52x10^{-3}$	66.51	$1.23x10^{3}$	8.1
752	30.0	$5.80x10^{-3}$	103.2	$4.60x10^{3}$	26.7
752	31.0	$5.60x10^{-3}$	123.63	$7.92x10^{3}$	44.9
752	33.0	$5.40x10^{-3}$	343.74	$1.66x10^{5}$	898.7
1175	0.0	$7.40x10^{-3}$	144.39	$1.26x10^{4}$	93.2
1175	1.0	$7.23x10^{-3}$	107.33	$5.18x10^{3}$	37.4
1175	2.0	$7.06x10^{-3}$	93.72	$3.45x10^{3}$	24.4
1175	3.0	$6.90x10^{-3}$	86.51	$2.71x10^{3}$	18.7
1175	4.0	$6.74x10^{-3}$	86.20	$2.33x10^{3}$	15.7
1175	6.0	$6.43x10^{-3}$	78.11	$2.00x10^{3}$	12.9
1175	9.0	$6.01x10^{-3}$	78.71	$2.04x10^{3}$	12.3
1175	11.0	$5.74x10^{-3}$	82.68	$2.37x10^{3}$	13.6
1175	13.0	$5.48x10^{-3}$	90.39	$3.09x10^{3}$	17.0
1175	14.0	$5.36x10^{-3}$	96.36	$3.75x10^{3}$	20.1
1175	16.0	$5.12x10^{-3}$	116.64	$6.65x10^{3}$	34.0
1175	17.0	$5.00x10^{-3}$	136.02	$1.05x10^{4}$	52.8
1175	18.0	$4.89x10^{-3}$	170.16	$2.06x10^{4}$	100.9
1175	19.0	$4.77x10^{-3}$	265.86	$7.87x10^{4}$	376.2

Table VI. ^{239}Pu Metal, Tuff, and H_2O Mixtures
Critical Parameters for Spheres Reflected With Tuff - H_2O Mixtures (continued)

(Si/^{239}Pu)1/0.77 (Atom ratio)	Water (wt %)	Density (kg/l)	Radius (cm)	Volume (liters)	Mass (kg Pu)
1570	0.0	5.54×10^{-3}	170.81	2.09×10^{4}	115.7
1570	1.0	5.41×10^{-3}	130.85	9.38×10^{3}	50.8
1570	2.0	5.29×10^{-3}	117.94	6.87×10^{3}	36.3
1570	3.0	5.16×10^{-3}	112.52	5.96×10^{3}	30.8
1570	4.0	5.04×10^{-3}	111.05	5.73×10^{3}	29.0
1570	5.0	4.93×10^{-3}	112.35	5.94×10^{3}	29.3
1570	6.0	4.82×10^{-3}	116.10	6.55×10^{3}	31.6
1570	7.0	4.71×10^{-3}	122.66	7.73×10^{3}	36.4
1570	8.0	4.60×10^{-3}	133.14	9.88×10^{3}	45.5
1570	9.0	4.50×10^{-3}	150.11	1.41×10^{4}	63.8
1570	10.0	4.40×10^{-3}	180.50	2.46×10^{4}	108.3
1570	11.0	4.30×10^{-3}	252.92	6.77×10^{4}	291.3
1570	11.2	4.28×10^{-3}	282.64	9.45×10^{4}	404.7
1570	11.3	4.27×10^{-3}	305.37	1.19×10^{5}	509.2
1850	0.0	4.76×10^{-3}	192.78	3.00×10^{4}	142.9
1850	1.0	4.65×10^{-3}	151.81	1.47×10^{4}	68.2
1850	2.0	4.54×10^{-3}	141.23	1.18×10^{4}	53.6
1850	3.0	4.44×10^{-3}	140.47	1.16×10^{4}	51.6
1850	4.0	4.34×10^{-3}	145.83	1.29×10^{4}	56.4
1850	5.0	4.24×10^{-3}	157.79	1.65×10^{4}	69.8
1850	6.0	4.14×10^{-3}	180.33	2.46×10^{4}	101.7
1850	7.0	4.04×10^{-3}	227.57	4.94×10^{4}	199.8
1850	8.0	3.94×10^{-3}	395.28	2.59×10^{5}	1023.5

Table VI. ^{239}Pu Metal, Tuff, and H_2O Mixtures
Critical Parameters for Spheres Reflected With Tuff - H_2O Mixtures (continued)

(Si/^{239}Pu)1/0.77 (Atom ratio)	Water (wt %)	Density (kg/l)	Radius (cm)	Volume (liters)	Mass (kg Pu)
2750	0.0	3.20×10^{-3}	361.34	1.97×10^{5}	632.4
2750	0.1	3.192×10^{-3}	357.04	1.91×10^{5}	608.7
2750	0.2	3.185×10^{-3}	355.58	1.88×10^{5}	599.9
2750	0.3	3.177×10^{-3}	356.77	1.90×10^{5}	604.5
2750	0.4	3.170×10^{-3}	360.42	1.96×10^{5}	621.8
2750	0.5	3.163×10^{-3}	366.48	2.06×10^{5}	652.2
2750	0.6	3.156×10^{-3}	375.04	2.21×10^{5}	697.3
2750	0.7	3.148×10^{-3}	386.45	2.42×10^{5}	761.1
2750	0.8	3.141×10^{-3}	401.17	2.70×10^{5}	849.5
2750	0.9	3.133×10^{-3}	420.01	3.10×10^{5}	972.6
2750	0.9	3.126×10^{-3}	444.23	3.67×10^{5}	1148.0

Table VII. ^{239}Pu, Tuff, and H_2O Reflected Spheres
Reactivity (k_{eff}) For a Si/^{239}Pu Ratio of 1570, Several Plutonium Masses, and Water Contents

A. (Si/^{239}Pu)1/0.77 = 1570
Mass Pu = 36.4 kg
Density = 4.71×10^{-3} kg/l
Volume = 7.73×10^{3} liters

% Water by wt	k_{eff}
7.0	1.000
6.11	1.006
5.21	1.010
4.26	1.010
2.23	0.980
1.14	0.925
0.0	0.754

B. (Si/^{239}Pu)1/0.77 = 1570
Mass Pu = 45.5 kg
Density = 4.60×10^{-3} kg/l
Volume = 9.88×10^{3} liters

% Water by wt	k_{eff}
8.0	1.000
6.25	1.017
4.36	1.024
2.28	1.0027
1.17	0.953
0.0	0.787

C. (Si/^{239}Pu)1/0.77 = 1570
Mass Pu = 63.8 kg
Density = 4.49×10^{-3} kg/l
Volume = 1.41×10^{4} liters

% Water by wt	k_{eff}
9.0	1.000
7.28	1.022
5.44	1.041
3.42	1.047
1.19	0.995
0.0	0.841

D. (Si/^{239}Pu)1/0.77 = 1570
Mass Pu = 108.3 kg
Density = 4.397×10^{-3} kg/l
Volume = 2.46×10^{4} liters

% Water by wt	k_{eff}
10.00	1.000
8.32	1.026
6.52	1.053
4.55	1.076
2.38	1.080
0.0	0.923

E. **(Si/^{239}Pu)1/0.77 = 1570**
Mass Pu = 404.7 kg
Density = 4.277×10^{-3} kg/l
Volume = 9.45×10^{4} liters

% Water by wt	k_{eff}
11.20	1.000
10.22	1.018
8.53	1.050
6.69	1.086
4.67	1.124
2.45	1.156
0.00	1.085

APPENDIX

SOIL COMPOSITION USED IN THE ONEDANT AND MCNP MODELS

The ONEDANT calculations were performed assuming an S_n order of 32 and the 16-group Hansen-Roach Cross Sections with P1 scattering. The spherical model consists of two zones. The inner zone assumes a homogeneous mixture of Pu-239 and SiO_2 or tuff and in some cases water. The inner zone contains approximately 200 fine mesh points. The outer zone is the 100-cm-thick reflector, which is assumed to be SiO_2 or tuff, and in some cases also contains water. The outer zone contains approximately 100 fine mesh points.

For a few special cases, we used the Los Alamos Monte Carlo Neutron Photon (MCNP) code operated in the k-code (eigenvalue) and using continuous energy cross sections based on the Evaluated Nuclear Data File, ENDF/B-V and ENDF/B-VI.

Table A.1 contains the actual composition of the tuff [4] and the elements and components that were used in the ONEDANT and MCNP models. Note that some of the cross section data for some of the elements were not available.

Table A.1. Soil Composition

Component	wt%
SiO_2	77.0
TiO_2	0.1
Al_2O_3	12.7
FeO	0.85
MnO	0.06
MgO	0.16
CaO	0.53
Na_2O	3.64
K_2O	4.97
P_2O_5*	0.01

Element	ppm by weight
Sc*	2.50
V	5.00
Co	0.16
Zn**	65.00
As	-
Rb*	160.00
Sr***	9.00
Zr	108.00
Sb***	0.33
Cs*	6.80
Ba*	43.00
Hf*	4.20
Ta	1.50
Th	24.00
U	4.40
La***	33.00
Ce**	75.00
Nd*	29.00
Sm	6.10
Eu	0.28
Gd	5.50
Tb***	0.32
Dy***	4.80
Tm*	0.48
Yb***	2.70
Lu***	0.39

* Cross section data not available in ONEDANT.

** Cross section data not available in MCNP.

*** Cross section data not available in both ONEDANT and MCNP.

Comparison of the Volume Displacement Model with the Porosity Model

The physical model used to calculate the atom densities for the critical radii and k_{eff} throughout this study has been the volume displacement model. That is, if, for example, 5 wt % water is assumed to be mixed with a dry mixture of tuff and plutonium, the volume occupied by the water displaces an equal volume of tuff and plutonium, thus reducing their densities. Another model can be justified and used. This second model recognizes that the tuff has a "porosity" of several percent, sometimes estimated to be as high as 11 %. Using this model, the water can be assumed to be simply added to the volume of tuff and plutonium, not changing their densities. A comparison is made below for two Si/Pu* ratios, 1850 and 1570; the displacement model data are taken from Table VI and reproduced here, in part. The porosity model results were obtained with the ONEDANT code and Hansen Roach cross sections.

Table A.2. Si/Pu* = 1570

Density Pu kg/l	Displacement water (wt%)	Model Critical Mass (kg)	Porosity Water (wt%)	Model Critical Mass (kg)
0.00554	0.0	115.7	0.0	115.66
0.00554	1.0	50.8	1.05	46.91
0.00554	2.0	36.3	2.087	32.16
0.00554	4.0	29.0	4.088	23.83
0.00554	6.0	31.6	6.01	24.69
0.00554	8.0	45.5	7.85	31.07
0.00554	10.0	108.3	9.63	57.55

Si/Pu* = 1850

Density Pu kg/l	Displacement water (wt%)	Model Critical Mass (kg)	Porosity Water (wt%)	Model Critical Mass (kg)
0.00476	0.0	14.29	0.0	142.8
0.00476	1.0	68.2	1.05	63.36
0.00476	2.0	53.6	2.08	47.97
0.00476	4.0	56.4	4.09	47.11
0.00476	6.0	101.7	6.01	77.43
0.00476	8.0	1023.5	7.85	493.81

These same data are plotted on Fig. A-1 to illustrate graphically the difference. The comparable figure in the body of the text is Fig. 16. The critical masses for the same water concentration can differ by factors up to about 1.4, depending on the amount of water. The pattern, however, is changed not at all and it is this pattern that determines the autocatalytic region of Fig. 17. Thus to use the porosity model would be equally correct, but the fundamental conclusions would be changed only in minor detail.

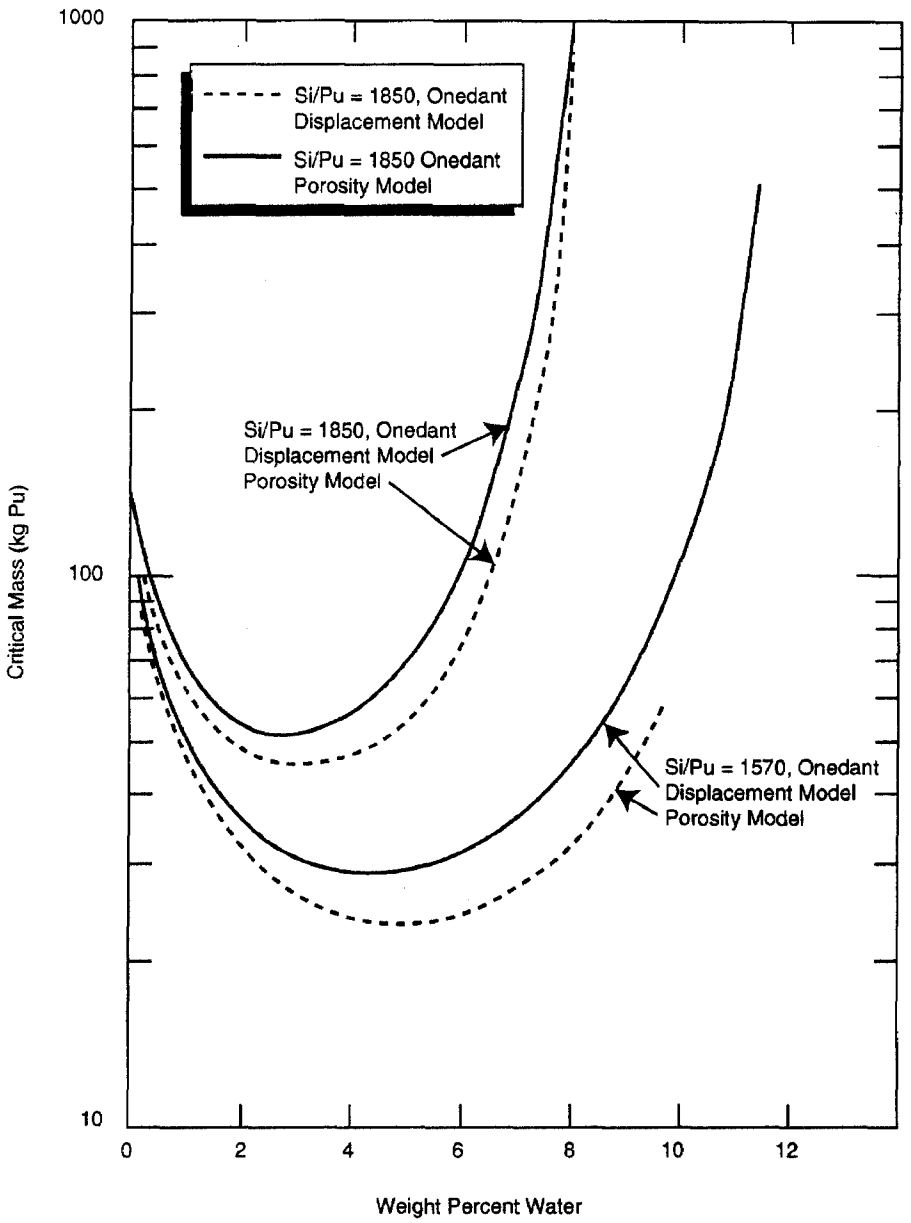

Figure A-1. Reflected critical mass of plutonium metal mixed with tuff and water vs weight percent water. The effect of two models for mixing water with the tuff are illustrated. These are the displacement model in which the volume of water displaces the appropriate volume of tuff and plutonium, and the porosity model in which the tuff is assumed to have an existing porosity of up to 11% of its volume. The water, then, is merely added without changing the density of the solid material. The two assumptions show different critical masses, but have little effect on the conclusions relating to autocatalytic power transients.

Comparison of ONEDANT and MCNP Calculated Results

A suggestion has been made that because the neutron spectrum of importance in at least part of this study is intermediate, neither fast neutron or thermal neutron, the calculated radii and k_{eff} would be better determined by using the MCNP computer program with the so-called continuous energy cross sections. This assumption is questionable, but to settle the matter a comparison has been made to ONEDANT data in Table VI and for Si/Pu* ration of 1850. The MCNP program calculates a k_{eff} most easily and these values of k_{eff} are compared to the k_{eff} = 1.0 critical radii calculations below, as taken from Table VI in the body of the text.

Table A.4. ONEDANT-MCNP Comparison

Si/Pu* = 1850

Density Pu kg/l	Water (wt%)	ONEDANT Radius (cm)	ONEDANT Mass (kg)	MCNP k_{eff}
0.00476	0.0	192.8	142.9	1.039 ± 0.0013
0.00476	1.05	147.0	63.4	1.0184 ± 0.0013
0.00476	2.08	134.0	48.0	1.00656 ± 0.0012
0.00476	4.0	133.2	47.1	0.99545 ± 0.00096
0.00476	6.0	157.2	77.4	0.99354 ± 0.00081
0.00476	7.85	291.5	493.8	0.99244 ± 0.00077

The data show that for the case with no water, the k_{eff} using MCNP is 1.039, meaning that the critical radius and mass would be smaller. However, when the water content reaches about 2%, the MCNP k_{eff} is essentially 1.0 and differences in the critical masses would be trivial. If these data were transferred to Fig. 16 the differences could scarcely be seen and the significant figure, Fig. 17, would not be changed.

REFERENCES

1. C. D. Bowman, and F. Venneri, "Nuclear Excursions and Eruptions from Plutonium and Other Fissile Material Stored Underground," Los Alamos National Laboratory, November 22, 1994, draft report.

2. C. D. Bowman and F. Venneri, "Criticality Issues for Thermally Fissile Material in Geologic Storage," Los Alamos National Laboratory document LA-UR-95-504 (January 1995).

3. C. D. Bowman and F. Venneri, "Underground Autocatalytic Criticality from Plutonium and Other Fissile Material," Los Alamos National Laboratory document, LA-UR-94-4022 (January 1995).

4. G. A. Cowan, "A Natural Fission Reactor," *Scientific American*, **235**, (1) 36 (July 1976).

5. Thomas Dey, Los Alamos National Laboratory, private communication (July 1995).

6. D. E. Broxton, R. G. Warren, F. M. Byers, and R. B. Scott, "Chemical and Mineralogic Trends Within the Timber Mountain-Oasis Valley Caldera Complex, Nevada: Evidence for Multiple Cycles of Chemical Evolution in a Long-Lived Silicic Magma System," *Journal of Geophysical Research* **94** (B5) 5961-5985 (May 10, 1989) Los Alamos National Laboratory document LA-UR-94-4022 (December 1994).

   Additional information on tuff and its properties can be found in

   6.a. R. F. Roy, A. E. Beck, and Y. S. Touloubian, "Thermophysical Properties of Rocks," in *Physical Properties of Rocks and Minerals*, Vol. II, W. R. Judd and R. F. Roy, Ed. (McGraw Hill, New York, 1981), pp. 409-502.

   6.b. J. R. Kaum and R. J. Bos, "Comparisons of Chemical and Nuclear Explosions: Numerical Simulations of the Non-Proliferation Experiment," Los Alamos National Laboratory report LA-12942-MS (June 1995).

7. R. D. O'Dell, F. W. Brinkly, Jr., and D. R. Marr, "User's Manual for ONEDANT: A Code Package for One-Dimensional, Diffusion-Accelerated, Neutral-Particle Transport," Los Alamos National Laboratory report LA-9184-M (February 1982).

8. B. G. Carlson, *The Numerical Theory of Neutron Transport*, in *Methods in Computational Physics*, Volume 1 (New York, Academic Press, 1963).

9. G. E. Hansen and William H. Roach, "Six and Sixteen Group Cross Sections for Fast and Intermediate Critical Assemblies," Los Alamos Scientific Laboratory report LA-2543-MS, (November 1961).

10. "MCNP, Monte Carlo Neutron Photon code, a General Monte Carlo Code for Neutron and Photon Transport," Los Alamos National Laboratory report LA-7396-M, Rev. 2 (1991).

11. "The Evaluated Nuclear Data File: Version V," available from and maintained by the National Nuclear Data Center, Brookhaven National Laboratory.

12. W. R. Stratton, "Criticality Data and Factors Affecting Criticality of Single Homogeneous Units," Los Alamos Scientific Laboratory report LA-3612 (July 1964 and September 22, 1967). The Pu-H_2O Data have been extended by one of the authors of this document.

13. H. C. Paxton and N. Pruvost "Critical Dimensions of Systems Containing U-235, Pu-239 and U-233," Los Alamos National Laboratory report LA-10860 (July 1987).

14. J. Robert Oppenheimer and Robert Serber, Letter to R.F. Christy and John A. Wheeler received December 31, 1942, quoted in "Chain Reaction of Pure Fissionable Materials in Solution," CP-400, January 1, 1943. The letter, apparently, has been lost.

15. W. R. Stratton, "Critical Dimensions of U(93.5)-Graphite-Water Spheres, Cylinders, and Slabs," Los Alamos Scientific Laboratory report LA-2955-MS (May 1962).

16. George P. Dix, Ratheon Services Corp., Las Vegas, Nevada, private communication (August 1995).

17. B. F. Gore, U. P. Jenquin, R. J. Serne, "Factore Affecting Criticality for Spent-Fuel Materials in a Geologic Setting," Pacific Northwest Laboratory, Richland, Washington, 99352, PNL-3791, UC-70.